

2

**AD-A258 347**

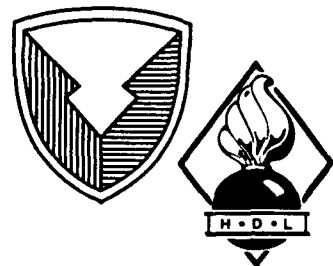


HDL-SR-92-2

September 1992

**High-Altitude Electromagnetic Pulse Survivability  
Assessment of the Harris RF-3200 Transceiver**

by William O. Coburn  
Eric Nguyen  
Ronald J. Reyzer  
Mark H. Mar



**92-30699**



U.S. Army Laboratory Command  
**Harry Diamond Laboratories**  
Adelphi, MD 20783-1197

The findings in this report are not to be construed as an official Department of the Army position unless so designated by other authorized documents.

Citation of manufacturer's or trade names does not constitute an official endorsement or approval of the use thereof.

Destroy this report when it is no longer needed. Do not return it to the originator.

REPORT DOCUMENTATION PAGE			Form Approved OMB No. 0704-0188	
Public reporting burden for this collection of information is estimated to average 1 hour per response, including the time for reviewing instructions, searching existing data sources, gathering and maintaining the data needed, and completing and reviewing the collection of information. Send comments regarding this burden estimate or any other aspect of this collection of information, including suggestions for reducing this burden, to Washington Headquarters Services, Directorate for Information Operations and Reports, 1215 Jefferson Davis Highway, Suite 1204, Arlington, VA 22202-4302, and to the Office of Management and Budget, Paperwork Reduction Project (0704-0188), Washington, DC 20503.				
1. AGENCY USE ONLY (Leave blank)	2. REPORT DATE September 1992	3. REPORT TYPE AND DATES COVERED Final, 1 Oct. 1989—1 Oct. 1991		
4. TITLE AND SUBTITLE High-Altitude Electromagnetic Pulse Survivability Assessment of the Harris RF-3200 Transceiver			5. FUNDING NUMBERS  PE: 62120	
6. AUTHOR(S) William O. Coburn, Eric Nguyen, Ronald J. Reyzer, and Mark H. Mar				
7. PERFORMING ORGANIZATION NAME(S) AND ADDRESS(ES) Harry Diamond Laboratories 2800 Powder Mill Road Adelphi, MD 20783-1197			8. PERFORMING ORGANIZATION REPORT NUMBER HDL-SR-92-2	
9. SPONSORING/MONITORING AGENCY NAME(S) AND ADDRESS(ES) National Communications System 701 S. Courthouse Rd. Arlington, VA 22204			10. SPONSORING/MONITORING AGENCY REPORT NUMBER	
11. SUPPLEMENTARY NOTES AMS code: 612120.H250000 HDL PR: E910E3				
12a. DISTRIBUTION/AVAILABILITY STATEMENT  Approved for public release; distribution unlimited.			12b. DISTRIBUTION CODE	
13. ABSTRACT (Maximum 200 words)  Harry Diamond Laboratories conducted a high-altitude electromagnetic pulse (HEMP) survivability/vulnerability assessment of a high-frequency transceiver system, the Harris Corporation RF-3200 transceiver and ancillary equipment. The non-developmental item and a hardened version of the RF-3200 system were both HEMP simulation tested. External transient protection devices were HEMP hardened at the various system electrical interfaces. The test and analysis results establish the RF-3200 transceiver system survivability when it is exposed to a HEMP threat environment.				
14. SUBJECT TERMS HEMP survivability, HF transceiver, HEMP simulator, TACAMO EMP simulator, non-developmental item			15. NUMBER OF PAGES 108	
			16. PRICE CODE	
17. SECURITY CLASSIFICATION OF REPORT Unclassified	18. SECURITY CLASSIFICATION OF THIS PAGE Unclassified	17. SECURITY CLASSIFICATION OF ABSTRACT Unclassified	20. LIMITATION OF ABSTRACT UL	

## Contents

	Page
Executive Summary .....	7
<b>1. Introduction</b> .....	<b>9</b>
1.1 <i>Objective</i> .....	9
1.2 <i>Scope</i> .....	10
<b>2. System Description</b> .....	<b>11</b>
<b>3. Pre-Test Analysis</b> .....	<b>12</b>
3.1 <i>Electrical Connections</i> .....	14
3.2 <i>HEMP Coupling Analysis</i> .....	15
3.2.1 <i>Antenna Coupling Analysis</i> .....	19
3.2.2 <i>Cable HEMP Coupling Analysis</i> .....	23
3.2.3 <i>HEMP Coupling to Internal Circuits</i> .....	28
3.2.4 <i>Circuit Survivability Analysis</i> .....	30
3.3 <i>Internal Transient Protection in the RF-3200</i> .....	32
3.4 <i>HEMP Survivability Analysis Conclusions</i> .....	33
3.4.1 <i>Power Supply Interfaces</i> .....	33
3.4.2 <i>Transceiver/Coupler Interfaces</i> .....	36
<b>4. Test Procedures for Unhardened System</b> .....	<b>39</b>
4.1 <i>HEMP Simulation</i> .....	39
4.2 <i>Unhardened System Configuration</i> .....	40
4.3 <i>General Test Procedures for the Unhardened System</i> .....	40
4.4 <i>Test Conduct for the Unhardened System</i> .....	41
<b>5. Test Results for Unhardened System</b> .....	<b>41</b>
5.1 <i>Test Data Summary</i> .....	45
5.2 <i>Conclusions</i> .....	46
5.3 <i>Recommendations</i> .....	48
<b>6. Test Procedures for Hardened System</b> .....	<b>48</b>
6.1 <i>Pulsed Illumination Tests</i> .....	49
6.1.1 <i>Hardened System Configurations</i> .....	49
6.1.2 <i>General Test Procedures for the Hardened System</i> .....	52
6.1.3 <i>Test Conduct for the Hardened System</i> .....	54
6.2 <i>Current Injection Tests</i> .....	59
6.2.1 <i>Power Supply Interface</i> .....	60
6.2.2 <i>Transceiver Interfaces</i> .....	61
<b>7. Test Results for Hardened System</b> .....	<b>61</b>
7.1 <i>Test Data Summary</i> .....	64

7.2	Conclusions .....	66
7.2.1	Direct Field Coupling .....	66
7.2.2	Field-to-Wire Coupling .....	67
7.2.3	Antenna Coupling .....	69
7.3	Recommendations .....	70
8.	HEMP Survivability Statement .....	71
	References .....	72
	Distribution .....	107

### Appendices

A.—	Test Data for Unhardened System .....	75
B.—	Test Data for Hardened System .....	89

### Figures

1.	Typical configuration for the RF-3200 system .....	13
2.	RF-3200 interconnect diagram .....	15
3.	RF-3200 front panel view .....	16
4.	RF-3200 rear panel connections .....	17
5.	HEMP response of a 46-m free-space dipole .....	18
6.	RF-1912 free-space antenna .....	20
7.	HEMP-induced response of the RF-1912 antenna at a height of 10 m .....	21
8.	HEMP response of a 46-m dipole at a height of 2 m .....	22
9.	Free-space dipole spectral response comparison for DE and FDE incident pulses .....	22
10.	Free-space dipole transient response comparison for DE and FDE incident pulses .....	23
11.	TACAMO EMP simulator .....	38
12.	Test configuration for the unhardened RF-3200 system .....	42
13.	Harmonic filter PWB A4 schematic diagram .....	47
14.	Test configuration IA without the transceiver .....	49
15.	RF-1912 antenna and RF-3282 coupler ground connections .....	50
16.	Test configuration IB without the transceiver .....	50
17.	Test configuration IB with the transceiver .....	51
18.	Test configuration II for the hardened system .....	52
19.	Test configuration III for the hardened system .....	52
20.	Measured TPD input current for a 50-Ω line .....	60
21.	Measured residual current for a 50-Ω load .....	60

## Tables

1. RF-3200 Electrical Connections .....	14
2. RF-382-01 Electrical Connections .....	18
3. Summary of Induced Antenna Current Peak Amplitudes Measured for Unhardened System .....	45
4. Summary of Peak E-Field Amplitudes Measured at Transceiver Location for Unhardened System .....	46
5. Summary of Measured Peak Current Amplitudes for Hardened System .....	65
6. Summary of Measured Field Amplitudes for the Hardened System .....	66
7. Summary of Pre- and Post-Test Calculated Hardness Margins for HEMP Field-to-Wire Coupling .....	69

DIRECT

<b>Accession For</b>	
NTIS GRA&I	<input checked="" type="checkbox"/>
DTIC TAB	<input type="checkbox"/>
Unannounced	<input type="checkbox"/>
Justification	
By _____	
Distribution/	
<b>Availability Codes</b>	
Dist	Avail and/or Special
A-1	

## Executive Summary

Harry Diamond Laboratories (HDL) is supporting the National Communications System (NCS) in the analysis and testing of a high-frequency (hf) transceiver and ancillary equipment to determine the system's ability to survive the high-altitude electromagnetic pulse (HEMP) early-time (E1) criteria of DoD-STD-2169A.\* The hf transceiver can serve as an alternative means of communication for elements of the NCS if the landline service is severely disrupted. The Harris Corporation (RF Communications Group) RF-3200 single sideband (SSB) hf transceiver has been nominated by the NCS to be pre-positioned at selected operating centers. The RF-3200 HF-SSB was selected because of the compatibility of its operating standard with existing installed equipment.

Initially HDL was asked to establish the HEMP survivability/vulnerability (S/V) of the Harris Corporation RF-3200 transceiver and ancillary equipment. HEMP simulation testing revealed that this commercial equipment was vulnerable to damage when exposed to a HEMP environment. Based on the test and analysis results, HDL made hardening recommendations. Transient protection devices (TPDs) were chosen and incorporated into the system as external parts. The HEMP S/V assessment process was then applied to the hardened system.

The program consists of pre-test analysis, HEMP simulation tests, and post-test analysis. The mid- and late-time components of the DoD-STD-2169A HEMP threat environment do not effectively couple HEMP energy to this system so the HEMP S/V assessment is with respect to the E1 component only. Test and analysis results based on other HEMP threat environments are appropriately extended to address the E1 threat. Determining the system S/V to other nuclear weapons effects and extending the test data to address the use of the RF-3200 system for communications connectivity are beyond the scope of this effort.

System-level HEMP hardness verification testing is best accomplished by a radiated pulse illumination (PI) test of the complete system in a typical (but worst-case) deployment configuration. Due to the unavailability of high-level PI testing facilities at HDL, the TACAMO EMP Simulator (TES) at the Naval Air Test Center (NATC), was used to produce the simulated HEMP environment. Of the possible system

---

\* DoD-STD-2169A, *High-Altitude Electromagnetic Pulse Environment*, 1985.

configurations, the dipole antenna and the maximum allowable cable lengths are chosen as the representative unhardened test article. The worst-case HEMP coupling to this system is obtained for the electric (E-) field oriented along the dipole antenna and the system cables, and the maximum field coupling to electronics that are mounted in a typical unshielded rack.

The unhardened system was shown to be vulnerable to damage from high-level pulsed electromagnetic environments. The simulation test results provided information on the failure threshold for the transceiver system. The primary concern for HEMP S/V was to limit the HEMP-induced antenna current without degrading the transceiver performance. External TPDs were subsequently incorporated into the system at the various electrical interfaces.

The hardened system was subsequently tested in a manner similar to that used for the unhardened system. The pass/fail criterion for HEMP survivability was that no failures be observed which could not be corrected by power cycling. The test results indicated arcing effects in the antenna feedline, which served to reduce the HEMP-induced threat at the antenna coupler. The measured data also indicated substantial current attenuation in both the antenna coupler and the transceiver power supply transformer. The system was not damaged after exposure to the maximum electromagnetic environment possible in the HEMP simulation tests. Based on the simulation test results, the post-test analysis, and engineering judgment, the hardened RF-3200 system, in a typical office building installation, can withstand exposure to the HEMP threat environment. Specific recommendations for the system installation are provided.

# 1. Introduction

Harry Diamond Laboratories (HDL) is supporting the National Communications System (NCS) in the analysis and testing of a high-frequency (hf) transceiver and ancillary equipment to determine the system's ability to survive the high-altitude electromagnetic pulse (HEMP) early-time (E1) criteria of DoD-STD-2169A [1]. The hf transceiver can serve as an alternative means of communication for elements of the NCS if the landline service is severely disrupted. The Harris Corporation (RF Communications Group) RF-3200 single sideband (SSB) hf transceiver has been nominated by the NCS to be prepositioned at selected operating centers. The RF-3200 HF-SSB was selected because of the compatibility of its operating standard with existing installed equipment.

The HEMP survivability assessment was accomplished in primarily two phases: HEMP simulation testing on an unhardened RF-3200 system and HEMP simulation testing on a hardened RF-3200 system. The unhardened system included the RF-382-01 antenna coupler and the RF-1940 dipole antenna and was tested during August 1990. The RF-3200 system, with the RF-3282 antenna coupler and the RF-1912 dipole antenna, was hardened with external protection devices and tested during August 1991. Current-injection (CI) testing on selected elements of the hardened system was undertaken during September 1991. The results for all phases of the survivability assessment are presented and discussed.

## 1.1 Objective

The primary objective of the HEMP survivability assessment for the RF-3200 is to establish the transceiver system survivability/vulnerability (S/V) when exposed to a HEMP threat environment. The transceiver was tested in an operational configuration including an antenna coupler and a typical broadband antenna. Simulation testing serves to evaluate the transceiver performance when subjected to incrementally increasing levels of a simulated HEMP environment. The test article was tested in both a hardened and an unhardened configuration, where the hardened configuration involves the installation of external transient protection devices (TPDs) at the various system electrical interfaces. The RF-3200 system was exposed to pulsed rf environments up to and including the maximum simulated HEMP environment.

Secondary objectives during testing were to document (1) performance degradations, (2) recoverable fault conditions, and (3) transient protection capabilities. Commercially available or nondevelopmental item (NDI) equipment that could be readily hardened to meet HEMP survivability requirements may be beneficial to the Army. The program results would have future applications if similar NDI equipment is incorporated into military systems.

## 1.2 Scope

The program consists of pre-test analysis, HEMP simulation tests, and post-test analysis. The HEMP S/V assessment is with respect to the DoD-STD-2169A threat environment, E1 component only. It can readily be shown that the later time components of the DoD-STD-2169A threat do not effectively couple HEMP energy to this system. The HEMP coupling analysis uses the unclassified Bell Laboratories double-exponential (DE) waveform [2] or a fast double-exponential (FDE) pulse as the incident HEMP waveform. Due to limited radiated pulse illumination (PI) capabilities for the DoD-STD-2169A HEMP environment, this type of testing is also with respect to the DE waveform. Additional testing attempts to address the system response to the E1 threat or the system S/V to the E1 waveform is established analytically. Results based on other threat environments are appropriately extended to address the E1 threat. Determining system survivability to other nuclear weapons effects is beyond the scope of this effort.

The pre-test analysis establishes the worst-case antenna/cable currents that could be expected when the system is exposed to a HEMP threat environment that has a DE or an FDE waveform. The pre-test analysis also identifies the worst-case HEMP-induced stress at the various system interfaces. The internal transient protection in the RF-3200 system is discussed. Radiated PI testing illuminated a representative test article, in both an unhardened and a hardened configuration, with peak pulsed electric (E-) field levels from about 5 to 45 kV/m. Several pulses at each E-field level were applied until upset or damage occurred or until the system was exposed to the maximum pulse level. External TPDs were chosen based on the pre-test analysis and the simulation test results for the RF-3200 system in an unhardened configuration. The RF-3200 system was subsequently tested in a hardened configuration using radiated PI HEMP simulation techniques.

The scope of the post-test analysis is limited to determining the upset or failure thresholds, if any, for the representative test article. The

pertinent test data are included and form the basis for a statement of the system HEMP S/V. The conclusions address the system HEMP S/V with regard to the E1 threat environment as specified in DoD-STD-2169A. Extending the test data to address the use of the RF-3200 for communications connectivity is beyond the scope of this effort.

## 2. System Description

The test article, as provided by the Harris Corporation (RF Communications Group), consists of the RF-3200 125-W HF-SSB transceiver, the RF-382-01 or RF-3282 continuous duty antenna coupler, the RF-3236R continuous duty power supply, and the RF-3238 continuous duty blower kit. The transceiver, power supply, and blower are rack mounted using the RF-3243 rack mounting kit. An RF-3252 dynamic hand microphone and an RF-3249 electret condenser desk microphone are supplied with the transceiver as standard equipment. The broadband antenna is the RF-1912, which can be connected as a high-radiation angle dipole or as a top-loaded vertical antenna. Alternative antennas are the RF-1940 antenna, which can be configured as a dipole or long wire antenna, a whip antenna up to 35 ft (10.7 m) in length, or a log-periodic antenna.

The RF-3200 transceiver has a power output of 125 W average, using the RF-3238 blower for thermal protection. The RF-3200 transmits from 1.6 to 30 MHz and receives from 0.5 to 30 MHz in 10-Hz steps. According to the manufacturer, the transmitter linear power amplifier (LPA) is fully protected from impedance mismatch, including open or shorted antenna conditions, and from thermal overload. The receiver has 30 V<sub>rms</sub> overload protection. The RF-3200 has diagnostic fault detection capability for excessive forward power, excessive reflected power, excessive voltage standing-wave ratio (VSWR), over-temperature, and antenna coupler fault conditions.

The RF-382-01 or RF-3282 antenna coupler automatically matches the transceiver 50- $\Omega$  rf input/output (I/O) to a variety of antenna types over the 0.5- to 30-MHz frequency range. The antenna coupler allows continuous operation at 125 W average power. The RF-382-01 coupler can be located up to 250 ft (76.2 m) from the transceiver; however, the RF-3282 coupler requires an rf coaxial cable no longer than 150 ft (45.7 m). Coupler tuning is fully automatic, either from memory or by an initial learning sequence. The antenna coupler will automatically cut-back or bypass the antenna I/O on over-temperature, over-voltage, or excessive VSWR fault conditions.

The broadband antenna could be the RF-1940 portable antenna kit, which consists of a 30-ft (9.1-m) coaxial cable (roughly 7-m RG-59B/U-supplied), a dipole adapter, two 23-m-long wires, each with storage spools and 70 ft (21.3 m) of cord with throw weights. The wire sections can be quickly deployed as a dipole or long wire antenna. The transceiver could also be deployed with a 9- to 35-ft (0.9- to 10.7-m) whip antenna or the RF-1912 high-radiation angle dipole; however, the worst-case transient stress is obtained with the 46-m center-fed dipole antenna (see sect. 3.2.1).

### 3. Pre-Test Analysis

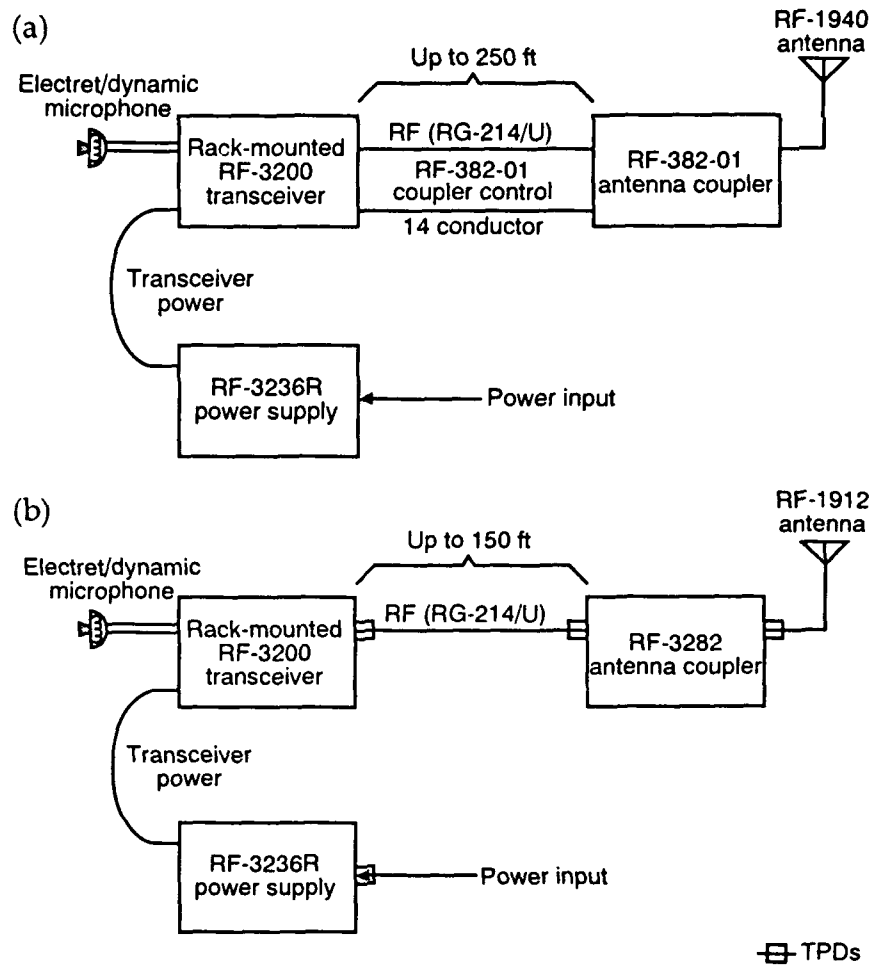
The first step in the HEMP S/V assessment process is the identification of all possible vulnerable elements of the system. Figures 1(a) and 1(b) show a typical deployment configuration for the unhardened and hardened RF-3200 transceiver systems, respectively. The test article consists of the following subassemblies:

- (1) RF-3200 transceiver,
- (2) RF-3236R continuous duty power supply,
- (3) RF-382-01 or RF-3282 antenna coupler,
- (4) RF-1940 or RF-1912 antenna kit,
- (5) RF-3252 or RF-3249 microphone, and
- (6) the associated cables.

This equipment complement is considered to be representative of the fielded transceiver system. Variations to the system include the antenna, the antenna coupler, and the microphone. The hardened system uses the RF-3282 antenna coupler rather than the RF-382-01 coupler. External TPDs are installed at each end of the rf line, at the coupler antenna I/O, and on the transceiver power input as shown in figure 1(b). The transceiver would normally be fielded in unshielded office buildings so that it would be exposed to nearly the full threat-level HEMP environment.

After the identification of the system elements, the next step is to eliminate those elements which are not mission essential. The transceiver could operate at a single frequency without an antenna coupler, into a broadband antenna or possibly without other system options; however, in this effort all system elements described above are considered mission essential. Upset criteria for this system have not been developed, so that a HEMP-induced failure of any system element

Figure 1. Typical configuration for the (a) unhardened RF-3200 system and (b) hardened RF-3200 system.



would determine the HEMP S/V of the entire system. It is important to note that landline communications are not considered part of the possible deployment configurations. The transceiver rear panel connector (A7J3) for ancillary equipment, such as computer terminals or modems, is not included in the S/V assessment, but should be addressed if it is used in the fielded transceiver system.

Some devices or subassemblies—cables and antennas as well as dipole adapter and antenna feed line—are normally considered inherently hard to HEMP effects. Any arcing that may occur due to the large HEMP-induced voltages would reduce the HEMP stress at the coupler antenna I/O. The HEMP-induced effects on the microphones are small, due to the small size of the microphones, so that the microphones can be considered inherently hard. The potentially vulnerable system elements can be reduced to the RF-3200 transceiver, the RF-3236R power supply, and the antenna coupler(s). The HEMP effects on these system elements include both direct field coupling and conducted interference on the electrical connections.

### 3.1 Electrical Connections

The RF-3200 transceiver has electrical connections only on the front and rear panels. Table 1 lists the electrical connections to the transceiver and the interconnect diagram is shown in figure 2 [3]. The front and rear panel views of the transceiver are shown in figures 3 and 4, respectively. The front panel headphone jack is included in table 1, but is not considered essential (and headphones were not supplied), so headphones were not used in the simulation tests or addressed in the S/V assessment. The rear panel connections, showing pin designations, are presented in figure 4. The rear panel accessory power connector, cw key, and accessory connector are included in table 1 and in figure 4, but were not connected in the test article or considered in the assessment process. For elements that are not considered in this assessment, the effect on the HEMP S/V would have to be addressed if those elements were used in the fielded system.

Table 1. RF-3200 Electrical Connections

Connector designator	Pin No.	Signal description	Connector location	Approximate length of associated cables
A2J3 (headset)	Phone jack	Headphone audio	Front panel	Not supplied
	1	Condenser mic		
	2	Mic A+		
	3	Handset sense		
A2J2 (microphone)	4	Earphone (+)	Front panel	1.5 ft coiled (roughly 3 ft total)
	5	Push to talk (+)		
	6	Push to talk (-)		
	7	Audio ground		
	8	Dynamic mic		
A7J9 (cw key)	cw jack	Optional cw key	Rear panel	Not supplied
A7J3 (accessory connector)	See fig. 5	Optional	Rear panel	Not supplied
ASW1 (antenna connector)	Type N	rf receive/transmit	Rear panel	Up to 250 ft RG-213/U 30 ft RG-58A/U supplied
ASA2 (dc power cable from RF-3236R)	1	13.6-Vdc power	Rear panel	5 ft coiled
	2	ground	(see fig. 5)	(inside rack)
P2 (accessory power switch connector)	P2-1 P2-2	13.6-Vdc power ground	Rear panel (see fig. 5)	Not used
Coupler power/control cable	See table 2	Multiconductor power/control cable	Rear panel (see fig. 5)	Up to 250 ft custom-built 100 ft supplied
Ground connection	Ground lug	Safety ground	Rear panel	Less than 10 in.

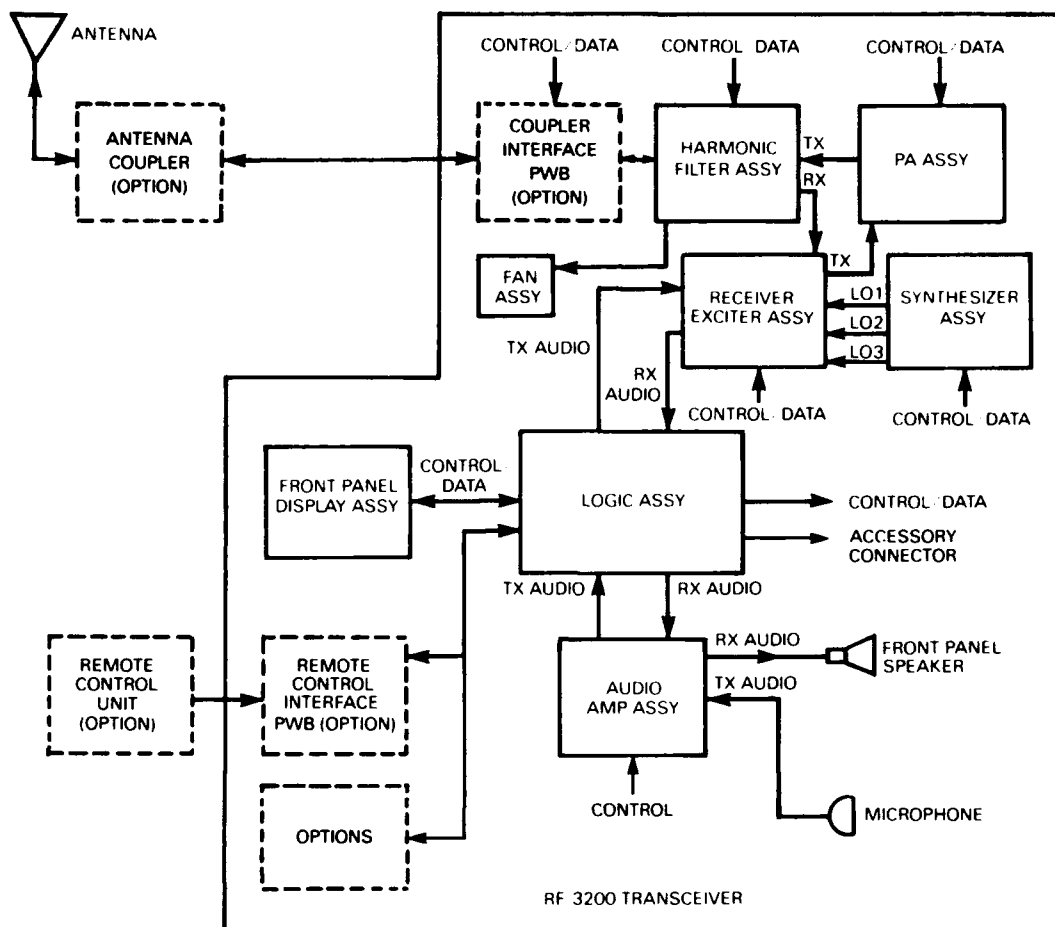


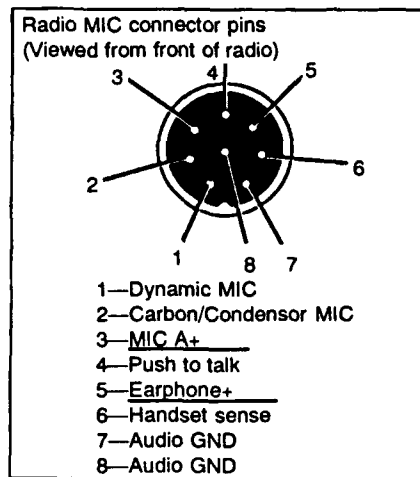
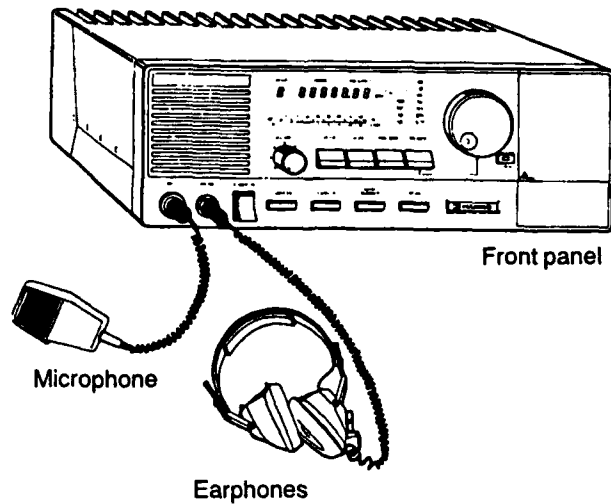
Figure 2. RF-3200 interconnect diagram.

The RF-382-01 antenna coupler has an rf transceiver connection (J1) and an rf antenna connection (J2) as described in table 2. This antenna coupler requires a separate power/control cable from the transceiver (J3) (see fig. 1(a)). Note that the RF-3282 antenna coupler has the same connections except that it uses only one multiplexed coaxial line (J1) for power, control, and communication (see fig. 1(b)). The RF-3236R power supply has an ac power input from the commercial power service and a permanently attached dc power output cable, as described in table 1.

### 3.2 HEMP Coupling Analysis

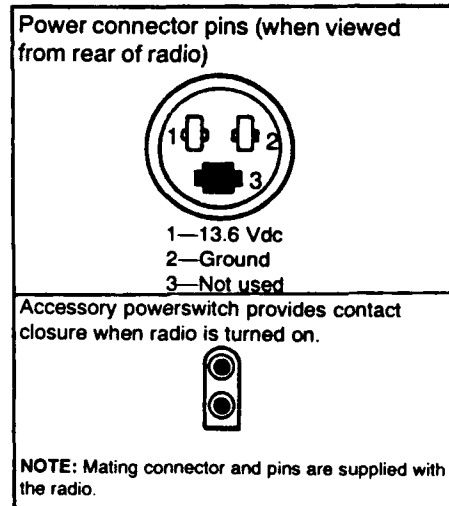
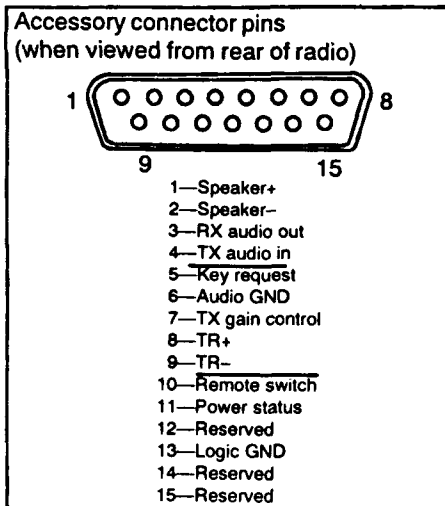
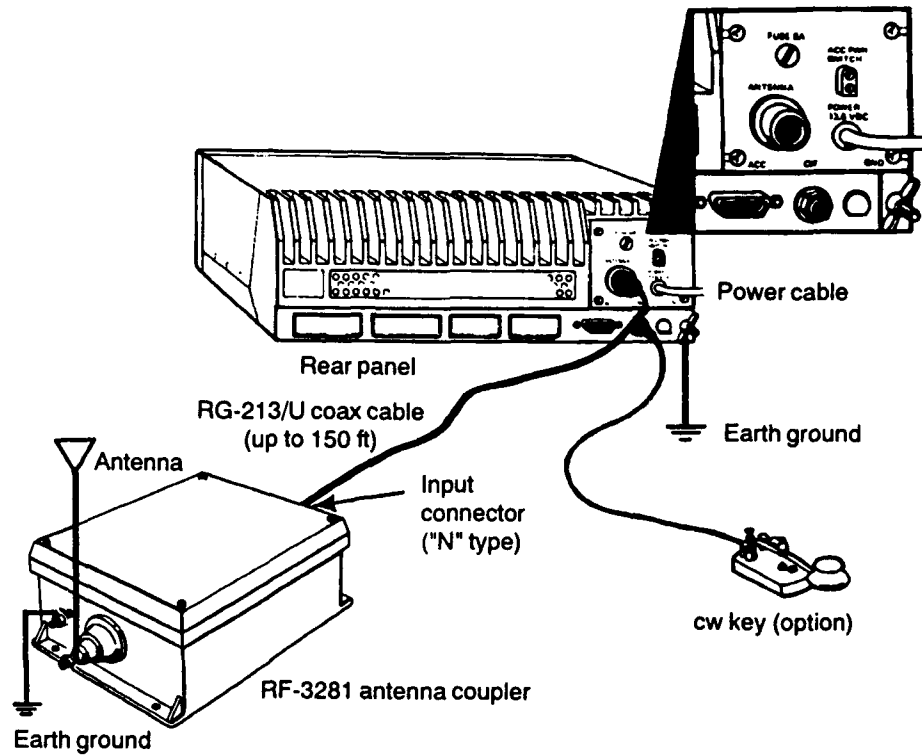
The RF-3200 transceiver is fairly well defined in terms of the possible coupling paths to interface circuits for a typical deployment configuration. The system is assumed to be deployed so that it would be exposed to nearly the full threat-level HEMP environment, as specified in the E1 component of DoD-STD-2169A. The coupling paths to the RF-3200 interface and internal circuits include direct field coupling and HEMP-induced transients on the dc power, microphone,

Figure 3. RF-3200 front panel view.



ground, and coupler connection(s). The possible coupling paths to the RF-3236R power supply interface and internal circuits include direct field coupling and HEMP-induced transients on the commercial power service and dc power cable. The possible coupling paths to the antenna coupler(s) interface and internal circuits include direct field coupling and HEMP-induced transients on the antenna, ground, and transceiver connection(s). HEMP coupling to ground straps and connections does not typically involve sensitive circuitry and is normally important only for safety considerations. The various ground connections are required for proper operation, so they are assumed to be electrically bonded and are not considered in the coupling analysis, but are monitored during simulation testing. Direct field coupling to internal circuits is estimated based on the worst-case coupling to the largest loop of wire that could be contained in a given enclosure.

Figure 4. RF-3200 rear panel connections.



An hf transceiver was previously tested under the Army NDI hardening guidelines program [4]. A Harris RF-350K transceiver system was chosen as a typical NDI to which general hardening guidelines were applied before CI testing. The results of this previous effort, in some cases, are directly applicable to the HEMPS/V assessment of the RF-3200 system. Information from previous tests or analyses that is applicable to the RF-3200 system is included as appropriate.

**Table 2. RF-382-01 Electrical Connections**

Connector designator	Pin No.	Signal description	Connector location	Approximate length of associated cables
J1 (rf LPA)	Type N	rf I/O to transceiver	Rear panel	Up to 250 ft RG-213/U 30 ft RG-58A/U supplied
J2 (rf antenna)	Lug nut	rf I/O to antenna	Front panel	20 ft RG-59B/U supplied
	A	Not connected		
	B	Not connected		
	C	Not connected		
	D	Ground		
	E	Operational status		
	F	+13.6-Vdc power		Up to 250 ft custom-built cable
J3 (power/control)	G	Key disable		
	H	Keyline	Rear panel	
	I	Not connected		100 ft supplied (14 pin)
	J	Tune power request		
	K	Retune		
	L	+13.6-Vdc power		
	M	Coupler bypass		
	N	Ground		
Ground connection	Ground lug	Safety ground	Front panel	Less than 10 in.

The HEMP coupling analysis is based on worst-case models of individual coupling paths. Synergistic and nonlinear effects are best determined through HEMP simulation testing. The coupling models used include monopole, dipole, and loop antennas, transmission lines, and transfer impedance models to calculate the coupling through braided cable shields. This section calculates the HEMP-induced stress at the various system interfaces under worst-case conditions. Section 3.3 addresses the existing internal transient protection in the test article subassemblies. The conclusions that can be drawn for the inherent hardness of the unhardened RF-3200 system are presented in section 3.4.

### 3.2.1 Antenna Coupling Analysis

The primary operational configuration chosen for the RF-3200 system is based on the worst-case HEMP-induced stress. The 46-m center-fed dipole antenna response, elevated high enough over ground to be considered in free-space, represents the maximum coupling configuration of the possible deployment configurations. When configured as a long wire antenna (or with the other antenna options) and exposed to the corresponding worst-case HEMP threat, the wire length is not sufficient to develop a larger HEMP-induced

stress than in the RF-1940 dipole deployment configuration. The worst-case coupling configuration is thus taken to be a 46-m centered dipole in free-space, illuminated by a horizontally polarized E-field which has a DE or an FDE waveform and a peak amplitude of 50 kV/m, and is incident from overhead. The HEMP S/V of other operational configurations are addressed based on the assessment results for the primary configuration.

The RF-1940 dipole plane wave impulse response was obtained with the Numerical Electromagnetics Code (NEC) and represents a highly accurate calculation of the antenna short-circuit current ( $I_{sc}$ ) in the frequency domain [5]. The  $I_{sc}$  impulse response is combined with the incident HEMP E-field spectrum, to obtain the HEMP-induced transient response through Fourier inversion. The HEMP-induced  $I_{sc}$  at the center of the RF-1940 antenna (located in free-space) is shown in figure 5. The peak current is roughly 2300 A and the resonant frequency is 3 MHz. For a 35-ft (10.7-m) monopole antenna, the HEMP-induced  $I_{sc}$  has a peak amplitude of about 2000 A with a resonant frequency of 7 MHz.

The HEMP-induced current for the RF-1912 dipole antenna is also calculated using the NEC. This antenna is mast mounted at a height of 30 ft (10.7 m) and is configured as a high-radiation-angle dipole as shown in figure 6(a). The HEMP-induced  $I_{sc}$  at the center of the antenna (located in free-space) is shown in figure 6(b) for horizontal polarization and overhead incidence. The peak  $I_{sc}$  is roughly 900 A, with a resonant frequency of about 6 MHz. The radiation pattern of

Figure 5. HEMP response of a 46-m free-space dipole.

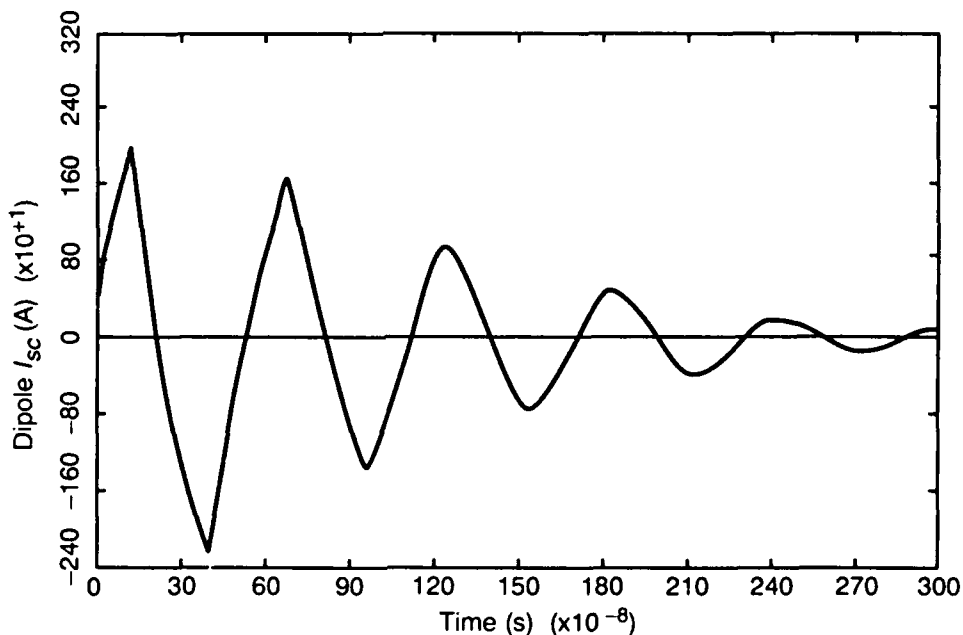
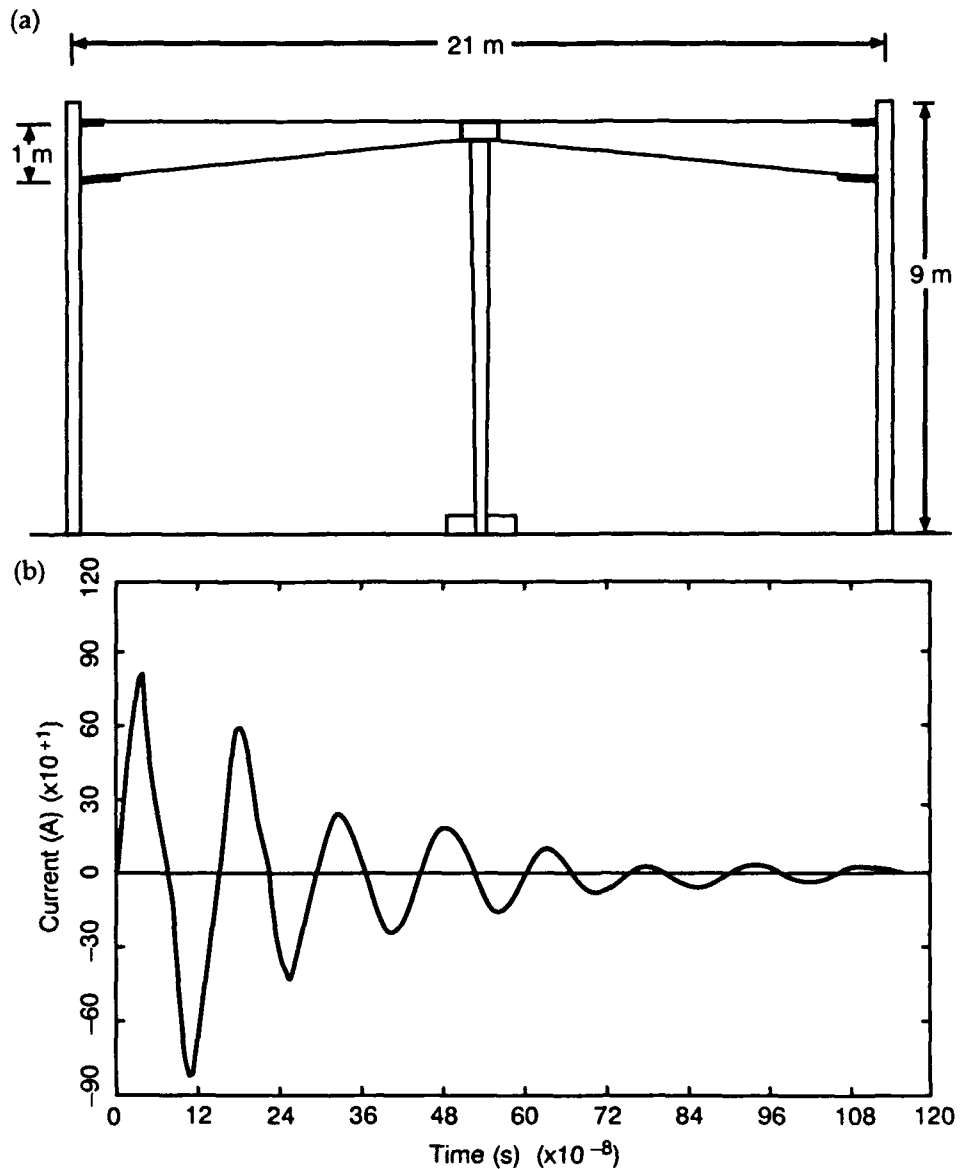


Figure 6. RF-1912 free-space antenna: (a) typical configuration and (b) HEMP induced response.

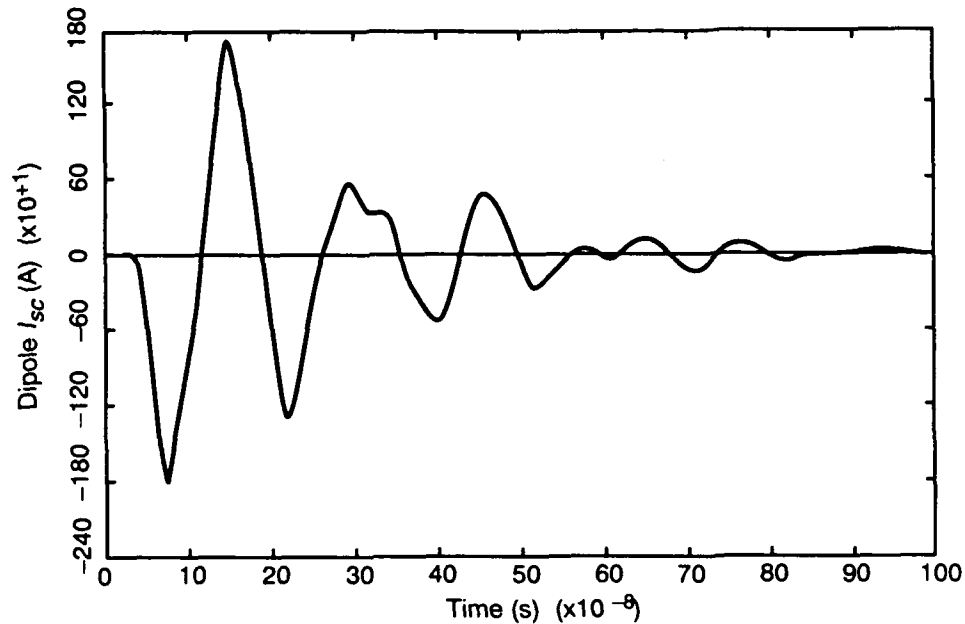


this antenna is enhanced at high-radiation angles when operated over a good ground plane. This is shown in figure 7 where the peak  $I_{sc}$  for an antenna height of 10 m is about 1800 A for a ground conductivity of 0.02 mhos/m and a relative permittivity of 15.

The corresponding open-circuit voltage waveform,  $V_{oc}(t)$ , is determined in the frequency domain from the antenna impedance. The peak  $V_{oc}$  can be approximated as  $E_0 h$  where  $E_0$  is the peak E-field amplitude along the antenna and  $h$  is the dipole half length. The peak load current ( $I_L$ ) is related to the peak  $I_{sc}$  through

$$I_L = I_{sc} Z_A / (Z_A + Z_L), \quad (1)$$

Figure 7. HEMP-induced response of the RF-1912 antenna at a height of 10 m.



where  $Z_A$  is the antenna impedance and  $Z_L$  is the antenna load impedance. Under matched conditions, then, the transient stress at the antenna coupler is  $I_{sc}/2$ ; however, the calculated  $I_{sc}$  represents an upper limit to the HEMP-induced stress and is a good approximation in the case of a dipole with a  $50\text{-}\Omega$  load.

The HEMP-induced transient response for the RF-1940 dipole, located at a height of 2 m over a lossy ground plane, is shown in figure 8. The ground plane is characterized by a conductivity of  $0.01\text{ mhos/m}$  and a relative permittivity of 15, which represents typical moist soil. As can be seen in the figure, the proximity of the ground plane serves to modify the antenna impedance and resonance characteristics and results in a peak  $I_{sc}$  of less than 900 A. Ground parameter variations are not investigated since the manufacturer recommends the RF-1940 antenna be deployed as far above the ground plane as possible to optimize the transceiver performance. For the purposes of the HEMP S/V assessment, the ground proximity effects are neglected so that system survivability to the worst-case HEMP-induced transient implies survivability for all other deployment configurations. Thus the RF-1940 dipole antenna, located high enough over the ground plane to be considered in freespace, represents the worst-case system deployment configuration for HEMP coupling.

The free-space RF-1940 dipole frequency domain response is shown in figure 9 for both the Bell Laboratories DE and an FDE pulse. The FDE pulse is obtained by increasing the DE pulse exponential risetime and

Figure 8. HEMP response of a 46-m dipole at a height of 2 m.

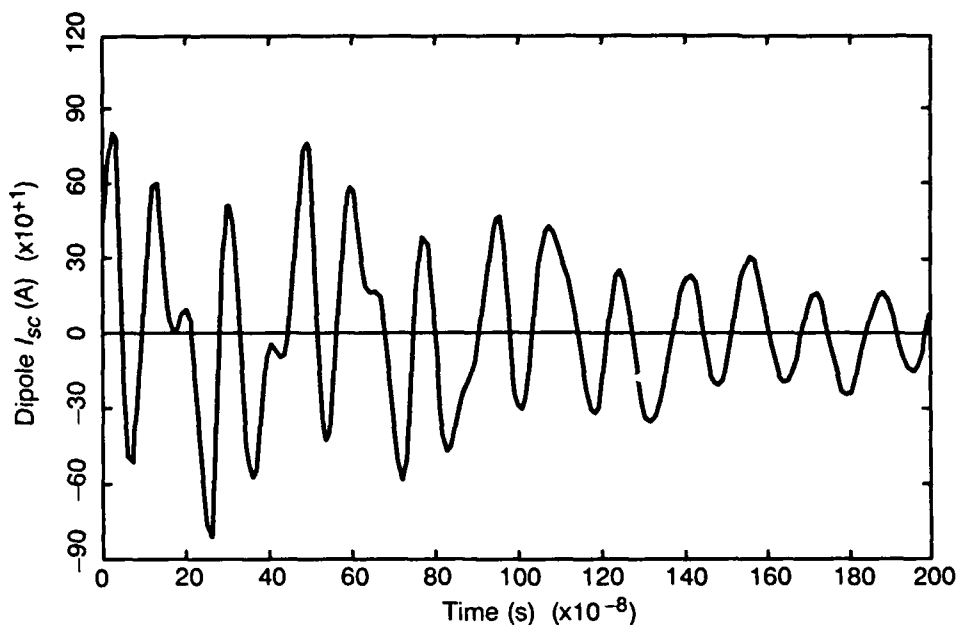
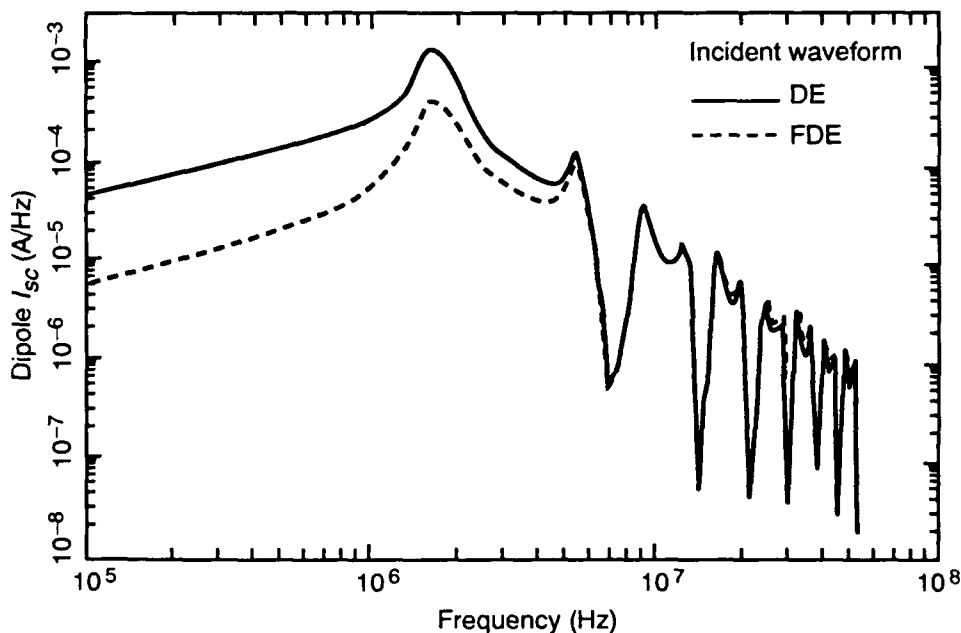
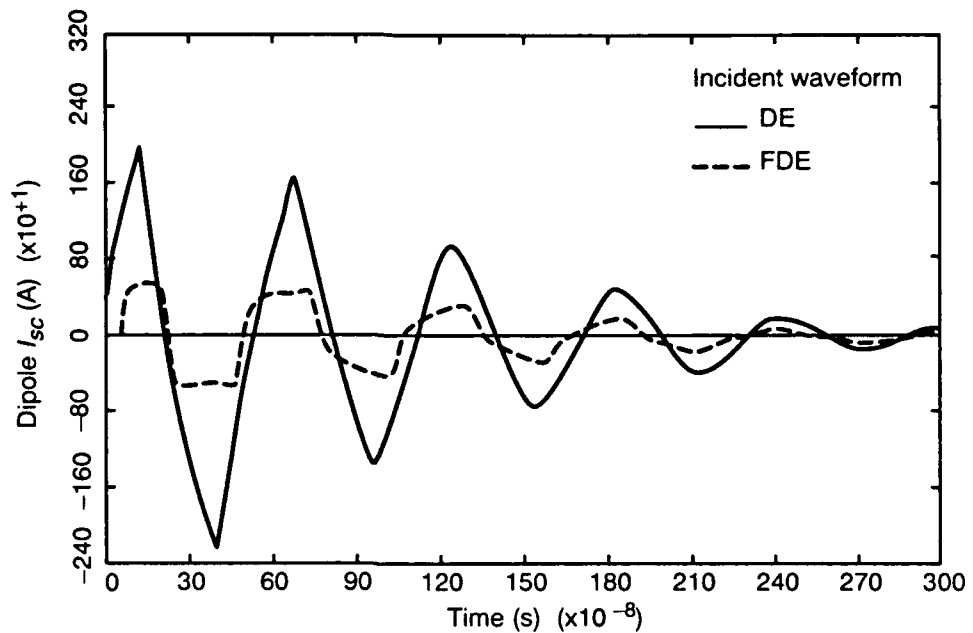


Figure 9. Free-space dipole spectral response comparison for DE and FDE incident pulses.



falltime parameters an order of magnitude. In the time domain the FDE pulse approximates the E1 waveform. As can be seen in the figure, the FDE has less low-frequency energy content but more hf energy content compared to the DE. The corresponding transient response is shown in figure 10 (the FDE response has been shifted in time), which implies that the FDE pulse is a less severe threat for this antenna deployment configuration. Similar conclusions would result for the RF-1912 antenna illuminated by an FDE pulse waveform.

Figure 10. Free-space dipole transient response comparison for DE and FDE incident pulses.



The FDE pulse could be a more severe threat for other deployment configurations or antennas (such as a 1-m whip antenna) compared to the DE pulse, but the maximum HEMP-induced peak transient is still given by figure 5. Similar conclusions would result for the E1 threat waveform; however, a faster risetime HEMP-induced transient could affect the operation of the surge protection circuits. The TPD clamping voltage increases proportional to the risetime of the stress waveform; however, the FDE pulse results in a significantly smaller HEMP-induced amplitude. For practical purposes, then, the E1 threat waveform represents a less severe stress to sensitive circuits but could lead to higher frequencies being coupled to these circuits. In those cases where this difference in frequency content can be neglected, survivability to the DE threat implies a high confidence in survivability to the DoD-STD-2169A E1 threat waveform.

### 3.2.2 Cable HEMP Coupling Analysis

The cables to be considered for the HEMP coupling analysis are the cable(s) between the transceiver and antenna coupler and the microphone cable. The antenna coupler is located close to the antenna, whereas the transceiver can be located up to 76 m away and connected by an RG-213/U coaxial cable (10-m RG-58A/U supplied). The RF-382-01 antenna coupler also uses a 14-conductor power/control cable (roughly 46 m supplied) which has a metal foil overall shield. The HEMP coupling to the antenna feedline (recommended to be as short as possible) is neglected since it is small compared to the HEMP-

induced antenna response. The cable deployment could be arbitrary, but the configurations considered are horizontal cables deployed near the ground.

A vertically polarized E-field, incident at a 22-degree elevation angle, on a 76-m horizontally oriented cable (modeled as a transmission line at a height of 0.1 m), would induce a cable shield current less than that for horizontal polarization. The case of a vertically polarized incident HEMP is neglected and the cables are considered to be oriented horizontally over a real earth. The soil conductivity, which would maximize the HEMP coupling and still represent typical moist soil, is considered to be  $10^{-3}$  mhos/m. The induced transient owing to an E1 threat waveform would be lower than that of the DE waveform since the cable response is proportional to the incident pulse width.

The microphone cable is modeled as a monopole antenna (since the cable shield is shorted to the transceiver) of length  $h = 1$  m, which corresponds to a resonant frequency of about 80 MHz. The HEMP-induced open-circuit voltage can be readily calculated from the incident field amplitude,  $E_0$ , as

$$V_{oc,HEMP} = E_0 h / 2 = 25 \text{ kV}. \quad (2)$$

For a wire radius of 2 mm, the source impedance of the induced transient pulse is  $626 \Omega$ , which leads to a short-circuit current of 40 A. The microphone cable is shielded but the shield parameters are not known, so we take the current attenuation at 80 MHz to be a factor of two for a worst-case coupling analysis. The peak cable shield current,  $I_s$ , is the HEMP-induced short-circuit current. This current is assumed to be attenuated by 6 dB in passing through the cable shield and appears as a bulk cable current. The HEMP-induced bulk current peak amplitude is then 20 A, which divides among the internal conductors. The HEMP-induced wire current for multiconductor cables is discussed in detail in the *Braided Shield Cables* section.

*Cables Lying on the Ground.* According to Vance [6], the HEMP-induced cable shield current, for cables lying on or near the ground, can be calculated according to:

$$I(t) = 10^6 (\epsilon_0 \epsilon_f / \sigma)^{1/2} E_0 D_H \exp(-t/t_f) \frac{2}{\sqrt{\pi}} \int_0^{\sqrt{t/t_f}} \exp(u^2) du, \quad (3)$$

where

$$\epsilon_0 = 8.85 \times 10^{-12} \text{ F/m},$$

$$\sigma = 10^{-3} \text{ mhos/m, and}$$

$$D_H = 1 \text{ for worst-case horizontally polarized illumination.}$$

For worst-case coupling, the incident E-field is taken to be a single-exponential pulse, horizontally polarized, with peak amplitude  $E_0 = 50$  kV/m and an exponential falltime,  $t_f = 250$  ns. The peak cable shield current is then

$$I_p = 6.1 \times 10^5 E_0 (\epsilon_0 t_f / \sigma)^{1/2} = 1434 \text{ A} \quad (4)$$

and its time of occurrence is  $t_p = 0.85 t_f = 213$  ns. For an FDE pulse,  $t_f = 25$  ns so that  $I_p = 453$  A and its time of occurrence is  $t_p = 21$  ns. The calculated HEMP-induced transient is applicable to cables longer than the critical line length or cables shorted to the soil at both ends. The peak current will be obtained for bare cables of length greater than the critical line length,  $L_c$ , where

$$L_c = 10^9 (\epsilon_0 t_f / \sigma)^{1/2} = 47 \text{ m} , \quad (5)$$

and for insulated cables of length

$$L_c > 5 \times 10^8 t_f [10 k \ln(b/a)]^{1/2} \quad (6)$$

where  $a$  = conductor radius,  $b$  = insulation radius, and  $k$  = insulation dielectric constant. For RG-213/U cable and dielectric jacket parameters, the 76-m cables under consideration will not develop the full peak current as calculated in equation (4), since  $L_c = 86$  m; however, the cable shield is effectively shorted to the soil at both ends through the equipment ground connections.

The worst-case HEMP-induced current pulse with peak amplitude,  $I_p$ , can be approximated by a DE waveform as follows

$$I_{sc}(t) = I_0 (e^{-bt} - e^{-at}), \quad (7)$$

with parameters

$$b = 4 \times 10^6 \text{ s}^{-1},$$

$$a = 2 \times 10^7 \text{ s}^{-1}, \text{ and}$$

$$I_0 = 2690 \text{ A} = 1.876 I_p.$$

The energy content of this pulse can be found by integrating the pulse power over time. A typical characteristic (surge) impedance,  $Z_0$ , for small cable heights over a lossy ground plane, is  $100 \Omega$ , which implies  $V_{oc,HEMP} = 140$  kV. To calculate the pulse energy content, integrate over all time, so

$$W = \int_0^{\infty} I_{sc}(t)^2 Z_0 dt = 2.35 \times 10^{-7} I_p^2 Z_0 J, \quad (8)$$

which leads to a HEMP-induced energy content of about 48 J.

**Braided Shield Cables.** The coupling of the HEMP-induced current on the cable shield to the cable inner conductors can be determined if the shield transfer impedance is known. Typical braided shield parameters are used to estimate the worst-case internal cable current. For multiconductor cables, an internal bulk cable current,  $I_B$ , is calculated and assumed to divide among the individual conductors. Based on the number of conductors and the termination impedances, a wire current,  $I_w$ , is calculated which represents the HEMP-induced individual pin currents.

The braided shield cable transfer impedance can be written as

$$Z_T = Z_d + j\omega M_{12}, \quad (9)$$

where  $Z_d$  represents diffusion of electromagnetic energy through the metal, based on the braided shield dc resistance per unit length,  $R_0$ . The second term is based on a mutual inductance,  $M_{12}$ , which represents penetration of the magnetic (H-) field through elliptical holes in the cable shield.

For RG-213/U cables,  $R_0 = 4.0 \text{ m}\Omega/\text{m}$  and  $M_{12} = 0.25 \text{ nH}/\text{m}$ . For RG-58A/U cables,  $R_0 = 13.7 \text{ m}\Omega/\text{m}$  and  $M_{12} = 0.53 \text{ nH}/\text{m}$  [6]. The power/control cable for the RF-382-01 coupler has a metal foil shield and is assumed to be characterized by the same parameters as RG-213/U. In the interest of presenting a concise HEMP coupling analysis, the bulk cable current is calculated at a discrete frequency so that the HEMP-induced stress is approximated by a damped sinusoid with a peak amplitude determined by the cable shield transfer impedance at this frequency. The resonant frequency associated with these cables corresponds to poor shield terminations (i.e., poor connector backshell conditions) and is calculated according to the resonant frequency of a dipole antenna of length,  $L$ , as

$$f = c/2L = 3 \times 10^8/2(76) \approx 2 \text{ MHz}. \quad (10)$$

This is probably representative of the RF-382-01 power/control cable, since the cable shield is not terminated at the transceiver and is pigtailed to the ground pin at the coupler connection. The dipole resonant frequency is not completely realistic for coaxial cable backshells, but is typically a better approximation than a monopole resonant frequency (i.e., 1 MHz). This results in a worst-case coupling

calculation since the induced current and voltage are directly proportional to the cable transfer impedance at the resonant frequency.

The inner conductor response depends on the transfer impedance and the internal cable termination impedances  $Z_1$  and  $Z_2$ . For 50- $\Omega$  coaxial cables,  $Z_1 + Z_2 = 100 \Omega$ . At 2 MHz the cable transfer impedance is 5.1 and 15 m $\Omega$ /m for RG-213/U and RG-58A/U, respectively. The open circuit voltage,  $V_{oc}$ , developed between the inner conductor and shield is

$$V_{oc} = I_{sc} Z_T L . \quad (11)$$

The HEMP-induced bulk current on the inner conductor is given by

$$I_B = I_{sc} Z_T L / (Z_1 + Z_2) . \quad (12)$$

For RG-58A/U, the magnitude of  $V_{oc}$  at 2 MHz is about 1635 V, and for RG-213/U, about 556 V. Thus for RG-58A/U,  $I_B \approx 16$  A, and for RG-213/U,  $I_B \approx 5.5$  A, with a 100- $\Omega$  source impedance.

For multiconductor cables the bulk cable core current is given by

$$I_B = V_{oc} / Z \quad (13)$$

where  $Z$  is a source impedance for multiconductor cables. A typical source impedance value estimated for multiconductor cables is a resistance of 100  $\Omega$  [7]. Under these approximations, the bulk cable core current on the RF-382-01 power/control cable is also 5.5 A. Below about 1 MHz, the bulk cable core current will be distributed among the  $N$  multiconductors according to the termination impedances at the interfaces. At higher frequencies, the bulk cable core current will be approximately equally distributed among the 14 conductors as follows (for  $N > 4$ ):

$$I_w^i = I_B (N)^{-1/2} = 5.5 / 3.74 = 1.5 \text{ A} , \quad (14)$$

where the superscript  $i$  denotes the individual conductor under consideration. The open-circuit voltage is 556 V as before, which implies a source impedance of 371  $\Omega$ . For  $N < 4$ , the worst-case wire current is taken to be  $I_B / 2$ . Thus for the coaxial cables, the HEMP-induced wire current is 8 A for RG-58A/U and is 2.75 A for RG-213/U. The wire current must be constrained to the common mode voltage,  $V_{oc}$ , as follows:

$$I_w^i < V_{oc} / R^i , \quad (15)$$

where  $R^i$  represents the wire termination resistance. It is important to

note that the multiconductor wire currents are common mode currents. Bipolar electronic circuits are vulnerable to differential mode currents so that a common mode to differential mode conversion factor is required. A conversion factor of 20 dB is a reasonable assumption for most well-balanced lines, which implies a differential mode current of about 0.15 A.

*Cable Connectors.* The coupling of the induced shield current to the inner conductors through the cable connectors is also caused by a transfer impedance. The cable connector transfer impedance comprises a dc resistance and a mutual inductance. For typical coaxial and multipin connectors, the transfer impedance mutual inductance values are orders of magnitude smaller than that associated with the cable shield, whereas the dc resistance is on the same order as the cable shield resistance. For the cable shields and connectors used in this system, the high-frequency coupling associated with connector leakage can be neglected compared to the leakage through the cable shield, except for the RF-382-01 coupler power/control cable. This cable has a metal foil overall shield, which is pigtailed to the ground pin at the coupler so that the connector and cable assembly would not provide a high degree of electromagnetic shielding. Hf coupling effects associated with the E1 pulse would be more prominent for this cable assembly than for typical coaxial cable connectors.

### 3.2.3 *HEMP Coupling to Internal Circuits*

The worst-case HEMP coupling to internal wires is based on the maximum coupling to the largest loop of wire that could fit inside a given enclosure. The internal coupling considered here includes the 13.6-V<sub>dc</sub> two-conductor power cable from the RF-3236R power supply to the transceiver, and hypothetical wire loops inside the power supply and transceiver enclosures. The 13.6-V<sub>dc</sub> power cable could be formed into a loop with a maximum area,  $A$ , of about 0.3 m<sup>2</sup>. The ac and dc power cables inside the rack are coiled and fastened to the rack with cable ties, which would later be cut to length during installation. This would be the recommended practice along with the avoidance of creating wire loops. HEMP coupling to the ac power cable within the rack is not calculated (but is monitored during simulation testing) since the HEMP-induced transient on the commercial power service is the worst-case stress to the power supply. Wire loops that could be formed within the transceiver and power supply enclosures would have a maximum area of about 0.07 m<sup>2</sup>.

Internal wires can collect HEMP energy and, if connected to sensitive circuits, can represent a viable coupling path to these internal circuits. Since the rack or enclosures are not an electromagnetic shielded

design, it is difficult to establish a shielding effectiveness (SE) for the enclosures. For worst-case coupling calculations, the threat-level incident HEMP amplitude is used for coupling inside the rack; however, the electronic enclosures and the rack combined could reasonably be expected to provide some attenuation of the peak field amplitude. For field-to-wire coupling inside the electronic enclosures, the peak field amplitude is assumed to be attenuated by 20 dB.

A loop antenna is resonant when the loop circumference is a full wavelength, so that the dc power cable would collect HEMP energy around 150 MHz and wire loops inside the equipment enclosures would be resonant around 300 MHz. The loop antenna impedance,  $Z$ , at resonance is primarily inductive so that the peak  $I_{sc}$  can be calculated directly. The peak  $I_{sc}$  induced in a loop antenna with inductance,  $L_A$ , can be calculated according to

$$I_{sc} = V_{oc}/Z = \mu AH/L_A , \quad (16)$$

where  $\mu$  is the permeability of free space (i.e.,  $12.57 \times 10^{-7}$  H/m) and  $H$  is the incident H-field normal to the loop. The incident H-field is assumed to be uniform over the loop area and to have a peak value of 133 A/m inside the rack and 13.3 A/m inside the electronic enclosures.

For the two-conductor dc power cable, the total wire radius is about 0.005 m, which could be formed in a loop of radius 0.3 m. This leads to a loop inductance of  $1.6 \times 10^{-6}$  H and a source impedance of 1500  $\Omega$  at 150 MHz. The HEMP-induced bulk cable current then has a peak value of 31 A and a damped sinusoid waveform. The worst-case wire current is taken to be a 150-MHz damped sinusoid with a peak value of 16 A and a peak HEMP-induced open-circuit voltage,  $V_{oc,HEMP} = 23$  kV. For short cables, a typical damping coefficient,  $Q$ , is about 24, so the pulse will decay to 50 percent of the peak amplitude in six cycles. Integrated over ten cycles, the corresponding energy content is about 0.1 J. The HEMP-induced load voltage would be much smaller for a typical load impedance. The corresponding energy content would be much smaller than the square pulse failure power of even the most sensitive circuits; however, device failure would depend on the actual HEMP stress waveform delivered to these circuits.

For hypothetical wire loops inside the electronic enclosures the wire radius is taken to be 0.005 m, which could be formed in a loop of radius 0.15 m. This leads to a loop inductance of  $4.5 \times 10^{-7}$  H and a source impedance of 848  $\Omega$  at 300 MHz. The HEMP-induced worst-case wire current is thus calculated to be a 300-MHz damped sinusoid with a peak value of 2.6 A and a peak  $V_{oc,HEMP} = 2.2$  kV. Inside the electronic

enclosure the HEMP-induced energy content (integrated over ten cycles) can be calculated to be about 0.8 mJ.

These transients are representative of the direct field coupling which could result under worst-case conditions. The HEMP-induced energy for this coupling mechanism may not be negligible; however, the power which could be delivered to internal circuits is small compared to typical device damage power levels. The analysis indicates the HEMP survivability of the transceiver system due only to direct-field coupling, which is verified during the threat-level PI tests, based on the system functional response.

### 3.2.4 Circuit Survivability Analysis

The Wunsch junction heating model [8] is based on empirical data and results in a thermal threshold which leads to a failure power,  $P_f$ , for device failure. The power for junction failure of semiconductor devices is dependent on the applied pulse duration and an empirically determined damage constant. For pulse widths from 100 ns to 1 ms, the failure power can be estimated according to

$$P_f = Kt^{-1/2} \text{ (in watts) ,} \quad (17)$$

where

$t$  = rectangular pulse width in seconds, and

$K$  = empirical damage constant.

A more general form of this equation is

$$P_f = At^{-B} \text{ (in watts) ,} \quad (18)$$

where  $A$  and  $B$  are both determined empirically. For semiconductor devices this power is dissipated according to

$$P_f = I_f V_{BD} + I_f^2 R_s \text{ (in watts) ,} \quad (19)$$

where

$I_f$  = junction failure current,

$V_{BD}$  = junction breakdown voltage, and

$R_s$  = surge resistance.

The failure current and voltage for a given semiconductor device can thus be calculated according to

$$I_f = \left[ -V_{BD} + (V_{BD}^2 + 4R_s P_f)^{1/2} \right] / 2R_s, \text{ and} \quad (20)$$

$$V_f = V_{BD} + I_f R_s. \quad (21)$$

The empirical damage data are based on rectangular pulses; however, HEMP-induced transients are usually damped sinusoids with a resonant frequency,  $f_r$ , and damping coefficient,  $Q$ , which are specific to individual coupling paths. A rectangular pulse to sinusoid conversion can be derived for  $Q > 8$  [9]. For a typical  $Q$  of 24, the equivalent pulse width is given by  $t = (2.57f_r)^{-1}$ . This model is applicable for square pulse widths greater than 100 ns, so that for hf transients, device failure should be based on empirical data.

To determine the inherent hardness of an interface or circuit requires knowledge of the  $I_f$  and  $V_f$ , which are propagated back through the circuit to determine the HEMP source at the circuit terminals that is required for failure. This failure current and voltage at the circuit terminals,  $I_T$  and  $V_T$ , are determined through circuit analysis and compared to the HEMP stress at the terminals. The HEMP-induced Thevenin voltage source,  $V_{oc,f}$ , required to provide a terminal voltage,  $V_T$ , is given by

$$V_{oc,f} = V_T(R_L + Z_s)/R_L, \quad (22)$$

where

$R_L$  = circuit (load) resistance and

$Z_s$  = HEMP-induced Thevenin-Norton source impedance.

The HEMP-induced Norton current source,  $I_{sc,f}$ , required to provide a terminal current,  $I_T$ , is given by

$$I_{sc,f} = I_T(R_L + Z_s)/Z_s, \quad (23)$$

where  $R_L$  and  $Z_s$  are as previously defined. For worst-case analysis purposes, the terminal currents and voltages are often taken to be equivalent to the device failure current and voltage (i.e.,  $I_T = I_f$  and  $V_T = V_f$ ).

A comparison of the Thevenin-Norton source parameters required for failure (i.e.,  $V_{oc,f}$  and  $I_{sc,f}$ ) to that determined in the HEMP coupling analysis (i.e.,  $V_{oc,HEMP}$  and  $I_{sc,HEMP}$ ) leads to a hardness margin (HM) for the circuit. The HM, in decibels, for a given circuit can be calculated by

$$HM = 20 \log(I_{sc,f}/I_{sc,HEMP}), \quad (24)$$

or by

$$HM = 20 \log(V_{oc,f}/V_{oc,HEMP}) . \quad (25)$$

The HM provides an estimate of the inherent hardness (or vulnerability) of a circuit. In those cases where the HEMP-induced Thevenin-Norton source impedance is much greater than the circuit load impedance (i.e.,  $Z_s \gg R_L$ ), the failure current simplifies to  $I_f = I_T$ , and

$$HM = 20 \log(I_T/I_{sc,HEMP}) . \quad (26)$$

In those cases where the HEMP-induced Thevenin-Norton source impedance is much less than the circuit load impedance (i.e.,  $Z_s \ll R_L$ ), the failure voltage simplifies to  $V_f = V_T$ , and

$$HM = 20 \log(V_T/V_{oc,HEMP}) . \quad (27)$$

### 3.3 Internal Transient Protection in the RF-3200

The RF-3200 transceiver has internal transient surge protection on the dc power supply input, the rf I/O connection, and when configured for the RF-382-01 coupler, at the power/control cable connection from the transceiver to the antenna coupler. The antenna couplers have surge protection at the rf I/O connector, at the antenna I/O connector, and for the RF-382-01 at the power/control cable connection. The protection at these interfaces is a combination of transZorbs, metal-oxide varistors (MOVs), rectifier diodes, and passive filtering. The available information for the transient protection capabilities in each of these areas as provided by the manufacturer, is included here for completeness.

The RF-3200 dc power input protection is afforded by two transZorbs. These two transZorbs will clamp a voltage spike on the supply line to a maximum of 32 V while shunting a total of 19 A to ground. Once clamped, passive inductor/capacitor filter networks slow the rise and fall times of the 32-V pulse and prevent damage to the radio circuits. The transceiver dc power supply input is also protected from negative voltage spikes with a rectifier diode placed across the power supply lines. This diode has the capability of handling 40 A of current and will clamp the voltage pulse to a maximum of -1 V. According to the Harris Corporation, the protection circuit has been verified to an 850-V, 40-A pulse with a rise time of 10 microseconds ( $\mu s$ ) and a fall time of 1000  $\mu s$ . The corresponding energy dissipation is calculated to be about 11 J.

The power/control cable interface to the RF-382-01 antenna coupler has transZorbs at the transceiver. The transZorbs are designed to

clamp a voltage pulse to a maximum of 59 V and are capable of handling up to 10 A of current. The components used in the transceiver rf I/O are designed to handle the voltages and currents present during normal transmission and during extreme load impedances. The voltage limit on the transceiver rf I/O is then determined by the voltage rating,  $V_{rated}$ , on the capacitors in the output filter, which is 500 V.

The power/control cable interface at the RF-382-01 antenna coupler is protected by a combination of MOVs, zener diodes, rectifier diodes, and passive filter networks. The diodes clamp a transient to a specific level, and the filter networks slow the rise and fall times of the pulse. The interface has been tested to a maximum pulse of 2500 V, 1000 A with a rise time of 1.5  $\mu$ s and a fall time of 13  $\mu$ s. The corresponding pulse energy can be calculated to be about 7 J.

The components at the antenna I/O of both the antenna couplers are designed to handle the normal operating voltages and currents of the transmitter into the extremes of impedance. The antenna I/O is also protected by a set of "arcballs" connected between the antenna coupler and ground. The arcball arrangement will protect the coupler at the antenna connector from peak spike voltages exceeding 8000 V. Based on the available information, protection at the coupler rf I/O is afforded by passive filtering.

### 3.4 HEMP Survivability Analysis Conclusions

We analyzed some of the existing internal transient protection in the RF-3200 equipment complement for HEMP S/V, since the protection circuits were not specifically designed to withstand HEMP-induced transients. We also attempted to establish the HEMP protection which these devices may afford. In some cases the S/V analysis is based on sensitive components at the various system electrical interfaces. If possible an HM is calculated (in dB) based on the worst-case HEMP-induced stress and the estimated strength at these interfaces.

#### 3.4.1 Power Supply Interfaces

The HEMP-induced transient stress on the transceiver dc power supply cable is due primarily to direct field coupling as calculated in section 3.2.3. The HM calculation is based on a P6KE6.8 transient suppressor rather than the Z2022 used (see A5A1 of ref. 3). The P6KE6.8 has a breakdown voltage of 6.8 V, whereas the Z2022 is 17.8 V, so the analysis uses the Wunsch damage constants and surge resistance of the P6KE6.8 [8], but the breakdown voltage of the Z2022, which should result in a fairly accurate HM calculation.

The HEMP-induced transient on the dc power cable is a 150-MHz damped sinusoid with a peak amplitude of 31 A and a source impedance,  $Z_s$ , of 1500  $\Omega$ . The published failure power of the P6KE6.8 is 30 kW and is used to represent the Z2022. The failure current is calculated to be 465 A, and is taken to be the terminal current required for failure. Since  $Z_s \gg R_L$ , the short-circuit current required for failure is equal to the terminal current,  $I_{sc,f} = I_T = I_f$ , and the HM can be calculated according to

$$HM = 20 \log(I_f/I_{scHEMP}) = 20 \log(465/31) = 24 \text{ dB} . \quad (28)$$

If the entire bulk cable current appears across the power supply lines, the HM is still 18 dB.

The HEMP-induced stress could be a negative polarity transient, so the protection circuit must also handle a  $V_{oc,HEMP} = -23$  kV. The Wunsch damage constants for a 1N4003 rectifier diode are used in the calculation rather than that for the 1N4004 diode used in the circuit. The only difference between these devices is the peak inverse voltage which is -200 V for the 1N4003 and -400 V for the 1N4004 [10], and corresponds to the breakdown voltage in reverse-bias. The published failure power for the 1N4003 is 1300 W and is used in the HM calculation, along with the reverse-bias breakdown voltage of the 1N4004, which should provide a fairly accurate HM calculation.

The terminal voltage required for failure is taken to be the calculated 420-V device failure voltage (i.e.,  $V_T = V_f$ ). The open-circuit voltage at the circuit terminals required for failure,  $V_{oc,f}$ , is based on an 18- $\Omega$  load resistance (see A5A2 of ref. 3) and will scale inversely with the load resistance according to

$$V_{oc,f} = V_f(18 + 1500)/18 = 35 \text{ kV} . \quad (29)$$

The HM for the power supply rectifier diode can be estimated from

$$HM = 20 \log(V_{oc,f}/V_{ocHEMP}) = 20 \log(35/23) = 4 \text{ dB} , \quad (30)$$

which would imply marginal survivability of this diode if subjected to threat-level, negative polarity transients.

Next, consider the power/control cable to the RF-382-01 antenna coupler and the HEMP-induced transient at the transceiver interface. The transient protection at the transceiver interface is not known exactly but is stated to be protected by transZorbs (see sect. 3.3). The HEMP-induced transient under worst-case conditions, as calculated in section 3.2.2.2, appears at both the transceiver and antenna coupler interfaces. Since this cable is assumed to be similar to RG-213/U, the

HEMP-induced wire current is small due to the *field-to-wire* coupling (i.e.,  $I_w = 1.5$  A with a source impedance of  $371 \Omega$ ) and has a 2-MHz damped sinusoidal waveform. For the P6KE6.8 transZorb previously described, and assuming the transceiver interface uses similar devices, the HM is

$$HM = 20 \log(I_{sc,f}/I_{sc,HEMP}) = 20 \log(465/1.5) = 50 \text{ dB} . \quad (31)$$

If the entire HEMP-induced bulk cable current (i.e., 5.5 A) appeared across one wire the HM would still be 38 dB.

The power/control cable interface at the RF-382-01 antenna coupler is protected by various devices which include 1N4004 diodes, so the analysis is done in the same manner as for the transceiver (i.e.,  $V_{oc,f} = 35$  kV). The HEMP-induced open-circuit voltage is only 556 V, which leads to

$$HM = 20 \log(35000/556) = 36 \text{ dB} . \quad (32)$$

If this cable has a single shield with shield parameters similar to RG-58A/U, the  $V_{oc,HEMP}$  is 1635 V and the corresponding HM is then about 27 dB. The power/control cable interface at both the transceiver and the RF-382-01 antenna coupler are thus considered hard to the HEMP *field-to-wire* coupling, under worst-case conditions, with an HM of more than 20 dB. The HEMP-induced transient conducted from the antenna could lead to a larger  $V_{oc,HEMP}$  and a negative HM such that TPDs would be recommended on the rf line to protect the interface circuits.

The conclusions that can be drawn from the analysis of the transceiver and RF-382-01 antenna coupler power supply circuits are that the existing transient protection can also provide HEMP protection. The protection devices would survive the calculated HEMP-induced transients. The residual HEMP stress after the protection devices cannot be determined analytically without data for the device performance as a function of the transient pulse parameters. The impact of the residual HEMP stress, synergistic effects, internal arcing, or other nonlinear effects on the system functional response are best determined through threat-level HEMP simulation under worst-case coupling conditions. The dc power for the RF-3282 antenna coupler is provided on the rf coaxial cable and is addressed in the next section.

The RF-3236R power supply commercial power input has some form of transient protection; however, insufficient data are available to analyze this interface for HEMP survivability. The HEMP-induced transient current under worst-case conditions could be a 500-A peak,

damped sinusoid with a resonant frequency of 100 kHz [11]. The power supply is believed to be protected by GE V275 series MOVs as in the RF-366 power supply [11]. In this case, the RF-3236R would probably be sufficiently hardened to HEMP, but the survivability analysis is inconclusive. An external TPD is thus recommended on the ac power input. The system functional response, when subjected to HEMP-induced transients on the commercial power service, is determined experimentally.

### 3.4.2 Transceiver/Coupler Interfaces

The front panel microphone input is another transceiver interface which must be addressed. The microphone cable is considered to be shielded so the HEMP-induced transient bulk current is taken to be a 80-MHz damped sinewave with a peak value of 20 A, as calculated in section 3.2.2. The microphone cable has eight conductors so the HEMP-induced wire current is then about 7 A (see sect. 3.2.2.2). For a multiconductor cable source impedance of 100  $\Omega$ , the corresponding open-circuit voltage is about 700 V. The voltage across the passive interface components is much lower due to the relatively large source impedance. The voltage rating of the capacitors associated with this input are 50 V [3], and the S/V analysis considers these capacitors as the sensitive interface component. The HEMP-induced voltage,  $V_{cap}$ , across a capacitive load depends on the capacitance, the source impedance, and the radian frequency,  $\omega$ . For a 1-nF capacitor (C16 on A2 of ref. 3), at 80 MHz,  $Z_s \omega C \gg 1$ ; so

$$V_{cap} = V_{oc,HEMP} / (Z_s \omega C) = 700 / (100 \times 5 \times 10^8 \times 10^{-9}) = 14 \text{ V} , \quad (33)$$

which leads to

$$HM = 20 \log(V_{rated} / V_{cap}) = 20 \log(50 / 14) = 11 \text{ dB} . \quad (34)$$

The microphone cable overall shield should perform better than assumed at 80 MHz, so that the analysis implies a high confidence in the HEMP survivability of this interface.

The rf I/O coaxial cable at both the transceiver and the antenna coupler(s) are designed with components that can handle the transient stress during both normal operating and fault conditions. The rf I/O is exposed to a HEMP-induced transient, owing to *field-to-wire* coupling, as calculated in section 3.2.2.2 at both the transceiver and the antenna coupler(s) (i.e.,  $V_{oc,HEMP} = 556 \text{ V}$  for RG-213/U or  $V_{oc,HEMP} = 1635 \text{ V}$  for RG-58A/U, with a source impedance of 100  $\Omega$ ). The HEMP survivability of the rf I/O on the transceiver, and on the antenna coupler, is determined by the voltage rating of the high-pass filter capacitors, which is 500 V. The HEMP-induced voltage across this

capacitor,  $C = 22 \text{ nF}$  (see fig. 11), can be calculated at 2 MHz according to equation (33). For an RG-213/U cable,

$$V_{cap} = 556 / (22 \times 10^{-7} \times 1.3 \times 10^7) = 19.4 \text{ V} . \quad (35)$$

The HM for the filter capacitors is then

$$HM = 20 \log(V_{rated}/V_{cap}) = 20 \log(500/19) = 28 \text{ dB} . \quad (36)$$

For RG-58A/U the corresponding HM is 19 dB, which would support the recommendation that only double-shielded coaxial cable be used.

The HEMP *field-to-wire* coupling to the cables between the transceiver and antenna coupler(s) should not impact the system HEMP S/V if these cables have transfer impedances similar to RG-213/U. Also the cable shields and connectors must be in sufficient condition to effectively attenuate the HEMP-induced transients. Due to the large HEMP-induced voltage from the cable shield to ground (i.e., 140 kV), the coupling to internal wires will be sensitive to the connector transfer impedance. Control of the cable connector backshell design would be a recommended HEMP-hardness dedicated design practice. Arcing and other nonlinear effects on the system functional response are best determined by HEMP simulation under worst-case coupling conditions.

The coupler antenna I/O connector has a HEMP-induced stress that is conducted from the antenna. Under worst-case conditions the entire antenna short-circuit current could appear at the coupler input connector and the corresponding voltage pulse has a peak amplitude that is large enough to form an arc across the transient protection arcball arrangement. Assuming the arcball will limit the peak HEMP-induced transient to 8000 V, the interface electronics would be protected since they were designed to handle this voltage level. However, the effect of the corresponding current transient cannot be readily calculated. The residual HEMP-induced stress after the input protection is difficult to calculate since the response time of the arcball arrangement (i.e., the time at which the arc will form) is not known. Under ideal conditions the HEMP-induced current would also be limited; however, the residual current could still be much larger than that associated with the transceiver normal operation. Since the coupler is designed to pass the antenna signals to the transceiver, current limiting is recommended on the rf I/O coaxial cable at both the transceiver and coupler. The S/V analysis is inconclusive in this area, so the impact to the system functional response is determined through simulation testing.

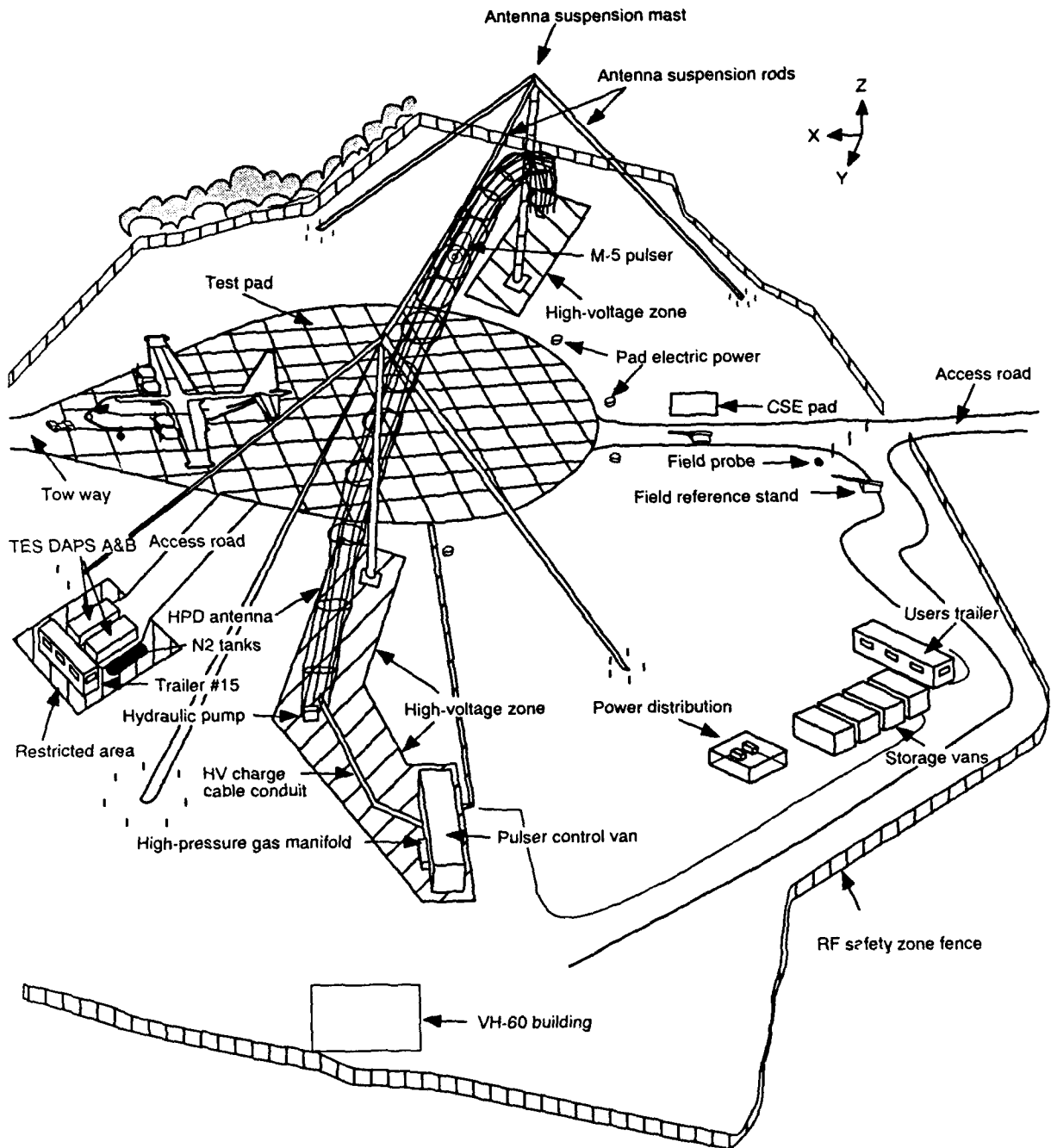


Figure 11. TACAMO EMP simulator.

## 4. Test Procedures for Unhardened System

There are basically two aspects of the HEMP S/V assessment process which require verification testing. The first part involves a verification that the TPDs installed in the test article operate as designed. In the case of the unhardened RF-3200 system the TPDs were not designed for HEMP protection, so adequate operation for HEMP hardness requires verification. The recommended validation test for the HEMP protection capability of TPDs is a laboratory direct-drive CI technique on an isolated device to completely characterize the HEMP protection capabilities of the device. Since the internal protection devices cannot be so characterized, the HEMP S/V must be based on the system functional response to the simulated HEMP environment.

The second aspect of the S/V assessment involves validating the HEMP hardness of the entire system. The preferred validation test technique is a radiated free-field PI test of the entire system in a typical deployment configuration. PI testing at sub-threat levels serves to substantiate the worst-case HEMP coupling configuration and the calculated HEMP-induced stress at the system interfaces. PI testing at threat level serves to verify the operation of TPDs and the completely deployed system S/V to the simulated HEMP environment.

The HEMP S/V assessment process is applied to a select group of electrical interfaces used on the RF-3200 transceiver system. The most important interfaces were identified in section 3.1 in terms of electrical connections. The simulation-induced stress waveforms should be representative of the HEMP-induced transients that could be expected at the interface of interest, as developed in section 3.2.

### 4.1 HEMP Simulation

System-level HEMP hardness verification testing is best accomplished by a radiated, free-field PI test of the complete system in a typical (but worst-case) deployment configuration. Due to the unavailability of high-level PI testing facilities at HDL, the TACAMO EMP Simulator (TES) at the Naval Air Test Center (NATC) (shown in fig. 11) was used to produce the simulated HEMP environment. Of the possible system deployment configurations, the RF-1940 dipole antenna, dipole adapter, RF-382-01 antenna coupler, rack-mounted transceiver, and power supply are chosen as the representative unhardened test article. The worst-case HEMP coupling to this system is obtained for the RF-1940 dipole antenna oriented parallel to the TES, the maximum cable lengths (oriented parallel to the TES) associated with the transceiver, and the maximum direct field coupling to electronics, which

are mounted in a typical unshielded rack. In all cases the unhardened system is exposed to incrementally increasing radiated pulse environments until the maximum pulse level is reached or damage occurs.

## **4.2 Unhardened System Configuration**

In the primary unhardened system configuration, the RF-1940 dipole antenna was oriented parallel to the TES and deployed at various locations and heights above the ground. The unhardened system was initially deployed at 60 m from the TES in a simulated HEMP environment having a peak E-field amplitude of about 16 kV/m. The rf I/O coaxial cable and the power/control line between the RF-382-01 antenna coupler and transceiver were oriented parallel to the TES. The maximum cable lengths associated with the transceiver are 76 m; however, only a 46-m power/control cable was supplied by Harris. The transceiver rf I/O to the antenna coupler would normally be up to 250 ft (76 m) of RG-213/U, but this was not supplied, so the system was tested with 100 ft (33 m) of RG-214/U (supplied by HDL). The frequency allocations for transmission were established by the NATC, and the transceiver would ideally be subjected to simulated HEMP environments while in the receive (RX) mode at the same frequencies, namely, 2.13, 7.595, and 24.43 MHz. Safety procedures during HEMP simulation are provided in the TES standard operating procedures [12] and are not reproduced here.

## **4.3 General Test Procedures for the Unhardened System**

HEMP hardness verification testing was accomplished in the primary unhardened system configuration described in the previous section. Initially the RF-1940 dipole antenna was deployed at 60 m from the TES at a height of 5 m. The RF-382-01 antenna coupler was on the ground, the cables were deployed parallel to the simulator on the ground, and the rack-mounted electronics were located about 30 m away from the antenna coupler on the ground. The test article used commercial electric power at the transceiver location. After proper grounding, the transceiver was in the RX mode at 2.13 MHz with the microphone keyed to tune the antenna coupler. HEMP simulation testing began in a radiated pulse environment with a peak E-field amplitude of about 16 kV/m while monitoring the induced current transients on the antenna line.

This test configuration was repeated at various pulsed field levels, relocating the system with respect to the TES. Ground and ac power connections were accomplished as required at each location. Commercial power was supplied through an extension cord routed to minimize the transients coupled to the transceiver power supply.

Ground connections were accomplished with ground rods or wire connections, as short as possible, to available grounding points on the TES concrete pad.

Functional testing was performed after each pulse by observing the transceiver self-diagnostic error messages and by verifying normal operational capability. The pass/fail criterion is that no failures be observed that cannot be corrected by power cycling or reprogramming. The transceiver has factory-programmed channels (Group A), which must be maintained throughout the simulation testing. User-programmed channels may require reprogramming, but given that the transceiver can be reconfigured for normal operation, this would not be considered a HEMP vulnerability.

#### **4.4 Test Conduct for the Unhardened System**

Initially the dipole antenna was deployed at the reference sensor location so that it was exposed to a peak E-field amplitude of about 16 kV/m. The RF-1940 dipole antenna was deployed 5 m above the ground and oriented parallel to the TES, centered on the TES centerline. The RF-382-01 antenna coupler was placed on the ground near the TES centerline. The cables to the transceiver were deployed on the ground and oriented parallel to the TES. The rack-mounted transceiver was located about 1 m above the ground, roughly 33 m off the TES centerline. The coupler and transceiver ground straps were connected to ground rods or other available ground connections. The external ac power cable was oriented perpendicular to the TES and located on the ground. Initial measurements were taken with the transceiver power off and then with the transceiver in the RX (standby) mode at a frequency of 2.13 MHz. The operation of the transceiver was verified after each pulse by keying the microphone and observing the transceiver functional response or fault conditions and any error messages. The test article was subsequently located at various distances from the TES with the RF-1940 dipole deployed on the ground.

### **5. Test Results for Unhardened System**

The first part of the test period involved HDL/NATC coordination, test article deployment and check-out, and instrumentation of test configuration for data acquisition (i.e., current and E-field measurements). The test article was deployed as described below and shown in figure 12. The coordinate system used to locate the various test object locations is shown in both figures 11 and 12. This coordinate system is centered on the TES centerline so that the x-axis represents the ground range from the pulser vessel. The slant range would be

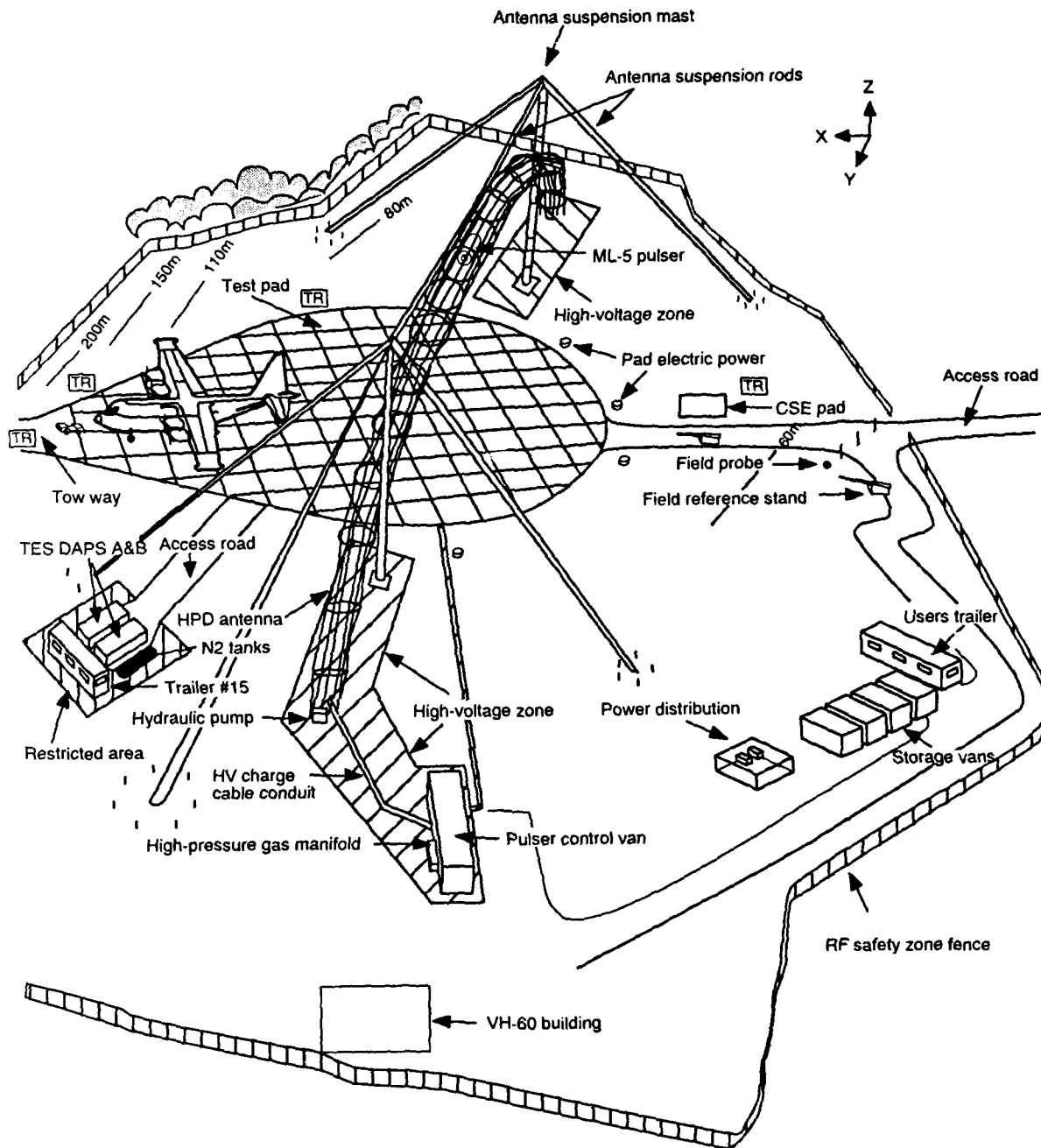


Figure 12. Test configuration for the unhardened RF-3200 system.

based on the normal pulser height of about 10 m. The distances shown are approximate for locations off the TES centerline.

The dipole antenna was initially deployed on wooden stands about 5 m above the ground, roughly 60 m from the TES with the dipole centered on the pulser centerline. The RF-382-01 antenna coupler was located on the ground beneath the dipole antenna. The rack-mounted transceiver was located on a workbench (roughly 1 m above the ground) at a location about 33 m from the centerline, parallel to the TES. Electric power was supplied by an extension cord to the closest 120-V receptacle. The transceiver and coupler ground connections were accomplished with ground rods driven at least 1 m into the soil. The system cables were deployed on the ground and parallel to the TES structure with the power cable oriented perpendicular to the TES (see fig. 12). The transceiver operation was verified in RX mode by tuning to local or national transmissions. Operation in transmit (TX) mode at the NATC frequency allocations (i.e., 2.13, 7.595, and 24.43 MHz) was verified by the front panel TX power LED indicators.

Simulation testing began on 28 August 1990. Several pulses were required before the induced antenna current was adequately documented. The induced current on the dipole antenna had a measured peak amplitude of about 130 A (see fig. A-10 in app A of this report) and corresponded to an incident E-field amplitude of 16 kV/m (as measured by the TES reference sensor). The transceiver operation was subsequently checked and it was discovered that the transceiver could no longer tune the coupler. The observable effect was that the transceiver front panel would continuously display the tuning message with no TX power LED indicators (i.e., no tune power). Power cycling did not return the TX section to normal operation. The RX power LED indicators and received signals demonstrated that the RX section was operational. Note that the fault indicator was not displayed. A Harris representative was scheduled to troubleshoot and repair the system.

Troubleshooting by the Harris representative was accomplished with the system as previously deployed except that the dipole antenna was laying on the ground. During this time the TES operations continued with the only effect on the RX section being the audible sound of the RX protection relay. Field measurements were completed at the transceiver (see fig. A-8 in app A) and coupler (see fig. A-9 in app A) locations but additional current measurements were not taken; however, the induced antenna current for the dipole on the ground at this location can be estimated to be about 60 A. Note that during the transceiver configuration programming by the Harris representative, the TES pulse did cause anomalies (i.e., display lockup) that were

corrected by power cycling. After replacing the receiver/exciter board with a spare, the fault indicator came on when the microphone was keyed, indicating a problem with the power amplifier board.

The Harris representative determined that the RF-382-01 antenna coupler and both the receiver/exciter and power amplifier boards of the transceiver were damaged. Replacement boards were obtained and configured to match the original system options. After installation the transceiver was configured without the coupler and normal TX/RX operation was verified with the transceiver directly connected to the dipole antenna. The test article was relocated to 200 m from the TES with the dipole antenna on the ground near the pulser centerline. The transceiver was 1 m above the ground and roughly 33 m off the centerline (see fig. 12). Initially the coupler was connected as in a normal deployment with the cables laying on the ground. Power was supplied by a portable generator and grounding was accomplished with ground rods.

No observable effects were noted for the test article deployed at the 200-m location. In this case, the current measurements indicated a current that was 20 percent larger on the rf line with the coupler than on the rf line without the coupler (see fig. A-3 in app A). This implies that, even though damaged, the coupler provided a better match to the antenna impedance than the 50- $\Omega$  cable. An explanation might be that the coupler failed in a tuned condition, so that at an RX frequency of 2.13 MHz, the coupler provided a reasonable match to a 3-MHz dipole at 5 m above the ground and so provided a reasonable match to the same dipole located on the ground. The test article was relocated to 150 m and deployed without the RF-382-01 coupler (see fig. 12). The system deployment, power, and grounding were as before, and no effects were observed. The induced antenna current had a peak amplitude of about 9 A (see fig. A-5 in app A). The dipole antenna was subsequently relocated to 110 m from the TES with the transceiver at the previous location.

Data acquisition resumed with the antenna at 110 m from the TES and deployed on the ground near the pulser centerline. The transceiver was roughly 150 m from the TES and located off the pulser centerline. The induced antenna current had a peak amplitude of about 13 A (see fig. A-5 in app A). No observable effects were noted. The test article was relocated to about 80 m from the TES (see fig. 12). The dipole antenna was deployed on the ground centered on the pulser centerline. The transceiver was roughly 33 m off the pulser centerline. Power and grounding were accomplished as in the previous configurations.

Several pulses were required to document the induced antenna current which had a peak amplitude of 45 A on the first measurement (see fig. A-6 in app A). System check-out found that the transceiver was damaged; however, the observable effects were not the same as in the previous case, when the TR was damaged. Since the transceiver was not configured for an antenna coupler, the tuning message was not displayed. As before, the TX power LED indicators demonstrated no TX power, but now the fault indicator came on whenever the microphone was keyed. Power cycling did not correct the fault condition.

## 5.1 Test Data Summary

A summary of the test results are provided in table 3 in terms of the horizontal E-field component measured at the dipole antenna and the corresponding induced antenna current. The exact system location and configuration can be found in the previous section and by reference to figure 12. In all cases the transceiver (TR) was in the RX mode at 2.13 MHz but deployed both with and without the coupler (CP). Although not shown, data were also collected for the transceiver in RX mode at the other allocated frequencies. If repeat data are available, the amplitudes presented are average values. The distances as shown are approximate. Except at the 60-m location, which is based on the TES reference sensor data, the E-field measurements were on the ground at the antenna location. As can be seen, the measured current amplitudes scale roughly with the measured E-field amplitudes. The measured current waveforms are included in appendix A.

A summary of the measured E-field amplitudes at the transceiver location is provided in table 4. The data are presented in terms of the

Table 3. Summary of Induced Antenna Current Peak Amplitudes Measured for Unhardened System

Dipole distance from TES (m)	Horizontal E-field at antenna	Induced antenna current (A)	Results
200 with CP	412 V/m	5.5	None
200 without CP	412 V/m	3.9	None
150 without CP	750 V/m	8.9	None
110 without CP	1.1 kV/m	13.9	None
80 without CP	4.9 kV/m	43.6	TR damaged
60 with CP	16 kV/m (elevated)	131	Both TR and CP damaged

CP = coupler  
TR = transceiver

**Table 4. Summary of Peak E-Field Amplitudes Measured at Transceiver Location for Unhardened System**

TR distance from TES (m)	Horizontal E-field	Vertical E-field	Radial E-field	Total E-field
200	779 V/m	678 V/m	233 V/m	1.1 kV/m
110	1.4 kV/m	861 V/m	—	—
80	4.3 kV/m	—	—	—
60	6.2 kV/m	11.9 kV/m	5.6 kV/m	14.5 kV/m

peak amplitude of each E-field component as measured at the front of the rack at the height of the transceiver (about 1 m). The data represent the ground interacted peak E-field amplitudes. If repeat data are available, the amplitudes presented are average values. The distances as shown are approximate. The total E-field amplitude is calculated as the vector sum of the measured E-field components. The observed effects on the transceiver are believed to be solely caused by the induced current conducted from the antenna, so the transceiver should be able to withstand E-field environments up to the measured levels. The measured E-field waveforms are included in appendix A.

## 5.2 Conclusions

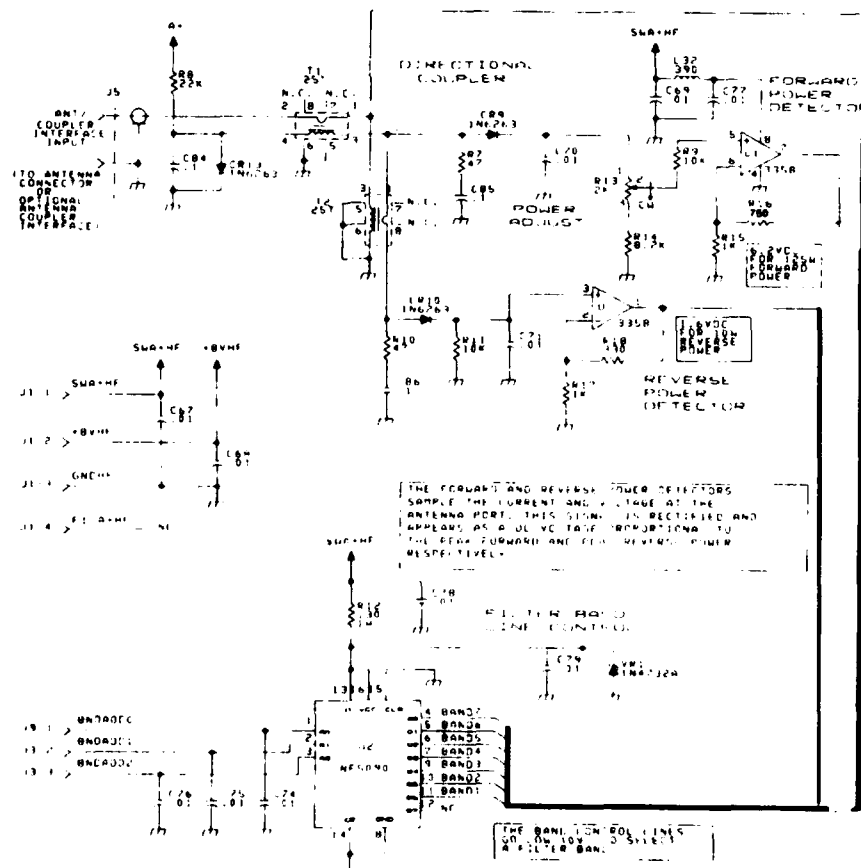
It is obvious that this commercial radio set is not hard to HEMP-induced transients. Although not verified, it is believed that a power-off condition would also result in a damaged transceiver and coupler if it were connected to an antenna during a HEMP event. The induced current levels which caused failure are such that connection to any of the optional antenna configurations would result in transceiver and coupler damage if subjected to a threat-level HEMP environment. Based on the test results it is believed that the RF-3200 transceiver would be vulnerable to high-level ambient electromagnetic environments and possibly to a lightning event.

The determination of the transceiver damage mechanism at the component level by Harris engineers indicated that component damage was limited to rectifier diodes in the forward and reverse power detectors. The damaged components were CR9, CR10, and CR13 where the 1N6263 diodes shown were actually 1N5711 low-current Schottky barrier diodes. The failure of CR13 would severely impair the transceiver performance; however, if CR9 and/or CR10 should fail, the transceiver would detect no forward and/or reverse power and so would not be able to effectively tune an antenna. Since the power amplifier output is detected but no forward and/or reverse

power is detected, a fault condition exists and the system is left in a non-operational mode.

Harris engineers estimate the 1N5711 diode failure current to be about 1 A, so it is unclear when CR13 actually failed. The current coupling through transformer T1 of figure 13 is about -28 dB so that the damage threshold for CR9 can be estimated at more than 25 A on the rf I/O coaxial cable. Since testing was accomplished at about 14 A on this line with no damage, but damage occurred at 43 A, the HEMP-induced failure threshold is between 14 and 43 A. Since this estimated failure threshold is larger than the HEMP-induced transient owing to *field-to-wire* coupling for an RG-214/U cable, the concern for the system HEMP S/V would be to limit the HEMP-induced antenna current without degrading the transceiver performance. The same diodes failed in the RF-382-01 antenna coupler; however, an RF-3282 antenna coupler will actually be used with this system, so the HEMP-induced failure of the RF-382-01 coupler is not discussed further. No matter which antenna coupler is used, HEMP survivability would require transient protection at the coupler I/O, which will not degrade the RF-3200 system normal operation.

Figure 13. Harmonic filter PWB A4 schematic diagram.



### 5.3 Recommendations

It is recommended that the RF-3200 system be retested under very structured conditions while both the transceiver and coupler rf I/O are protected by in-line coaxial TPDs that provide current limiting. The device chosen is a Fischer Custom Communications, Inc. (FCC), 350-V coaxial spark gap (part #FCC-350B-350), to be located at both the transceiver and coupler interfaces. The coupler antenna I/O also requires some form of transient protection. The device chosen is an FCC 12,000-V gas tube surge arrestor (part #FCC-350A-12000-IL23/U). HEMP simulation testing on the deployed system then establishes the HEMP S/V of the hardened system when exposed to threat-level HEMP environments. This information is required before the HEMP survivability of the RF-3200 system can be established, even though the various interfaces can be adequately protected with an external TPD, because of the direct field coupling to this unshielded system. It is believed that adequate protection on the antenna and rf line would result in a survivable system (possibly without an antenna coupler) since damage owing to the *direct-field* coupling would not be expected. HEMP protection on the commercial power line is also recommended. The device chosen is an ac power line protector manufactured by MCG, which has a 415-V clamping level.

## 6. Test Procedures for the Hardened System

For the hardened RF-3200 system (which includes the RF-3282 antenna coupler), external TPDs were chosen specifically for HEMP protection. The HEMP S/V of the hardened system is based primarily on threat-level HEMP simulation and the system functional response. The most important electrical connections to be addressed are as follows:

- (1) 13.6-Vdc power input on the transceiver,
- (2) microphone input on the transceiver,
- (3) rf I/O on the transceiver,
- (4) rf I/O on the antenna coupler,
- (5) antenna I/O on the antenna coupler,
- (6) ac power input on the power supply, and
- (7) dc power output on the power supply.

Variations to the equipment used at these connections include the microphone and antenna. These variations to the basic equipment complement are addressed in the S/V assessment. Variations that are not addressed could impact the system S/V and so would not be recommended.

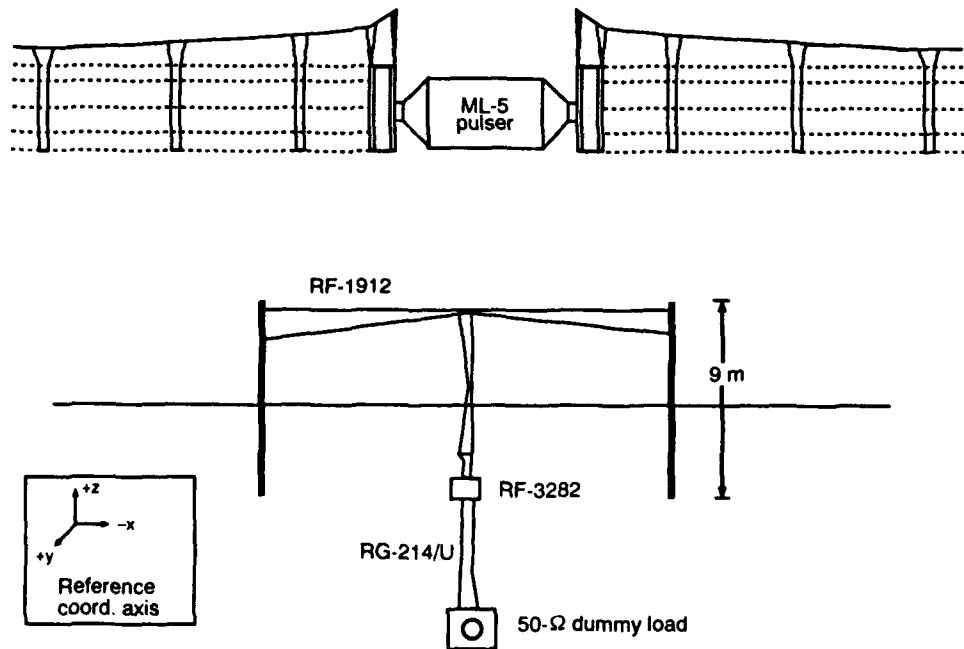
## 6.1 Pulsed Illumination Tests

For the hardened system, the representative test articles are the RF-1912 mast-mounted antenna, the RF-3282 antenna coupler, and the rack-mounted electronics. Note that the maximum cable length associated with the RF-3282 coupler is 150 ft (45.7 m) rather than 250 ft (76.2 m) for the RF-382-01 coupler. Testing was again conducted at the TES using the same reference coordinate system (see fig. 11). The HEMP simulation testing for the hardened system was conducted during the period 19–23 August 1991. The pass/fail criterion for HEMP survivability is that no failures be observed which cannot be corrected by power cycling.

### 6.1.1 Hardened System Configurations

The initial test configuration used only the fully deployed RF-1912 antenna and the RF-3282 coupler. This setup is referred to as test configuration 0, which includes the RF-3282, even though it is unpowered and unterminated. Test configuration IA, without the transceiver, used a 50- $\Omega$  resistive load as shown in figure 14. The initial tests served to document the RF-1912 induced antenna current

Figure 14. Test configuration IA without the transceiver.



without the RF-3200 and its associated electronic components. The RF-3282 antenna coupler was located underneath the TES and grounded as shown in figure 15. The measurements documented the coupling to the RF-1912 antenna in the simulated HEMP environment under various antenna load conditions. The RF-1940 antenna was also deployed and connected in parallel with the RF-1912 antenna while the coupler was still connected to the 50-Ω load. This is test configuration IB without the transceiver, as shown in figure 16. This configuration served to establish the induced current on the combined antenna feedlines with the coupler in an unpowered state.

The RF-3200 was subsequently deployed for minimum coupling to the transceiver electronics. In this setup, test configuration IA with the

Figure 15. RF-1912 antenna and RF-3282 coupler ground connections.

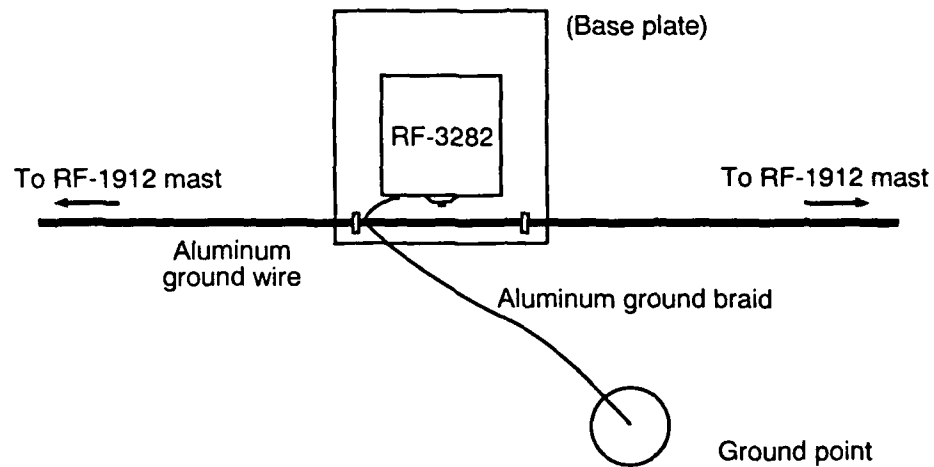
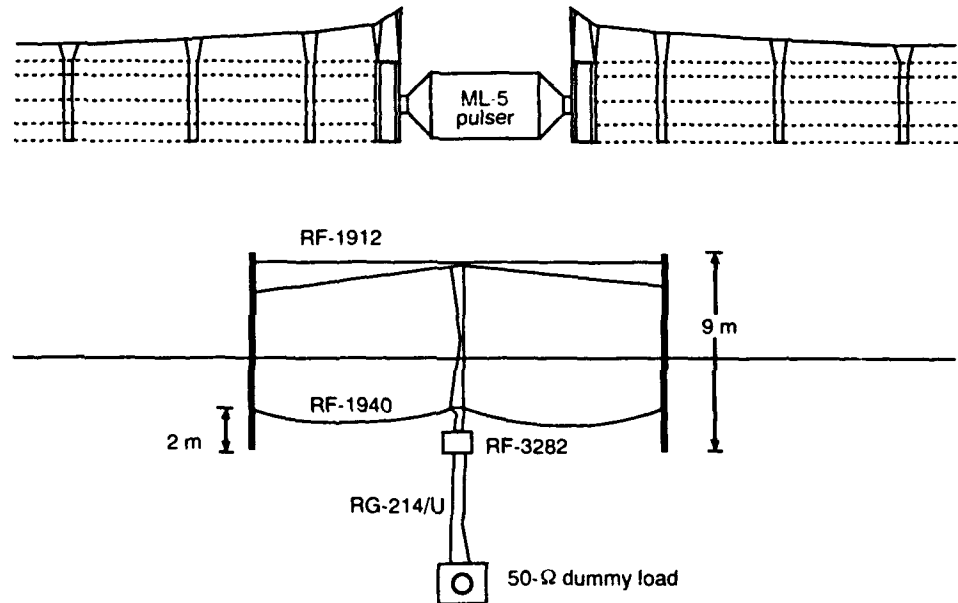


Figure 16. Test configuration IB without the transceiver.



transceiver, the RF-1912 was as before (e.g., positioned parallel to the TES) while the coaxial cable to the transceiver was deployed perpendicular to the TES. Test configuration IB with the transceiver included connecting the RF-1940 dipole antenna, deployed at a height of about 2 m as shown in figure 17, along with the RF-1912 antenna. This configuration maximized the induced current at the coupler antenna I/O by connecting both antennas in parallel.

The system was then configured for maximum coupling to both the RF-1912 antenna and the transceiver electronics. This was done by moving the rack-mounted electronics to a dielectric stand directly underneath the TES at a height of 5 m, while leaving the antenna in its previous position as shown in figure 18. This deployment is referred to as test configuration II, which maximized the coupling to the fully deployed test article in the simulated HEMP environment.

Test configuration III maximized the coupling to the transceiver electronics while minimizing the coupling to the antenna. For this last test configuration, the RF-1912 antenna was replaced with the RF-1940 antenna, or a length of aluminum wire, in a monopole configuration. The RF-1912 antenna was not moved because of time constraints but was completely disconnected from the test article. Test configuration III was implemented by positioning a vertical monopole antenna under the TES while leaving the transceiver directly under the raised pulser at a height of 5 m, as shown in figure 19.

Figure 17. Test configuration IB with the transceiver.

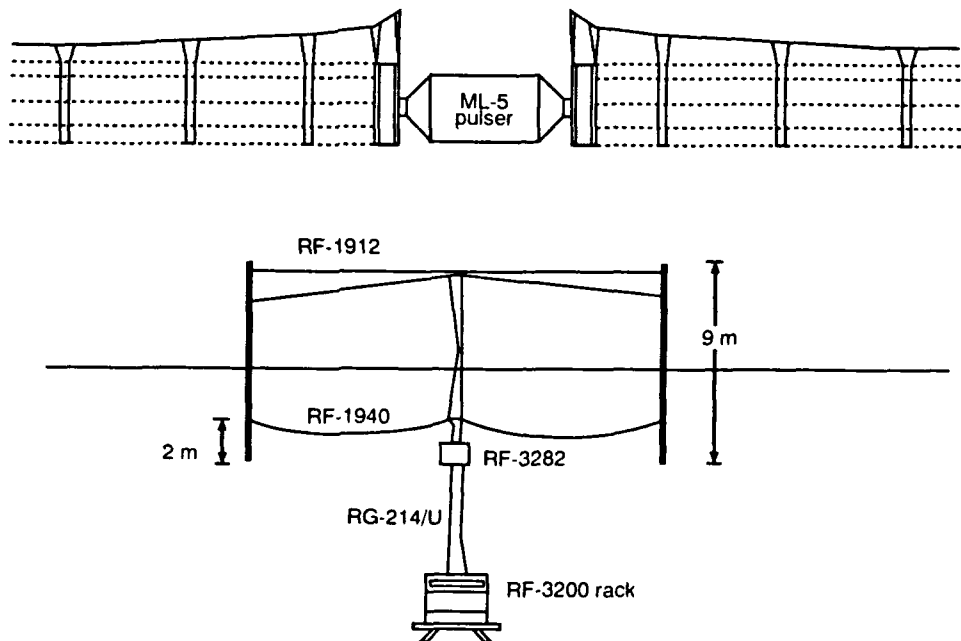


Figure 18. Test configuration II for the hardened system.

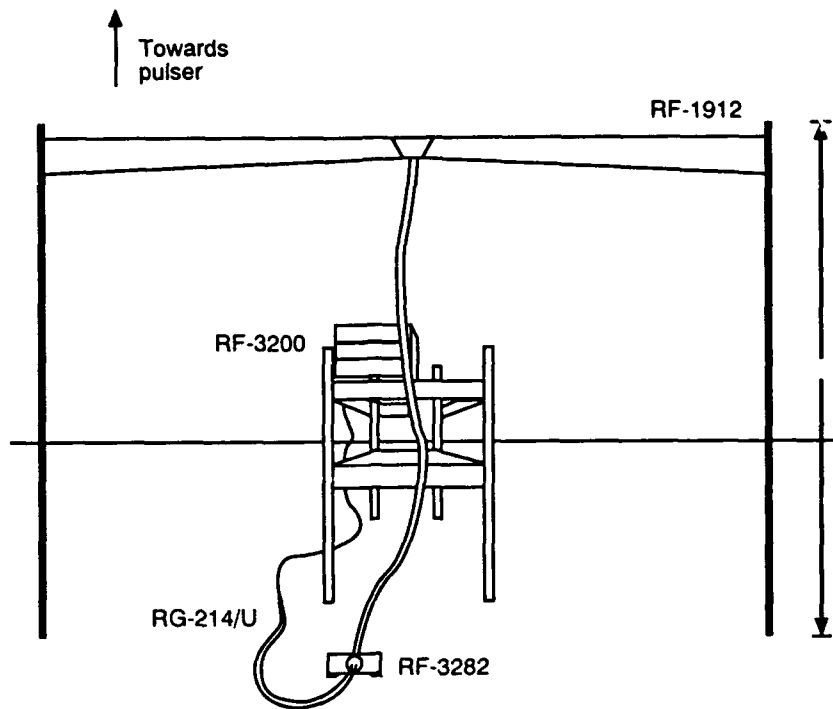
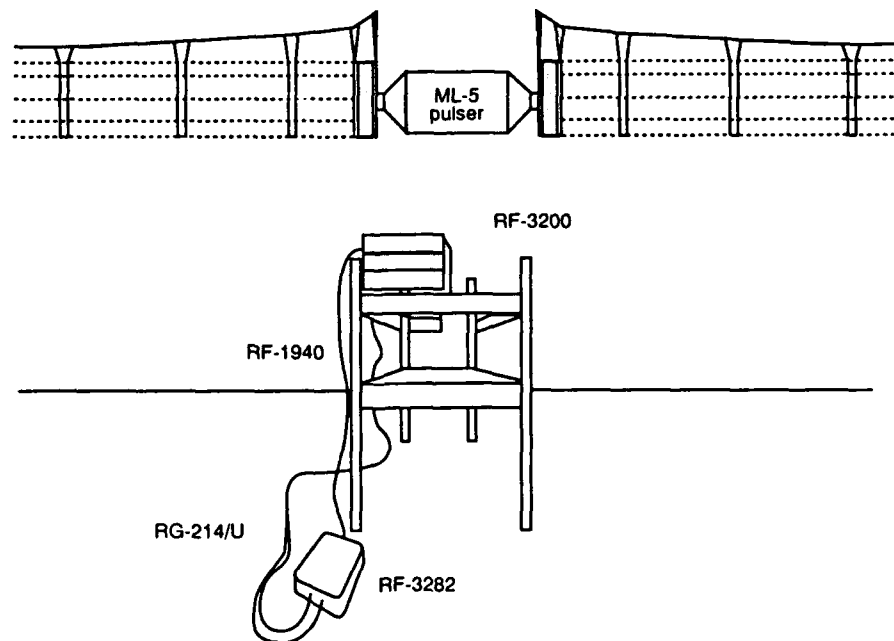


Figure 19. Test configuration III for the hardened system.



### 6.1.2 General Test Procedures for the Hardened System

HEMP hardness verification testing was accomplished in primarily four different system configurations (test configurations 0, I, II, and III). Test configuration 0 was the initial system deployment without

the transceiver or the 50- $\Omega$  load. Test configuration I, either with or without the transceiver, was further subdivided into test configurations IA and IB to distinguish between the use of only the RF-1912 antenna and the use of both the RF-1912 and RF-1940 antennas, respectively. The test object was exposed to various simulated environments determined by the location and orientation of the system elements relative to the TES. Minimum coupling to the antenna and cables was achieved by orienting them perpendicular to the TES. Maximum coupling to the entire system required that the antenna be parallel to the TES and that the transceiver be directly underneath the TES (test configuration II). Maximum coupling to the transceiver electronics alone is achieved by minimizing the coupling to the antenna and system cables with the transceiver directly under the TES (test configuration III).

Commercial power was supplied by a standard 120-V, 60-Hz outlet at the test site. An extension cord was used to provide ac power as required. Grounding was accomplished with tinned copper ground braids to the available ground points on the TES concrete pad. These connections were made as short as possible (i.e., about 5 m) to reduce coupling effects. In each test configuration the RF-3200 was left in RX mode at each of the three NATC allocated frequencies and, in some cases, it was left in RX mode at 10 MHz. These tests were designed to determine the effects of the simulated HEMP environment on the system functional response.

Throughout the testing period E-field and H-field sensors were used to document the simulated environment. The RF-3282 antenna coupler monitor points included the antenna feedline(s), the coupler rf I/O both before and after the TPD, and the coupler ground connection. Monitor points at the RF-3200 rack included the RG-214/U coaxial cable shield current, the RG-214/U center conductor current both before and after the TPD, the ac power line bulk current (e.g., three conductors), the microphone cable(s) shield current, and the transceiver ground connection. Monitor points inside the RF-3200 rack included the ac power line bulk current after the MCG415 power line protector, and the bulk cable current (e.g., two conductors) from the RF-3236R power supply. During test configuration III, the induced shield current on both the dynamic and electret microphone cables was measured.

Functional response testing was accomplished after each pulse by checking the RF-3200 LED display for any diagnostic error messages and by verifying the system operational capabilities. Communication with the on-site hf equipment verified the operational capability of the

TX/RX functions. Data acquisition and processing was provided by the NATC Data Acquisition and Processing System (DAPS) [13].

### 6.1.3 *Test Conduct for Hardened System*

Simulation testing began by instrumenting the test article for data acquisition and making the final connections between the RF-1912 antenna and the RF-3282 antenna coupler. The mast-mounted RF-1912 antenna had been previously deployed. The RF-1912 was configured as a high-radiation angle dipole exactly 20 ft (6.1 m) away from and parallel to the TES. The antenna was positioned with a tilt of 15 deg, away from the TES, to prevent its possible collapse and tangling with the pulser cage wires. It had a total vertical height of about 9 m. This setup is referred to as test configuration 0. With both leads to the RF-1912 antenna shorted to ground, the measured current on one lead had a peak amplitude of about 125 A with a resonant frequency of 12 MHz, since each leg of the RF-1912 antenna responded like a top-loaded monopole antenna.

The coupler, with a transient surge protector in front of its antenna I/O connection, was positioned directly underneath the center of the RF-1912 at (6,0,0) and left on top of its associated base plate. The surge protector used was the FCC-350A-12000-IL23/U gas-tube type. The coupler was grounded by routing an aluminum wire through both of the RF-1912 mast base plates and the coupler base plate. A tinned copper ground braid (roughly 5 m long) was then strung from this connection at the coupler base plate to a ground point at the test site (see fig. 15). With the RF-1912 in this configuration and no connection to the coupler rf I/O, measurements of the current on the coupler lead gave an average peak value of 122.4 A. Measurements on the ground braid gave an average peak value of 115.6 A. Thus test configuration 0 documented the induced current on the RF-1912 with the RF-3282 coupler in an unpowered and unterminated condition. In some cases the measured waveform indicated that arcing occurred in the antenna feedline. As in the case of the shorted antenna feedline, the resonant frequency was about 12 MHz, which indicated that an arc served to short both legs of the antenna to ground.

A 50- $\Omega$ , 600-W resistive load was connected to the coupler rf I/O using a 33-m section of RG-214/U coaxial cable. The load was positioned at (18,0,0) so that the adjoining cable would be perpendicular to the TES. Two TPDs were installed at each end of the coaxial cable, one at the coupler connection and one before the load connection. Both of these TPDs were FCC-350B-350 coaxial spark gaps. This is referred to as test configuration 1A without the transceiver, which was re-

placed by the 50- $\Omega$  load (see fig. 14). Measurements on the coupler lead and ground braid had average peak values of 125.0 and 133.7 A, respectively. This configuration documented the RF-1912 induced antenna current with the coupler unpowered, but terminated in a 50- $\Omega$  load. The additional contribution to the coupler ground braid current was due to the induced current on the coaxial cable shield. The measured RF-1912 antenna current in some cases had the expected dipole resonant frequency, while subsequent measurements indicated that arcing occurred in the antenna feedline.

Test configuration IB without the transceiver included both the RF-1912 antenna and the RF-1940 dipole connected to the unpowered coupler (see fig. 16). The RF-1912 was left in the previous position and the RF-1940 dipole antenna was attached (at a height of about 2 m) between the two masts supporting the RF-1912. The coupler remained at (6,0,0) with the 33-m section of RG-214/U cable attached from its rf I/O to the 50- $\Omega$  load. All the TPDs were in place.

With the RF-1912 connected to the coupler antenna I/O, and the RF-1940 feedline (RG-58A/U) shorted to ground, the induced current amplitude at the coupler was about 125 A, as before. Measurements at the coupler rf I/O before and after the TPD had average peak values of 3.1 and 3.3 A, respectively. The RF-1912 was then replaced with the RF-1940 dipole and the same measurements were repeated. The measured peak current on the RF-1940 antenna was about 100 A with a resonant frequency of about 2 MHz, as would be expected. Since the RF-1940 dipole was closer to the ground than the RF-1912, the driving E-field was reduced and arcing in the dipole adapter was not evident from the measured data. The measured current had average peak values of 3.8 and 3.6 A before and after the TPD at the coupler, respectively. With both antennas connected to the coupler antenna I/O, the average values were 7.9 and 8.0 A before and after the TPD, respectively. The combined antenna feedlines were measured in this last configuration and the measured waveform is the superposition of the 2-MHz RF-1940 antenna current and the 12-MHz RF-1912 antenna current. The coaxial cable center conductor measurements thus indicated current dissipation in the antenna coupler.

The rack-mounted electronics (this included the RF-3200 transceiver, the RF-3236R power supply, and the RF-3238 blower kit) were then deployed on top of a workbench at (18,0,1) and connected to the coupler rf I/O with the 33-m section of RG-214/U coaxial cable. This is referred to as test configuration IA with the transceiver for only the RF-1912 antenna, and as test configuration IB with the transceiver for both antennas connected (see fig. 17). The TPD, which had been used

in front of the 50- $\Omega$  load, was now connected in front of the transceiver (at the rack feedthrough connector). The transceiver had been previously configured for operation at the NATC frequency allocations (i.e., 2.13, 7.595, and 24.430 MHz) before the testing period. However, it was decided to first test the transceiver in an unpowered and ungrounded deployment, which represents an indeterminate antenna load configuration.

For test configuration IB with the transceiver operational, the RG-214/U and ac power cables are deployed on the ground. The induced current waveform on these cables is as expected (see sect. 3.2.2.1). The average peak amplitude is about 70 A for the RG-214/U induced shield current and about 180 A for the ac power cable bulk current. The measured bulk current on the dc power cable has a peak amplitude of about 3 A and a dominant frequency of 273 kHz. These data indicate the band-pass filter characteristic of the RF-3236R power supply transformer.

With the transceiver fully operational, both antennas were used again. The rack was still on top of the workbench at (18,0,1). The transceiver was fully configured and left on in RX mode. It was set at 10 MHz, i.e., a local radio station, to determine the effects, if any, of the simulated HEMP environment upon its operating characteristics. It was observed that the frequency setting was incremented to 10.003 MHz after three pulses. Measurements taken on the combined antenna feedlines did not yield a true measure of the combined antenna currents; however, the measured waveform has a dominant frequency of about 10 MHz, which indicates the matched load effect of the transceiver compared to test configuration IB without the transceiver.

Measurements taken on the transceiver ground lead indicated an average peak value of 131.9 A. These data can be understood from the measured bulk current on the ac power cable (about 180 A) and the shield current on the coaxial cable (about 70 A). That is, roughly one-third (i.e., 60 A) of the induced current on the ac power cable appears on the neutral wire and flows to chassis ground. This current would be combined with the coaxial cable shield current at the transceiver ground connection and result in about 130 A on this line. Note that the measured current on the dc power cable is only about 3 A, which indicates negligible direct field coupling and a common-mode rejection ratio (CMRR) of about 27 dB in the RF-3236R power supply transformer.

The transceiver was again left on in RX mode and tuned to 10 MHz. HEMP simulation had the same effect on the transceiver, although

now the frequency setting was decremented instead of incremented. Checks after each pulse showed that the frequency decreased by 1 kHz. This problem was solved by enabling the "frequency-lock" feature on the transceiver. Measurements on the RG-214/U coaxial cable at the transceiver rack showed an average peak shield current of 69.4 A. Measurements were then taken on the coaxial cable center conductor at the rack before and after the TPD. These currents had average peak values of 28.6 and 29.0 A, respectively. These currents were in response to an average peak current of 321.4 A measured on the combined RF-1912 and RF-1940 feedlines, which represent the maximum induced current at the antenna coupler. The data indicate arcing effects in the RF-1912 antenna feedline, combined with the normal response of the RF-1940 antenna, which serves to limit the maximum induced current at the coupler.

The rack-mounted transceiver was then placed on top of a stand at (0,0,5). This was test configuration II, which results in the maximum direct field coupling to the transceiver electronics (see fig. 18). The transceiver was again left on in RX mode at each of the allocated frequencies. Functional checks were made on the transceiver after each pulse. The objectives of these tests/inspections were to (1) determine the effects of the simulated environment, if any, upon the transceiver and (2) observe if the TX/RX functions were still operational. On this date, only the RF-1912 antenna was used. The radiated pulse had a variety of effects upon the transceiver. At times, both the LED display on the transceiver was scrambled and the front panel controls were locked, and at other times only the prior effect was observed. Power cycling was necessary to fix both situations. The scrambled display made the LED segments unintelligible, which made it difficult to determine the frequency setting for the transceiver. The TX/RX functions were still operational, although communication with the NATC facilities was garbled. This was probably due to center frequency drift for the transceiver in upper sideband mode. Since this identified susceptibility could be corrected by power cycling, it did not represent a HEMP vulnerability.

Measurements taken on the RF-1912 antenna lead showed an average peak current of 143.9 A. This documented the maximum induced antenna current for the RF-1912 into a matched load where the corresponding induced current for a 50- $\Omega$  load was 125 A. Measurements taken on the coaxial cable center conductor, before and after the TPD at the transceiver, showed average peak values of 21.4 and 19.1 A, respectively. These measurements indicated that non-linear effects were not significant for the coaxial cable TPDs.

It is interesting to note that in this configuration, the current waveform induced in the RG-214/U cable and the ac power cable are as expected for cables laying on the ground, except for a sharp early-time pulse. This early-time response is due to the vertical E-field coupling to the vertical runs of cable required to reach the transceiver at (0,0,5). This part of the induced waveform is directly proportional to the vertical component of the E-field. The ac power cable is deployed in basically the same manner as in test configuration IB (except for an extension cord used for the vertical run), so that the induced current amplitude for the horizontal cable response is roughly the same. The RG-214/U cable is basically looped back to the transceiver at (0,0,5) in this configuration so that the induced current amplitude is roughly one-half of that measured in test configuration IB. As expected, the early-time response is about the same for both cables since the vertical length of cable and the driving E-field is about the same. The measured current on the dc power cable also exhibits this early-time response characteristic and a dominant frequency of 273 kHz. As before, the steady-state transformer response leads to a peak amplitude of about 3 A, but the early-time peak amplitude is about 5 A.

The RF-1912 antenna was subsequently replaced with the RF-1940 antenna in a monopole configuration. By uncoiling only half of the entire dipole and resting the unwound portion on the top of the stand, a monopole antenna of about 5-m vertical height was constructed. In order to accommodate this new configuration, the coupler was moved to the base of the stand at (1,1,0). The rack-mounted electronics were still positioned at (0,0,5). This is referred to as test configuration III (see fig. 19). Measurements of the monopole antenna current had an average peak value of 66.8 A. An average peak value of 72.7 A was measured on the coaxial cable shield at the transceiver rack, while about 69 A was measured at the coupler. The coupler ground connection was measured to have a peak current of about 66 A, while the transceiver ground connection had a peak current of about 113 A, which indicates the contribution of the induced current on the ac power cable to the transceiver ground connection.

Authorization was obtained to change the highest allocated frequency to 23.245 MHz because of other transmissions on 24.430 MHz. The RF-1940 monopole configuration was also replaced with a 5-m section of aluminum wire connected in the same manner. The effects of simulation testing before and after the frequency adjustment remained the same. The LED display was again scrambled. This new configuration resulted in a peak current of 70.1 A on the monopole antenna with the coupler in by-pass mode (since it was not required to tune this antenna).

After a few pulses, the test configuration was switched back to the RF-1940 dipole antenna. This was due to the fact that the transceiver required the coupler to tune the monopole antenna only at 7.595 MHz so that the coupler was in by-pass mode at the other allocated frequencies. Next, the dynamic microphone was connected to the transceiver and its cable was extended vertically for a total length of about 1 m. The measured vertical component of the E-field was about 20 kV/m at this location. Measurements on the microphone cable had an average peak value of 17.2 A. The dynamic microphone was then replaced with the electret microphone and similar measurements were taken. Currents measured on the extended cable showed an average peak value of 42.8 A.

No observable effects on the TX/RX functions were noted even with the microphone key locked during pulse testing. The simulation results for the two different microphones can be understood in terms of coupling to a top-loaded monopole antenna which increases the antenna effective length and reduces the antenna resonant frequency. The electret microphone represents a capacitive top-load and has an induced response (when scaled to a threat-level amplitude) about twice the calculated threat and a lower resonant frequency. The dynamic microphone represents an inductive top-load and the induced current amplitude (when scaled to a threat-level) is about as calculated; however, the resonant frequency is lower than expected. The microphone cable connected to the rack-mounted transceiver has a resonant frequency of about 20 MHz.

## 6.2 Current Injection Tests

Direct current-injection (CI) testing for the hardened RF-3200 system involved direct-drive test techniques for validating the operation of selected external TPDs for HEMP protection without affecting the normal system operation. Additional CI tests were not conducted due to time constraints. The CI testing that was accomplished verified the clamping level of the coaxial cable TPDs for a low-level transient pulse. At an input level just above the TPD clamping threshold (i.e., 350 V), the TPD operation could be measured.

The TPD was tested in a 50- $\Omega$  system using a 50- $\Omega$  resistive load. A representative example of the measured input current is shown in figure 20, which corresponds to a peak input voltage of about 1000 V. The corresponding residual current is shown in figure 21. At input voltage levels much higher than the TPD clamping threshold, the peak residual voltage is limited to about 75 V. Since the injected transients were similar to HEMP-induced transients, which are on much shorter

Figure 20. Measured TPD input current for a 50-Ω line.

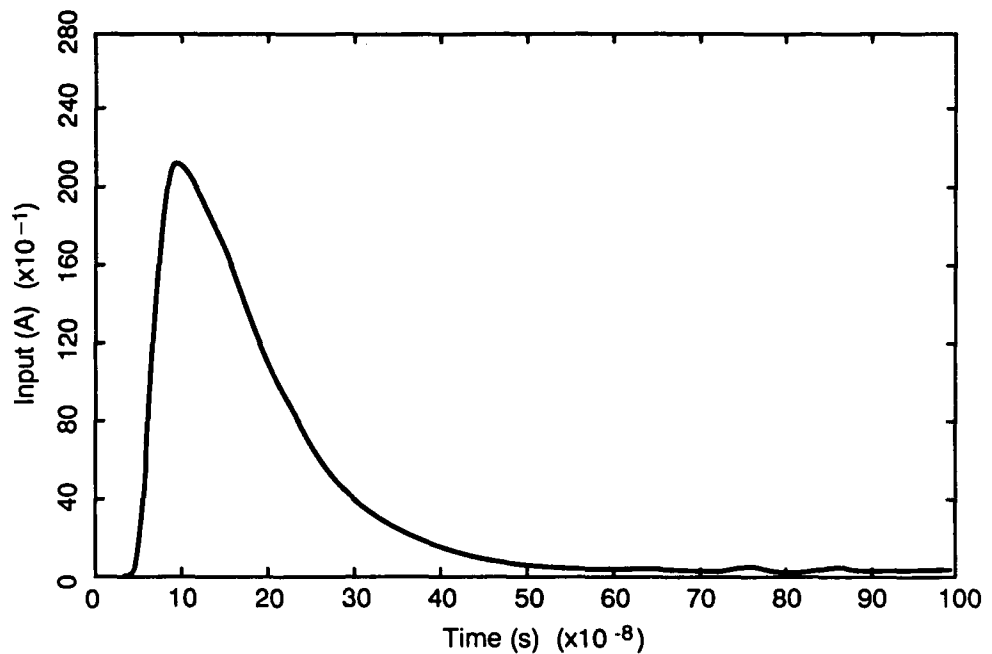
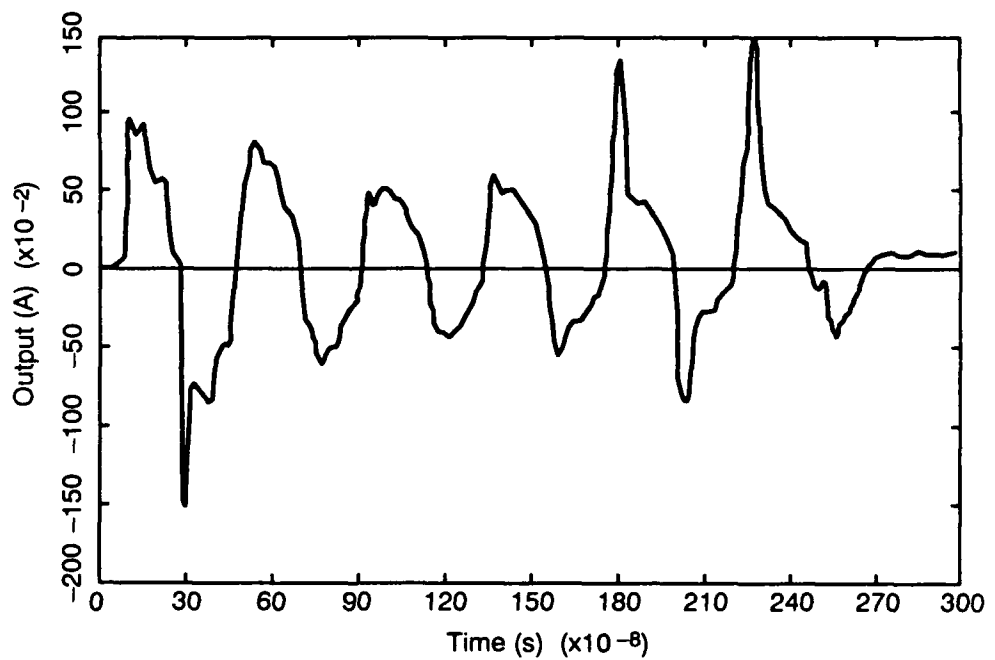


Figure 21. Measured residual current for a 50-Ω load.



time scales than the operational signals, it could be readily seen that the TPD response would not affect the system operation.

### 6.2.1 Power Supply Interface

Under the NDI program, CI testing was accomplished on an RF-366 power supply using an input current with a peak amplitude of 500 A

[11]. The RF-366 was tested under operational conditions with no effect on the system functional response. The power supply had no external protection devices and internal MOV protection devices similar to the RF-3236R power supply. Thus the NDI program CI test results should extend directly to the RF-3236R power supply; however, since these results have not been completely verified for the RF-3236R, the confidence in HEMP survivability is reduced. In terms of mission requirements, the RF-3200 transceiver is designed to operate from 13.6 Vdc power so that it can always be configured for battery operation.

The HEMP-induced stress at a wall receptacle would actually be much lower for typical commercial power systems since the effect of transformers, surge arrestors, and installation/distribution practices all serve to reduce the HEMP-induced transients which propagate throughout an office building. A strength level was established for the ac power input during the PI testing. That is, the RF-3236R has been shown to withstand the measured bulk current at the ac power input during the PI testing (a peak amplitude of about 180 A). Thus, if the residual HEMP stress after the ac power line protector, corresponding to a threat-level input, is less than the measured strength of the RF-3236R, survivability to the threat-level input is verified. Since time constraints did not permit additional CI testing on the MCG power line protector, the HEMP S/V of the RF-3236R power supply is based on the PI test results, previous CI test results on a similar power supply, and on engineering judgment.

### 6.2.2 *Transceiver Interfaces*

During the PI testing, the antenna, antenna cable, and rf cable are deployed so as to simultaneously couple the largest stress to the associated transceiver circuits. The PI testing establishes the coupled waveform and how the induced stress propagates through the system. The peak stress at the transceiver and coupler rf interfaces was imposed during the PI testing because arcing limited the induced current at the coupler. Thus additional CI tests are not required. The transceiver system survivability to the HEMP-induced antenna current has been verified based on the system functional response during and after the PI testing. For similar antennas, arcing effects will limit the HEMP-induced stress to the strength level verified in the PI tests.

## 7. Test Results for Hardened System

The initial test configurations for the hardened system were designed to establish the induced current conducted from the antenna to the RF-

3282 coupler. This was done in order to avoid damage to the transceiver early in the test period. The results for the RF-1912 alone, the RF-1940 alone, and the combined antennas connected to the RF-3282 (which was terminated into a 50- $\Omega$  resistive load) indicated that the maximum differential mode current was about 8 A, which is lower than the failure threshold established for the unhardened system (i.e., between 14 and 43 A). Test configurations IA and IB without the RF-3200 transceiver established the induced differential mode current conducted from the antenna for the unpowered but terminated RF-3282 coupler.

The rack-mounted electronics were then included but deployed roughly 18 m from the TES. Test configurations IA and IB with the RF-3200 were conducted with the transceiver in RX mode at the allocated frequencies. No observable effects were noted owing to the direct field coupling to the transceiver electronics. This is as expected, since the E-field at the transceiver location was only about 3 kV/m (see table 5 on p 65), which is less than the E-field exposure for the unhardened system.

For the fully configured system, the measured center conductor current from the combined antennas was only about 29 A at the transceiver. This demonstrated the matching effect of the RF-3282 coupler compared to test configuration IB without the transceiver. Although the TPDs were installed, the data indicated that the induced transients were not sufficient to trigger their operation (i.e., the measured current waveform before and after the TPDs were roughly the same). This implies that the measured center conductor current was not a completely differential mode current because the corresponding voltage level (i.e., 1450 V) would have triggered the TPD as can be seen by comparing figures 20 and 21. It is believed that the shorted RF-1912 response results in a common mode current rather than a normal differential mode signal.

The data for the RF-1912 antenna indicate a peak antenna current of only about 125 A and a current somewhat larger for the RF-1940 dipole. For the RF-1912 antenna feedline shorted to ground, the measured current peak amplitude is about 125 A and has a waveform characteristic of each feedline responding as a capacitive top-loaded monopole antenna roughly 11 m long (see fig. B-5(a) in app B). The measured waveform for the normal configuration of the RF-1912 and RF-3282 coupler indicates arcing in the antenna feedline (see fig. B-5(d) in app B). The sinusoidal frequency is about twice what would be expected, as was observed in the RF-1912 shorted antenna response of test configuration 0. The measured data indicated that each leg of the

RF-1912 antenna structure could be modeled as a capacitive top-loaded monopole antenna when arcing effects serve to short the antenna feedline to ground.

These results imply arcing effects in the RF-1912 antenna feedline connection. Evidence of arcing was confirmed at the RF-1912 feedline connection by a visual inspection which indicated discoloration. A microscopic inspection revealed burned and pitted markings on the antenna feed wires. The measured current amplitude indicates a voltage breakdown at around 11 kV. This is consistent with the air breakdown across a 0.6-cm gap. For sharply pointed to roughly spherical electrodes in dry air, the threshold for voltage arc-over across this gap spacing can be calculated to be from about 4 to 14 kV, respectively. This arcing served to limit the RF-1912 induced current so that the maximum current amplitude at the coupler for the combined antennas is only about 300 A (see fig. B-7). The measured waveform represents the superposition of the RF-1940 dipole response and the RF-1912 top-loaded monopole response.

Although the induced voltage at the coupler antenna I/O is on the same order as the gas tube firing voltage (i.e., 12 kV), there is no evidence that this TPD was conducting. Non-linear effects due to TPD operation were not evident; however, the measured current at the coupler rf I/O was substantially reduced compared to the induced antenna current. The data thus indicate the CMRR of the antenna coupler. With the coupler in an unpowered state and terminated into a 50- $\Omega$  load, the current attenuation from the antenna I/O to the load was about 30 dB. With the coupler and transceiver in a normal RX configuration, the coupler attenuated the current by about 20 dB. Since the current was attenuated but did not appear on the ground connection, it must have been rejected by the RF-3282 coupler. This trend would be expected at all RX frequencies unless the transceiver was tuned to exactly the antenna resonant frequency, in which case the induced differential mode voltage could trigger the TPDs.

The transceiver was subsequently deployed underneath the TES at a height of 5 m. The transceiver was exposed to a total E-field amplitude of about 36 kV/m. This E-field exposure affected the transceiver LED display and front panel controls. In the various test configurations the TX/RX frequency may have been changed, the LED display was scrambled, and the front panel controls may have been affected. In all cases power cycling corrected the observed effects and normal TX/RX operations could be restored. Thus the observed effects indicate a HEMP susceptibility but do not represent a HEMP vulnerability. This is because the mission requirements for this system lead to a pass/fail

criterion for HEMP S/V that allows system upset without damage. The system withstood the maximum induced antenna currents and the maximum E-field exposure possible in the simulated environments.

Measurements on the ac and dc power cables in test configuration IB indicated no non-linear effects due to the operation of the MCG power line protector. As expected, the induced current on the ac neutral line flows directly to the transceiver ground connection. Since the bulk wire current was divided approximately equally among the conductors, the load impedances must be similar (i.e., low impedance loads). Thus the voltage from wire-to-ground is at most a few hundred volts, which is not sufficient to activate the power line protector.

The measured bulk current on the dc power cable in test configuration IB with the RF-3200 was about 3 A, which dominated any hf transients owing to the field-to-wire coupling. Since this peak current was due only to the induced bulk current on the ac power cable phase wires (about 120 A), the CMRR that could be associated with the RF-3236R power supply is about 30 dB. The power supply transformer has the characteristics of a band-pass filter with a resonant frequency of 273 kHz.

In test configuration II, vertical lengths of the coaxial and ac power cables were required to reach the transceiver. The effect of the vertical E-field coupling to these vertically oriented sections of cable is readily evident in the measured current as an early-time response, which is directly proportional to the vertical E-field. This early-time response also appears on the dc power cable with the peak amplitude attenuated roughly 25 dB, due to the RF-3236R power supply transformer response.

## 7.1 Test Data Summary

The following table summarizes the available test data for each of the last four test configurations with the transceiver. Table 5 provides the total E-field peak amplitude calculated at the antenna location and the corresponding induced antenna current. In general, these values represent an average of a series of measurements. The measured E-field components are used to calculate the total E-field (i.e., the vector sum) at various locations. The measured data for the coaxial cable shield current on the RG-214/U cable are also shown in table 5, but these data are not available in all configurations. The effects listed in table 5 correspond to the transceiver being left on, in RX mode, during the simulation testing.

**Table 5. Summary of Measured Peak Current Amplitudes for Hardened System**

System configuration	Total E-field at antenna (kV/m)	Induced antenna current (A)	Total E-field at transceiver (kV/m)	Coaxial cable shield current (A)	Transceiver functional response
IA	41.8	125	2.9	—	No observed change. TX/RX satisfactory at all frequencies.
IB	41.8	321	2.9	69	No observed change. TX/RX satisfactory at all frequencies.
II	41.8	144	30.6	—	LED display scrambled. TX/RX satisfactory at all frequencies.
III	19.5	67	30.6	73	LED display scrambled. RX satisfactory.

Although not shown in table 5, tests were also conducted in which the transceiver was manually tuned to a single frequency (10 MHz) instead of a frequency previously programmed into the transceiver memory. It was discovered that this made a difference in the observed effects. It appears that the tuning display is more vulnerable to HEMP effects when it is set to a frequency not previously stored in memory. During test configuration IA with the transceiver, for example, it was observed that the frequency setting was incremented after each pulse. Likewise for test configuration IB with the transceiver, although instead of incrementing the tuned frequency, the setting was decremented. In both cases, however, the TX/RX functions were unaffected and communication capability was confirmed at the original frequency setting. The effect was even more severe for test configuration II. This time, the LED display was scrambled and the transceiver controls were found to be locked. Power cycling was necessary to return control to the transceiver front panel. Fortunately, however, the RF-3200 memory remained intact and unaffected so this functional response does not represent a HEMP vulnerability.

During the last configuration, communication with the on-site hf equipment was not possible at the highest NATC frequency due to other transmissions. Although the allocated frequency was later changed to 23.245 MHz, reception in upper side band mode was still garbled and barely perceptible. This effect seemed to be due to the

changed TX/RX center frequency, and effective communication required power cycling.

Table 6 is a summary of all the measured E-field and H-field components. All of the values shown are measurement averages. Those values which have been left blank were not measured. The total E-field is the vector sum of all three measured components. All location coordinates are expressed in meters with respect to the TES coordinate system and represent only approximate distances. The data indicate that the assumption of a radiated plane wave pulse is not completely valid at the test object locations.

## 7.2 Conclusions

The PI testing served to expose the RF-3200 system to a simulated HEMP environment. No failures were observed that could not be corrected by power cycling.

### 7.2.1 Direct Field Coupling

The effects of the direct field coupling to the system electronics were obvious but did not represent a HEMP vulnerability. When exposed to a threat-level environment, a significant difference in the system functional response would not be expected. In addition, some degree of attenuation would be afforded by even an unshielded office building, so that the transceiver would actually be exposed to a HEMP environment similar to that shown in table 6 at location (6,0,9). The coupler would be installed on its base plate as in the PI tests so that the

Table 6. Summary of Measured Field Amplitudes for Hardened System

Location	Quantity	Measured field component			Total field (kV/m)
		X	Y	Z	
(6, 0, 0)	E-field	16.5 kV/m	2.9 kV/m	2.9 kV/m	17.0
(6, 0, 9)	E-field	41.8 kV/m	—	—	—
(18, 0, 0.6)	E-field	15.6 kV/m	1.4 kV/m	1.5 kV/m	15.7
(0, 0, 5)	E-field	30.6 kV/m	2.7 kV/m	19.5 kV/m	36.4
(6, 0, 0.3)	H-field	—	132.9 A/m	—	—
(18, 0, 0.3)	H-field	—	130.7 A/m	—	—
(18, 0, 1)	H-field	—	133.6 A/m	—	—
(0, 0, 5)	H-field	—	152.6 A/m	—	—

threat-level environment would likewise be reduced and the direct field exposure would be similar to that shown in table 6 at location (6,0,0). Since the effects of the direct field coupling on the RF-3282 antenna coupler were not obvious, the coupler should also survive a threat-level HEMP environment without damage.

Thus, based on the PI test results and engineering judgment, the hardened RF-3200 system, in a typical office building installation, could withstand exposure to the HEMP threat environment. The risetime of the TES environment is faster than the DE waveform but slower than the E1 waveform; however, the effect of the additional hf coupling to this system should not significantly affect the system functional response. In addition, the peak amplitude of the E1 waveform is more readily attenuated by a building structure and/or equipment cases compared to the DE waveform. Thus, based on the PI test results and engineering judgment, the RF-3200 system would also withstand the direct field coupling associated with the E1 threat.

### 7.2.2 *Field-to-Wire Coupling*

The coupling to the cables associated with the RF-3200 system was as expected. Leakage through the coaxial cable shield was not apparent in the measured data compared to the signal conducted from the antenna. When the shield current is scaled to a threat-level amplitude, the leakage through the cable shield is a negligible contribution to the total HEMP-induced stress at the transceiver. The PI testing thus verified the hardened RF-3200 system (i.e., using the RF-3282 coupler) survivability to the HEMP *field-to-wire* coupling to the coaxial cable. For the E1 waveform, the induced cable shield current would be smaller, owing to the shorter pulsewidth compared to the simulated environment. The enhanced hf leakage through the cable shield is still a negligible contribution to the total HEMP-induced stress at the transceiver. Thus the RF-3200 system would withstand the *field-to-wire* coupling to the coaxial cable, which would be associated with the E1 threat.

The microphone input on the transceiver front panel was addressed during the PI tests. The microphone cable was oriented for worst-case coupling during the PI testing. Testing was under operational conditions, so the survivability of this interface was established, at the measured levels, from the transceiver functional response during and after the PI testing. When scaled to a threat-level, the induced stress amplitude is similar to the threat used for the microphone input on the RF-350K. This interface was previously CI tested to a microphone cable shield current amplitude of 70 A, which had a waveform with

significantly more energy content than that measured during the PI testing [11].

The microphone cable shield should provide more attenuation at 20 MHz than assumed in the S/V analysis (see sect. 3.4.2). Assuming a current attenuation of 20 dB, the threat-level HEMP-induced bulk cable current is about 7 A. For  $I_w = I_B/2$  and a multiconductor cable source impedance of 100  $\Omega$ , we have  $V_{oc,HEMP} = 350$  V at 20 MHz. The voltage across the input capacitors can be calculated to be about 28 V so that the HM = 5 dB (see sect. 3.4.2). Note that the capacitor rated voltage is taken to be the dc value which leads to a very conservative analysis. Since the microphone interface for the RF-3200 is like the RF-350K, the system HEMP survivability is verified based on the RF-3200 functional response during the PI tests, the CI tests conducted on the RF-350K, and the calculated HM.

The transceiver dc power input has a worst-case HEMP-induced  $I_{sc}$ , as calculated in section 3.2.3; however, the induced load current is determined by PI testing. This interface is addressed during the PI testing by orienting this cable for maximum coupling. The cable was formed in a loop and the induced current was monitored with the rear panel of the rack removed. The induced current waveform on the dc power cable was dominated by the response of the power supply transformer. The direct field coupling to this line was negligible and the system HEMP survivability was verified based on the transceiver functional response to the residual stress after the power supply.

The CMRR owing to the transformer response of the RF-3236R power supply was measured to be about 27 dB. Thus even for a 500-A HEMP-induced peak wire current (i.e., a bulk current of 1500 A), the residual HEMP-induced bulk current at the transceiver dc power input is a damped sinusoid with a peak amplitude of about 67 A and a resonant frequency of 273 kHz. If the entire threat-level bulk current appeared as a wire current it is still much less than the 465-A failure current of the transZorb at the transceiver dc power input (see sect. 3.4.1). The HM can be calculated to be more than 16 dB. Under reverse bias, the energy content of this threat-level stress waveform is much less than the 1300-J failure level of the diode at this interface. Thus no damage to the RF-3200 would be expected for a severe worst-case HEMP-induced current on the ac power line. Based on the PI test results, the calculated HM, and engineering judgment, the RF-3200 dc power interface is considered hard to a threat-level environment. Based on the PI test results, the NDI program CI tests, and engineering judgment, the RF-3236R is also considered hard to a threat-level environment. Since the threat-level stress for an E1 waveform would be

similar or lower, these interfaces are also hard to the E1 threat environment.

A summary of the calculated HMs are shown in table 7. Also included are the revised HMs based on the available test data extrapolated to a worst-case threat as discussed above. The RF-3236R power supply S/V is based primarily on the NDI test program. The RF-382-01 antenna coupler power/control interface at the transceiver is summarized in table 7, but test data were not available to revise the HM. Similarly, the current attenuation associated with the rf line could not be verified so the test data do not allow a revised HM calculation. As can be seen, the revised margins associated with the HEMP *field-to-wire* coupling are positive and indicate system survivability for this coupling mechanism. For the E1 waveform the HM results would be similar or smaller.

### 7.2.3 Antenna Coupling

Although the HEMP-induced current on the antennas that could be used with the RF-3200 system is substantial, the PI testing demonstrated that typical antenna feed structures cannot support these high-voltage transients. Arcing in the antenna feedline would occur at some level for any practical antenna configuration, except possibly a monopole antenna. In this case, the TPD at the coupler connection would serve to limit the HEMP-induced transient. Assuming the voltage at the coupler antenna input would be limited to about 12 kV, the peak input current amplitude would be less than 300 A. Since the combined antennas resulted in an input current greater than 300 A, the HEMP survivability of the RF-3282 coupler has been verified to this level. The HEMP-induced antenna current would be substantially reduced for an E1 threat environment as shown in figure 10, such that the HEMP survivability of these interfaces to the E1 waveform is directly verified by the PI test results.

Table 7. Summary of Pre- and Post-Test Calculated Hardness Margins for HEMP Field-to-Wire Coupling

System interface	Pre-test HM	Post-test HM
RF-3200 rf input	28 dB	28 dB
RF-3200 microphone input	11 dB	5 dB
RF-3200 dc power input	24 dB	16 dB
RF-3236 ac power input	NDI test	NDI test
RF-382-01 power/control	36 dB	36 dB

The PI testing also demonstrated the CMRR of the antenna coupler (without damage) and the corresponding reduction in the peak amplitude of the residual current. The survivability of the RF-3200 transceiver is thus verified to this residual current level (i.e., 29 A) and is considered to be hard to the HEMP-induced current conducted from the antenna. The hf coupling effects associated with the E1 waveform have been shown to be insignificant except for small antennas. The enhanced coupling which could occur for short monopole antennas would be attenuated by the RF-3282 coupler so that the RF-3200 system is considered to be hard to the HEMP-induced antenna currents which would result from the E1 waveform.

### 7.3 Recommendations

Radiated PI testing on the fully deployed RF-3200 system established the system survivability to the simulated HEMP environments. The test results demonstrated those aspects of the system response which determine the HEMP-induced stress at the various system interfaces. Based on a typical air-gap, which would be associated with a dipole antenna feedline, one can conclude that arcing effects would occur at an antenna  $V_{oc,HEMP}$  of less than about 14 kV. The PI test results also established the CMRR associated with the RF-3282 antenna coupler and the RF-3236R power supply.

Based on the test and analysis results, several recommendations can be made for the hardened system to be installed in typical office buildings. It is recommended that the RF-3282 coupler always be connected, even if unpowered or in by-pass mode, since it serves to reduce the HEMP-induced stress at the transceiver. It is recommended that a fast-response-time gas tube with a clamping voltage between 8 and 12 kV always be installed at the coupler antenna connection. This provides a high confidence in HEMP survivability for this system when used with an arbitrary antenna. For the same reason it is recommended that coaxial cable TPDs be installed at both the coupler and transceiver connections. It is also recommended that a power line protector be installed on the ac power input to provide high confidence in HEMP survivability for an arbitrary commercial power service. Thus, although the operation of the TPDs was not evident in the PI test results, their proper installation increases the confidence level in the RF-3200 system survivability to a HEMP threat environment or other high-level electromagnetic environments such as lightning.

The TPDs initially chosen for the RF-3200 system are believed to be more than adequate for HEMP protection without affecting the nor-

mal system operation. Laboratory CI tests confirmed this assertion for the coaxial cable TPDs. The peak voltage on the coaxial cable during operation with a kilowatt amplifier can be calculated as

$$V_p = 1.4 \times (P \times R)^{0.5} = 1.4 \times (1000 \times 50)^{0.5} = 313 \text{ V.} \quad (37)$$

The transient response of the TPD should limit the HEMP-induced voltage to less than three times this peak operating voltage. Thus the Fischer 350-V TPDs should be adequate for HEMP protection. The MCG power line protector should also limit the HEMP-induced voltage to less than three times the normal peak operating voltage (i.e., 504 V). Since the MCG gas tube has a clamping level of 415 V, this device should be adequate for the slow-risetime HEMP-induced transients which propagate from the commercial power grid through-out an office building.

An additional recommendation is that only double-shielded coaxial cables be used with this system. In this case the HEMP-induced stress coupled through the cable shield would always be less than that conducted from the antenna coupler. That is, under worst-case conditions for RG-213/U cable, the HEMP-induced stress owing to field-to-wire coupling is only 3 A, whereas the unhardened system has been shown to be hard to a larger differential mode signal on this line. The PI test results also demonstrate that good ground connections are required at the transceiver and coupler to divert the HEMP-induced transients on the coaxial cable shield and the ac power line. Although the analysis results for the microphone cable(s) indicate system survivability to the HEMP-induced stress at this interface, the PI test results demonstrated that reduced coupling could be obtained by using the electret microphone exclusively.

## 8. HEMP Survivability Statement

The authors believe that the hardened RF-3200 transceiver system, in a typical office building installation, is survivable when exposed to the E1 HEMP threat environment. Unfortunately there are several factors which serve to reduce the confidence level associated with this statement. Since the system was not exposed to the full threat-level incident E-field amplitude, it can only be concluded that it can withstand the direct E-field coupling up to a level of roughly 46 kV/m, which was the maximum horizontal E-field component measured at the transceiver location. As discussed in section 7.2, the location of the system elements as installed implies that they would not be exposed to the full threat-level environment; however, this restriction imposes constraints

on how the transceiver system is fielded. Thus the manufacturers recommendations must be followed in deploying the antenna and coupler and in making the appropriate ground connections.

Additional areas of uncertainty are the effect of the HEMP-induced transient on the commercial power service and the antenna. As previously discussed, the threat-level HEMP-induced transient on the ac power line, even if greater than 180 A, should not impact the system survivability. The HEMP-induced antenna current is the primary area of uncertainty in that the effect of a large differential mode current amplitude conducted from the antenna could not be investigated. If an antenna used with this system could deliver a large HEMP-induced differential mode current amplitude to the antenna coupler, it could adversely affect the system. However, the protection devices as installed are designed to protect the coupler and transceiver, in this case. Unfortunately, this could not be verified under this program. Additional PI testing at higher E-field levels and threat-level CI testing would be required to reduce or alleviate these uncertainties.

## References

1. DoD-STD-2169A, *High-Altitude Electromagnetic Pulse Environment*, 1985.
2. Bell Laboratories, *EMP Engineering and Design Principles*, New Jersey: Technical Publication Department (1975).
3. Harris Corporation RF Communications Group, *RF-3200 Series Product Line Service Manual*, Publication No. 10212-0300 (June 1988).
4. R. Strayer, S. Skovgaard, and T. Hill, *Final Report for EMP Demonstration Test*, Mission Research Corporation, MRC/COS-R-953 (August 1989).
5. G. J. Burke and A. J. Poggio, *Numerical Electromagnetics Code (NEC)—Method of Moments*, NOSC TD116 (1977), revised (1980).
6. E. F. Vance, *Coupling to Shielded Cables*, John Wiley & Sons, Inc. (1978).
7. *DNA EMP Handbook (U)*, Defense Nuclear Agency, DNA2114H (5 July 1979). (CONFIDENTIAL)
8. *EMP Assessment Handbook*, Air Force Weapons Laboratory, AFWL-TR-78-60 (April 1980).
9. *System Survivability in the Nuclear Age*, IRT Corporation (1985).
10. *Semiconductor Diode D.A.T.A. Book*, 33rd ed., D.A.T.A., Inc., Orange, NJ (1973).

11. R. Strayer et al, *EMP Hardening Guidelines for Army Nondevelopmental Items*, Mission Research Corporation, MRC/COS-R-890 (7 April 1989).
12. *Standard Operating Procedures for the TACAMO Electromagnetic Pulse Simulator*, Electronic Systems Department, Systems Engineering Test Directorate, Naval Air Test Center, Patuxent River, MD 20670-5304.
13. *Instrumentation Suite Test Preparation Guide*, BDM Management Services Co., II (29 May 1990).

## **Appendix A.—Test Data for Unhardened System**

Selected examples of the available test data are included in this appendix for all the various unhardened system test configurations. The data have been corrected, in the frequency domain, for the effects of the measurement probe and the data acquisition system. The data are presented in terms of both the corrected transient response measurements and the corresponding calculated spectral content. The locations shown are with respect to the coordinate system shown in figures 12 and 13 of the main report. Test point locations at a height of 1 m denote the transceiver location. Test point locations on the ground (or at a height of 5 m) denote the antenna location.

Figure A-1\* presents the measured electric (E-) field components at the transceiver location (200,30,1). The ground interacted horizontal E-field (fig. A-1 (b)) has a large initial pulse and a small late-time tail. For most systems, this E-field can be represented as an impulse so that the system response could be approximated by the system impulse response. Note that the radial and vertical E-field components near the ground have similar waveforms off the TES centerline. On the TES centerline, the horizontal and vertical E-field components near the ground have similar waveforms, as would be expected for a dipole radiator over a ground plane. The data also indicate that off the TES centerline, the vertical E-field component is significant compared to the horizontal component.

Figure A-2 presents the measured E-field components on the ground at the antenna location (200,10,0). The effect of the ground interaction is to reduce the amplitude of the horizontal component and effectively double the amplitude of the vertical component. The corresponding induced antenna current measurements are shown in figure A-3. As can be seen, the antenna responds as if driven by an impulse, with a fine structure that depends on the driving E-field spectral content. Note that the RF-382-01 antenna coupler, although damaged, serves to tune the dipole antenna so that more current would be delivered to the load. This effect can be seen in the frequency response by the broader dipole resonance obtained without the antenna coupler. This coupler serves to tune the antenna fundamental resonance (i.e., a lower Q-factor), but also tunes the higher order modes which can be seen in the transient response.

---

\*Figures are found at the end of this appendix.

## Appendix A

Various measurements of the ground-interacted horizontal E-field are shown in figure A-4. Note that at a fixed height above the ground, the peak amplitude scales approximately according to the range from the TES. For the E-field measurements on the ground at the antenna location (i.e., fig. A-4 (b) and (c)) the corresponding induced antenna currents are shown in figure A-5. Note that the induced current amplitudes scale roughly with the distance, and the induced transient is dominated by the antenna fundamental resonance.

Figure A-6 presents the measured horizontal E-field at the transceiver and antenna locations at roughly 80 m from the TES. Note the difference in the ground interacted E-field waveforms where the peak amplitude is heavily dependent on the height above ground. The waveform characteristics are more strongly dependent on the distance off the TES centerline. The measured antenna current corresponding to figure A-6 (b) is shown in figure A-7. The induced current at later times is proportional to the derivative of the driving E-field.

The measured E-field components at the transceiver location  $(-60, -30, 1)$  are shown in figure A-8. The transceiver was exposed to a predominantly vertically polarized E-field since it was located off the TES centerline. The measured E-field components at the location  $(-60, 0, 0)$  are shown in figure A-9. Since the E-field components were measured on the ground, the vertical E-field component exhibits the largest amplitude. The antenna was actually elevated 5 m and exposed to a horizontal E-field component of roughly 16 kV/m, which had a waveform similar to figure A-6 (a).

The corresponding induced antenna current is shown in figure A-10 (a). This measurement was taken with the RF-382-01 coupler tuning the antenna. The effects of the coupler can readily be seen in that the antenna resonances are more narrow and the higher order modes are enhanced. The transient response also indicates the contribution of higher order resonances and that the response is not readily damped.

The induced current on the RF-382-01 coupler ground cable was also measured and is shown in figure A-10 (b). Since the antenna is operated with respect to this ground connection, the antenna and ground cable currents should be similar. The discrepancy indicates a capacitive effect which prevents the higher frequency components of the induced current from flowing to ground. This effect can be seen in the frequency domain response and may contribute to the damage mechanism associated with the antenna coupler.

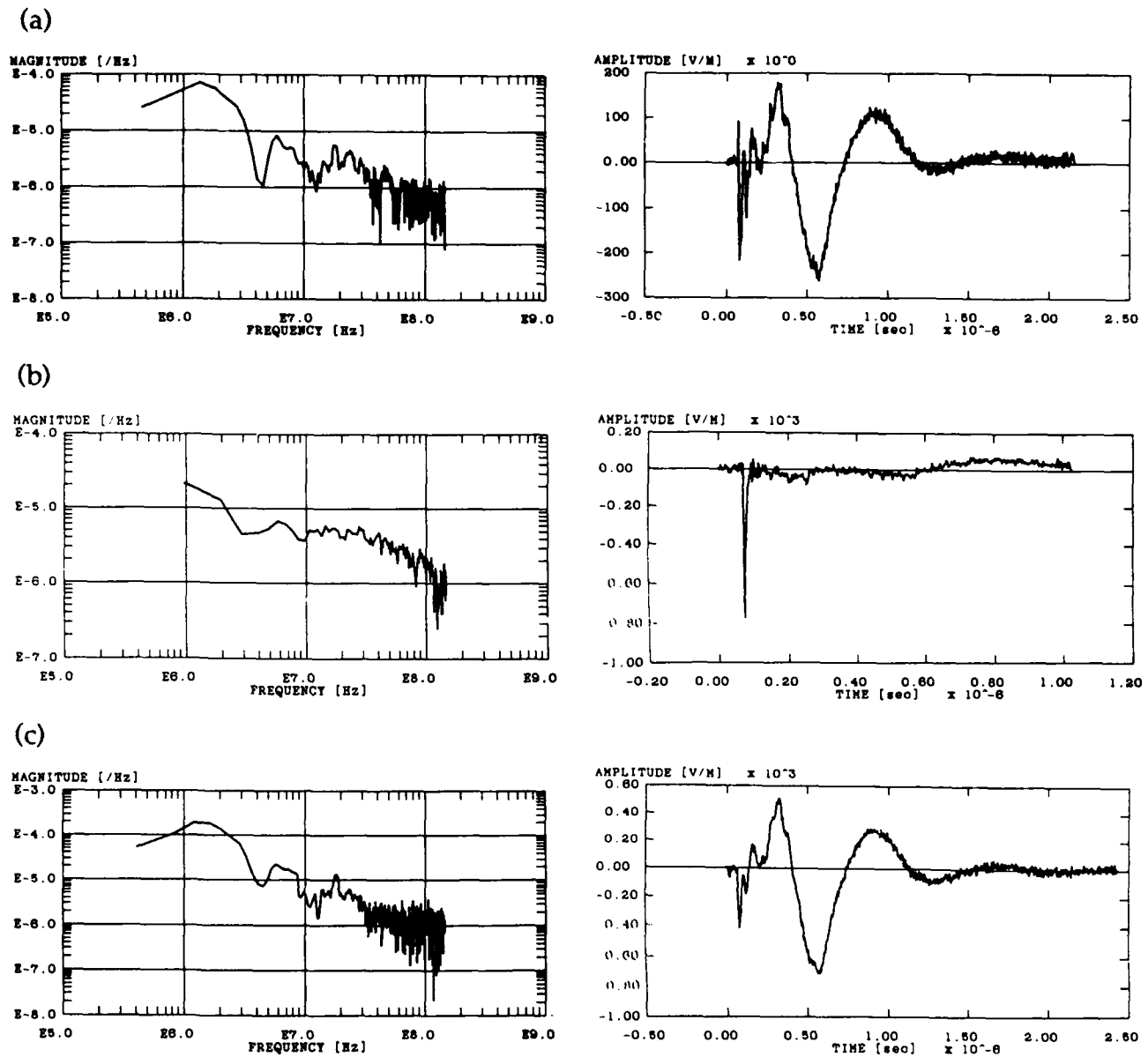
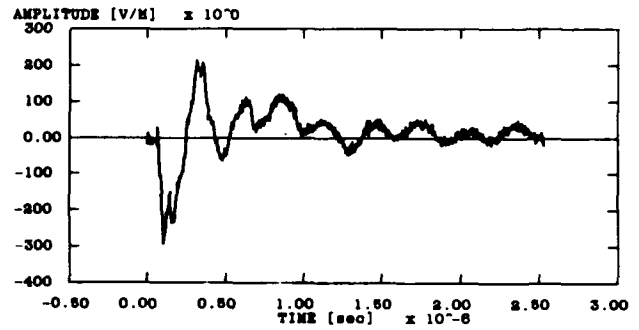
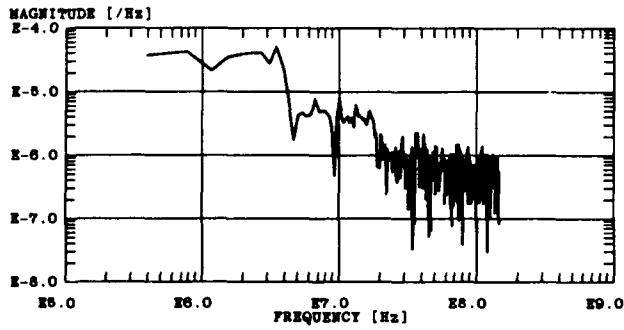


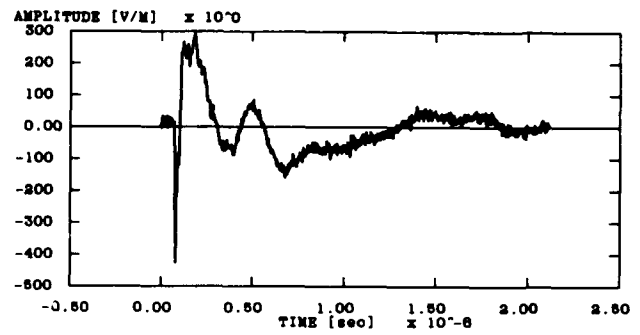
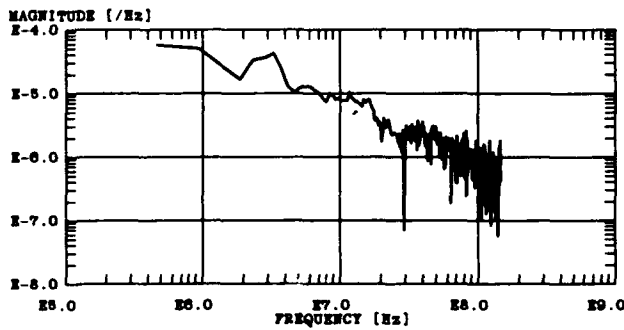
Figure A-1. Measured electric field components, magnitude and amplitude, at location (200, 30, 1): (a) radial (x-component), (b) horizontal (y-component), and (c) vertical (z-component).

# Appendix A

(a)



(b)



(c)

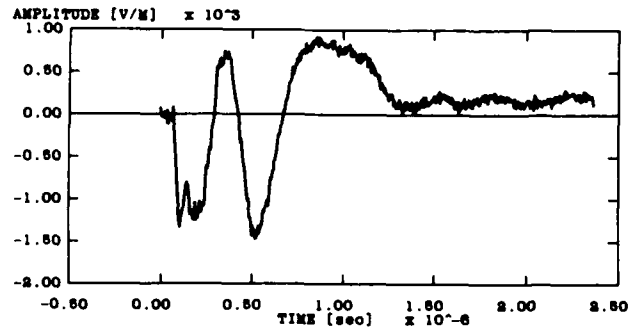
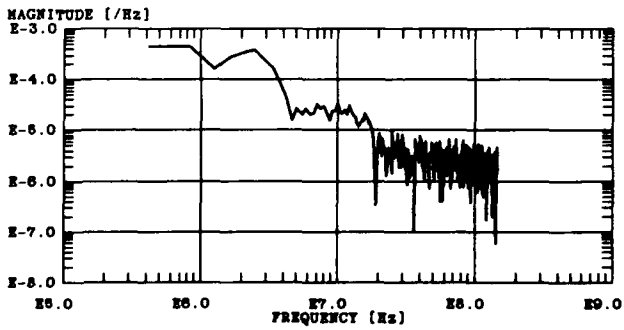
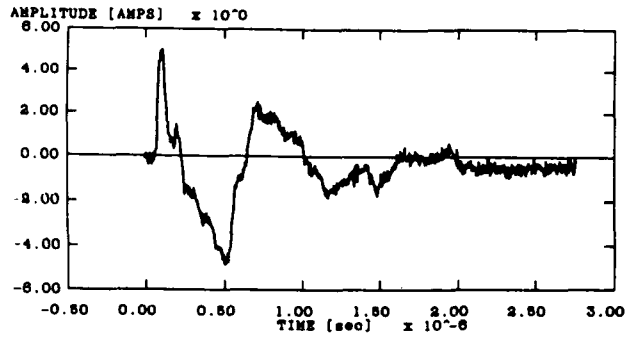
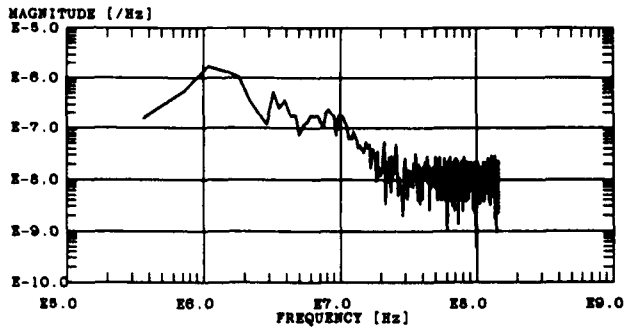


Figure A-2. Measured electric field components, magnitude and amplitude, at location (200, 10, 0): (a) radial (x-component), (b) horizontal (y-component), and (c) vertical (z-component).

(a)



(b)

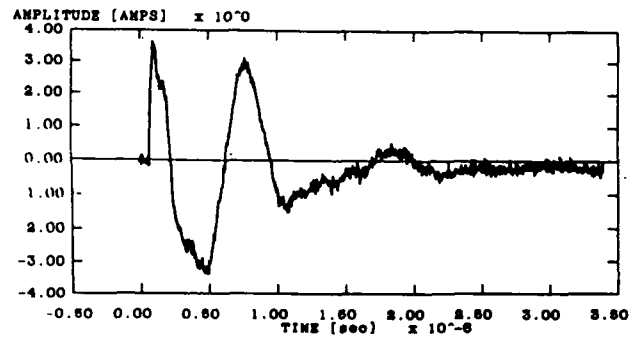
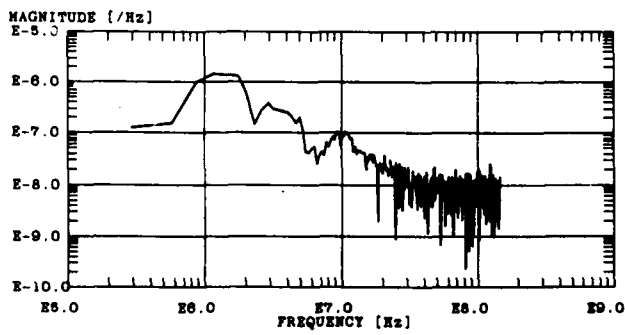
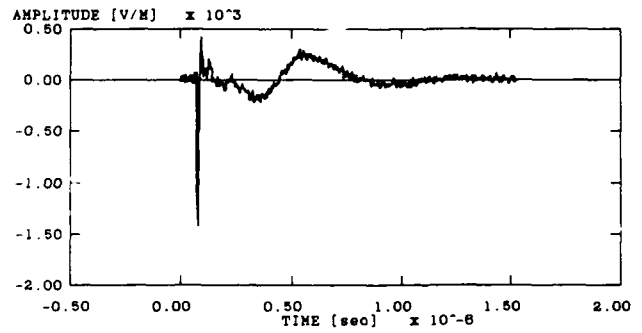
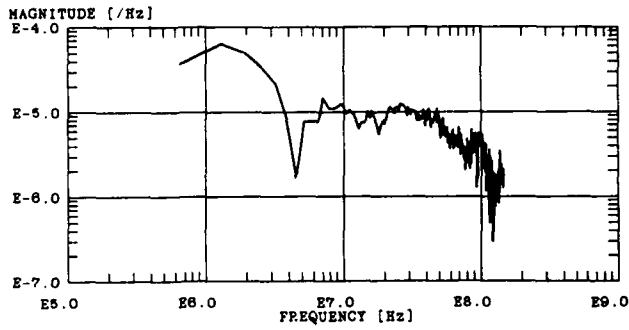


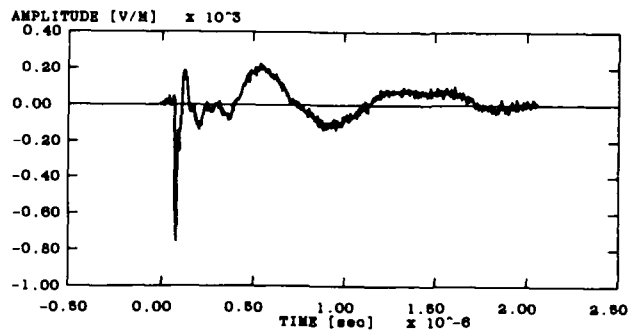
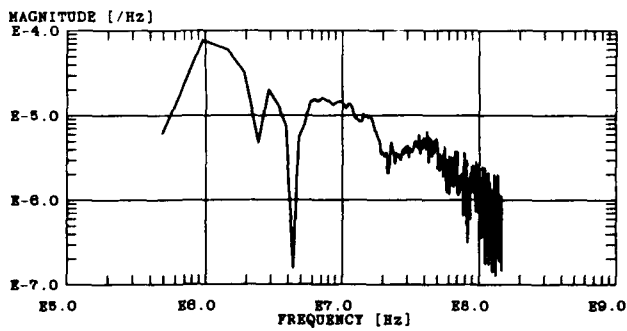
Figure A-3. Measured antenna current at location (200, 10, 0): (a) with the antenna coupler and (b) without the antenna coupler.

# Appendix A

(a)



(b)



(c)

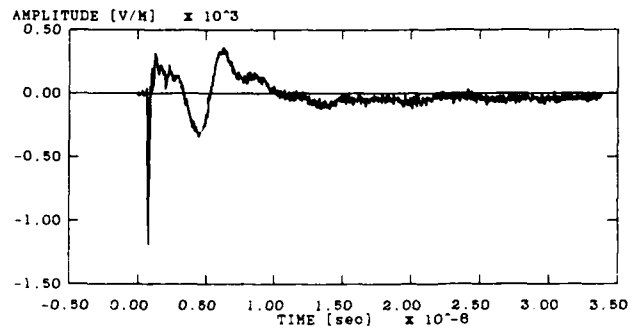
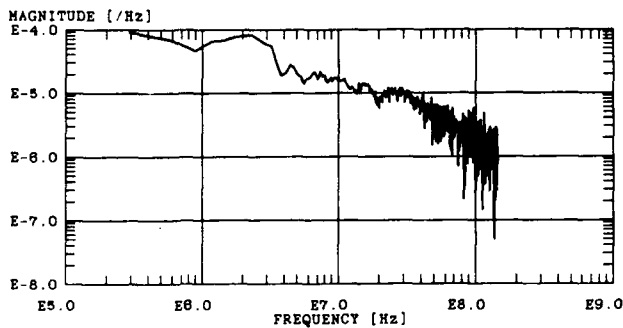
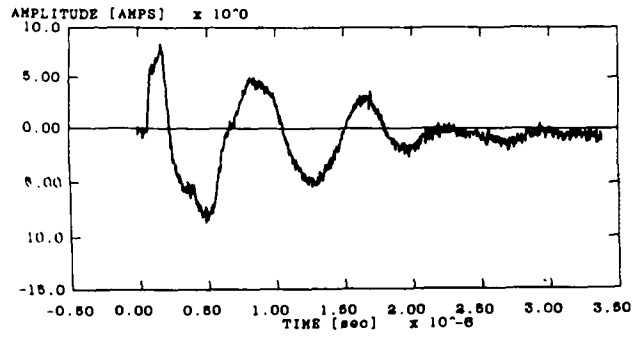
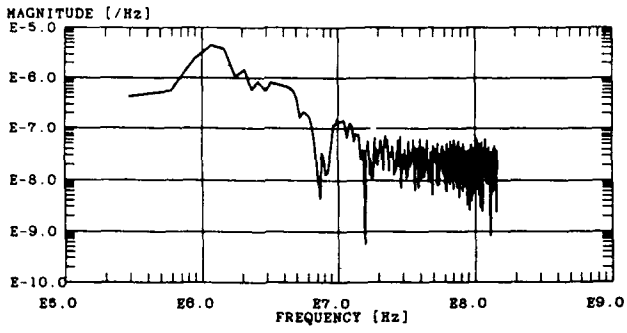


Figure A-4. Measured horizontal (y-component) electric field at locations: (a) (150, 30, 1), (b) (150, 10, 0), and (c) (110, 10, 0).

(a)



(b)

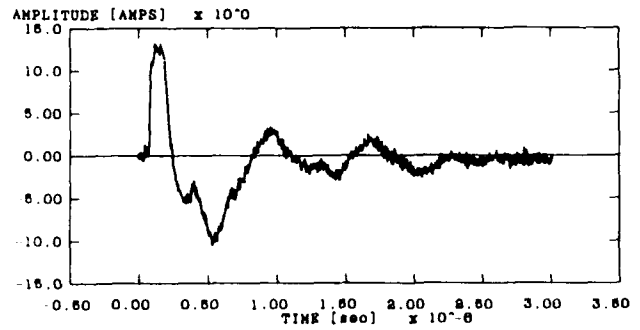
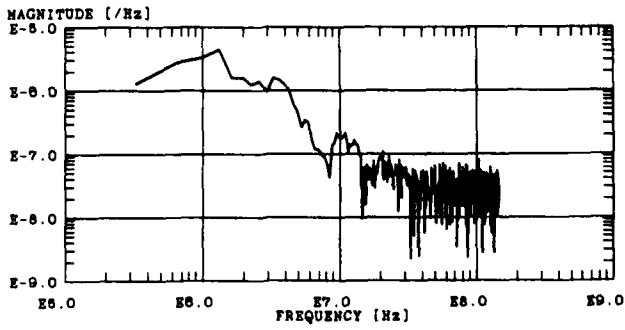
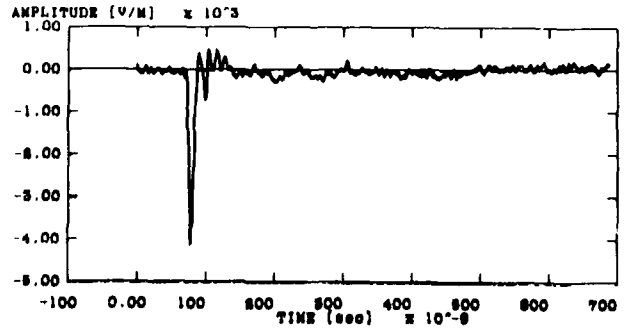
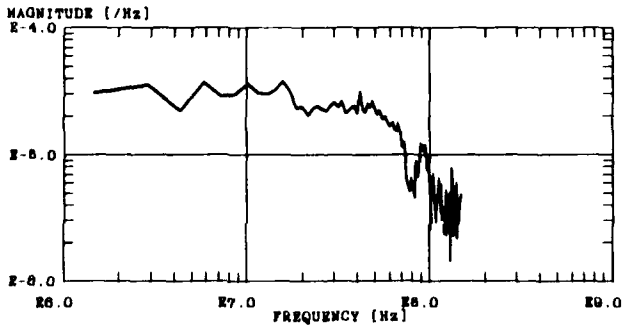


Figure A-5. Measured antenna current at locations: (a) (150, 10, 0), and (b) (110, 10, 0).

# Appendix A

(a)



(b)

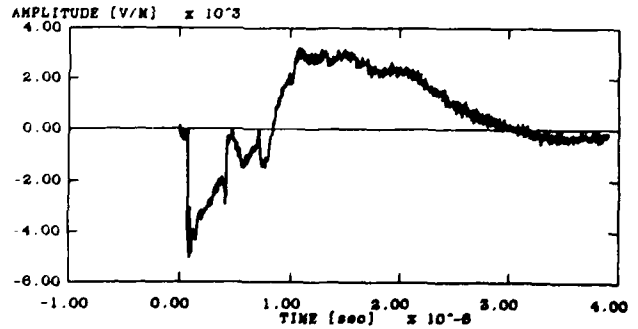
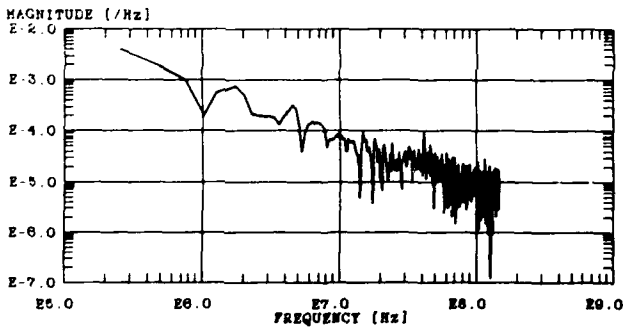
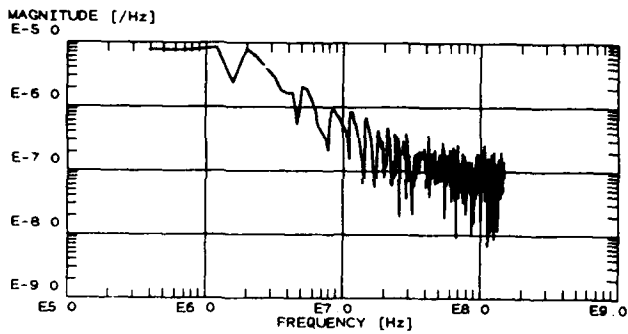


Figure A-6. Measured horizontal electric field (y-component) at locations: (a) (80, 20, 1) and (b) (80, 0, 0).

(a)



(b)

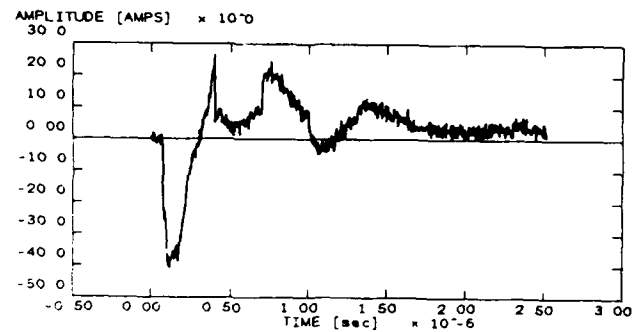
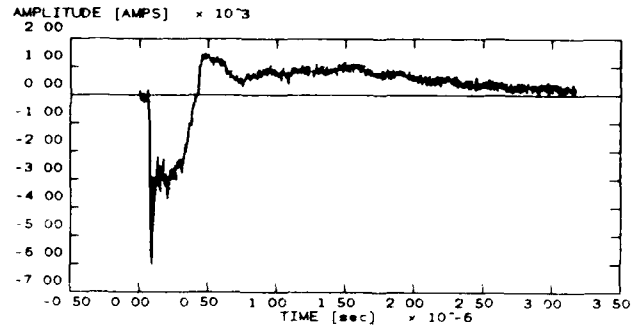
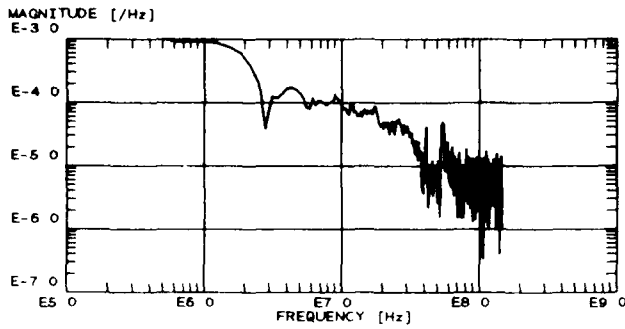
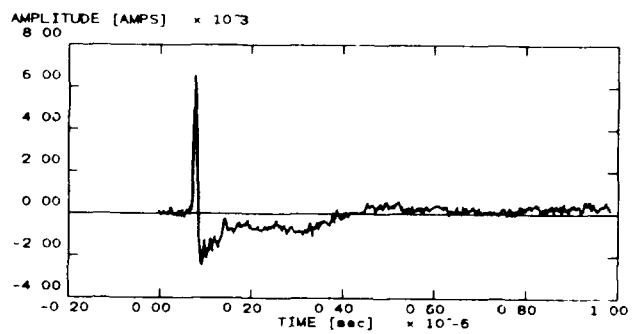
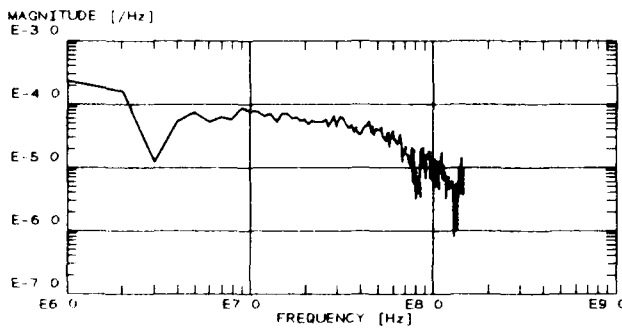


Figure A-7. Measured antenna current at location (80, 0, 0): (a) magnitude and (b) amplitude.

(a)



(b)



(c)

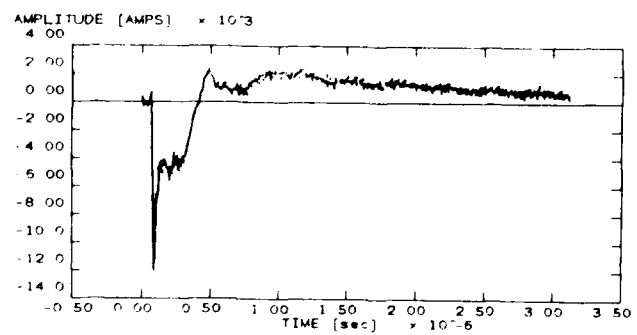
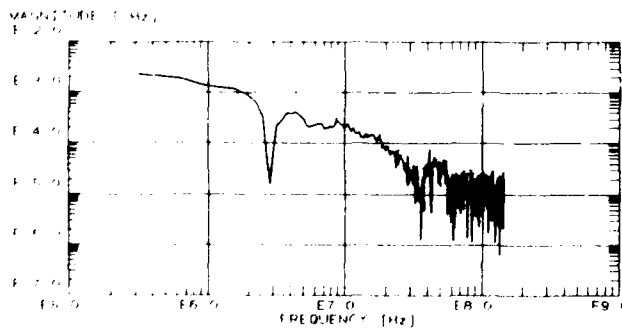
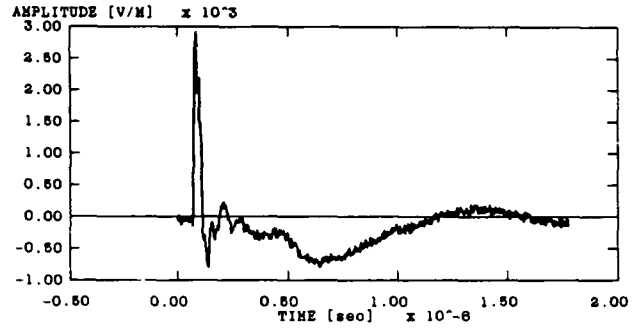
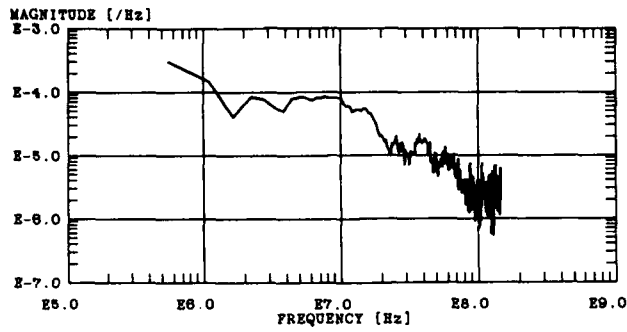


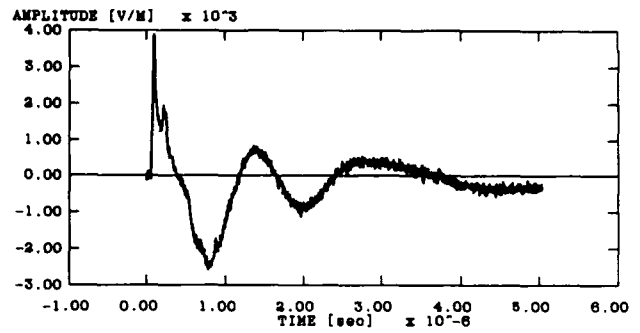
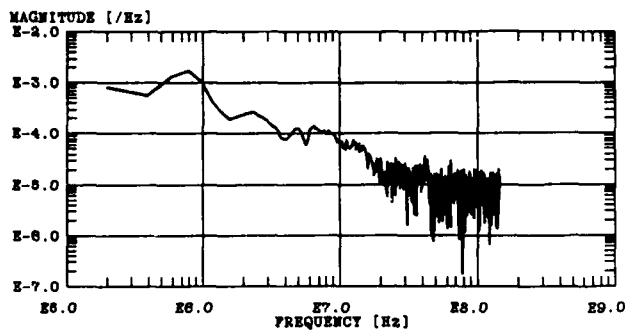
Figure A-8. Measured electric field component, magnitude and amplitude, at location (-60, -30, 1):  
 (a) radial (x-component), (b) horizontal (y-component), and (c) vertical (z-component).

# Appendix A

(a)



(b)



(c)

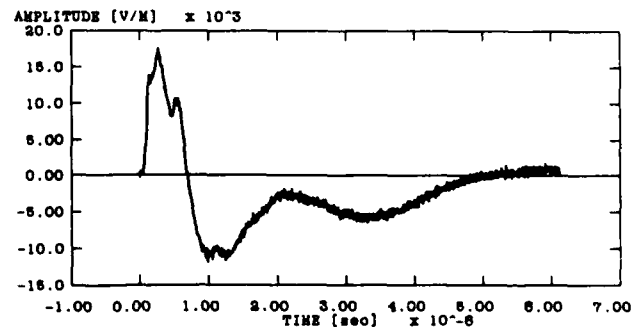
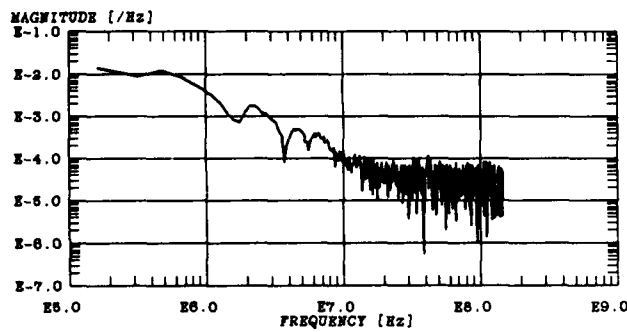
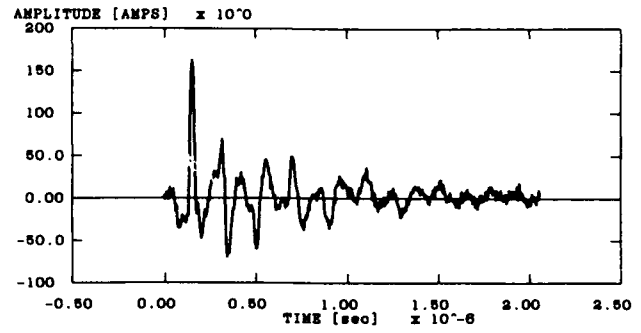
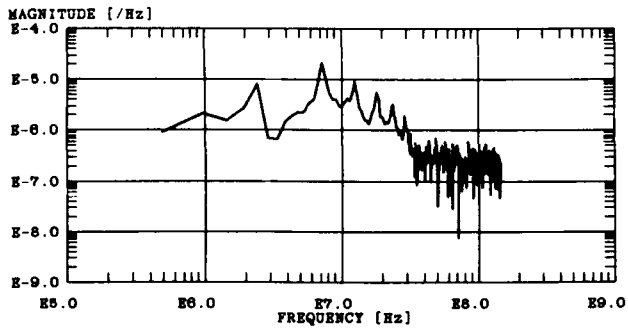


Figure A-9. Measured electric field component, magnitude and amplitude, at locations (-60, 0, 0): (a) radial (x-component), (b) horizontal (z-component), and (c) vertical (z-component).

(a)



(b)

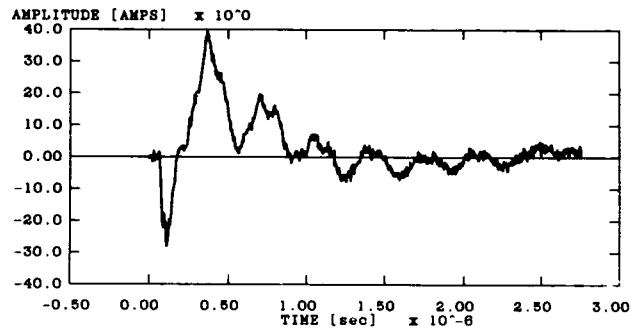
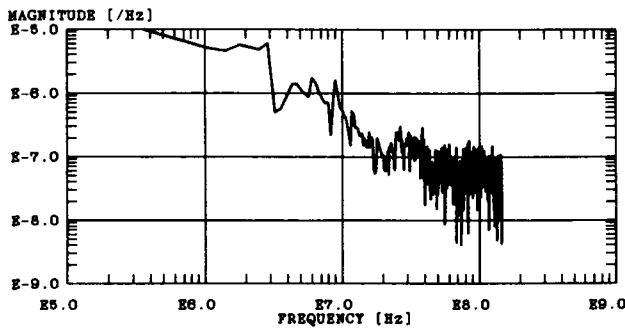


Figure A-10. Measured currents at location (-60, 0, 5): (a) antenna current and (b) coupler ground cable current.

**Appendix B.—Test Data for Hardened System**

This appendix presents typical examples of the data taken for each of the hardened system configurations. The graphs shown are for the corrected data, which have been processed in the frequency domain to remove the response of the data acquisition system. Both the time- and frequency-domain plots are shown for each measurement. The coordinates listed with each plot are with respect to the reference coordinate system shown in figure 12 of the main report. These coordinates are in meters with all fractions rounded to the nearest integer.

Figure B-1\* is a measurement of the electric (E-) field components at the transceiver location (18,0,1). The three sets of graphs show the radial (x-component), horizontal (y-component), and vertical (z-component) E-field components in both the time and frequency domains. The horizontal E-field component is shown in figure B-1 (b). In general, these waveforms show the expected characteristics for a horizontal dipole over a ground plane and resemble those measured in the unhardened configuration (see app. A). Figure B-2 presents all the measured E-field components at the coupler location (6,0,1). Figure B-3 shows the E-field at the transceiver while it was positioned on top of a stand at (0,0,5). The vertical E-field, shown in figure B-3 (c), was used as a rough estimate of the driving E-field for the RF-1940 monopole configuration as well as the microphone cable(s). The horizontal component of the E-field at location (6,0,9) is shown in figure B-4. This measurement indicates the maximum E-field that drives the RF-1912 dipole antenna.

The next five sets of data, figures B-5 (a) through (e), are measurements of the current on the RF-1912 antenna feedline in different test configurations. In figures B-5 (a) and (b), both antenna leads have been shorted to ground. Figure B-5 (a) is a measurement of one of the shorted leads and figure B-5 (b) is a measurement of both shorted leads. Note that the reduced current amplitude in figure B-5 (b) is due to current cancellation from the combined feedlines. Figures B-5 (c) and (d) are measurements of the antenna lead with the RF-1912 connected to the coupler antenna I/O and a 50- $\Omega$  load connected to the coupler rf I/O. Figure B-5 (c) shows a response which indicates arcing in the antenna feedline and figure B-5 (d) shows the expected response. The last measurement in this set, figure B-5 (e), shows the current measured on the RF-1912 antenna lead at the coupler input with the transceiver connected to

---

\*Figures are found at the end of this appendix.

## Appendix B

the coupler rf I/O. The tuning effect of the transceiver and coupler can readily be seen in comparing the measured data taken under the various antenna load configurations.

Figures B-6 (a) and (b) show the current measured on the RF-1940 feedline during different test configurations. For figure B-6 (a), the RF-1940 was configured as a horizontal dipole and connected to the coupler antenna I/O with the 50- $\Omega$  load connected to the coupler rf I/O. In figure B-6 (b), the RF-1940 is configured as a vertical monopole antenna connected to the coupler antenna I/O with the transceiver connected to the coupler rf I/O. Due to the fact that both of these plots show the expected frequency characteristics, it is possible to conclude that the RF-1940 feedline did not exhibit arcing effects (unlike the RF-1912 dipole). Figure B-7 is a measurement with both the RF-1912 and RF-1940 dipoles connected to the coupler and the transceiver connected to the coupler rf I/O. These data, included for comparison purposes, clearly show the superposition of the earlier two plots, figures B-6 (a) and B-5 (e).

Figures B-8 (a) and (b) are current measurements on the RG-214/U coaxial cable shield and center conductor, respectively. Note that the peak at 10 MHz in figure B-8 (b) is because during this measurement, the transceiver was tuned to a frequency of 10 MHz (WWV radio). These data represent the received signal at the transceiver and indicate effective attenuation of the cable shield current. Figures B-9 (a) and (b) are current measurements on the ac power line in Test Configuration IB, with the transceiver before and after the MCG415 power line protector, respectively. These may be considered normal responses as the waveform in figures B-9 (a) and (b) are the same, although they are shown on different time scales.

Note the difference in Test Configuration II as shown in figures B-10 (a) and (b), which are identical measurements on the power line before and after the MCG415, respectively. The early-time pulse on these two plots is due to the manner in which the power cable and RG-214/U coaxial cable were routed to the transceiver. In figures B-9 (a) and (b), the transceiver was located on the ground (see fig. 18 in the main report) so there was no problem connecting the cables to the transceiver. In figures B-10 (a) and (b), however, the transceiver was positioned on top of the stand at a height of 5 m (see fig. 19 in the main report) and connecting the cables to the transceiver required a 5-m vertical section of cable. The vertical component of the

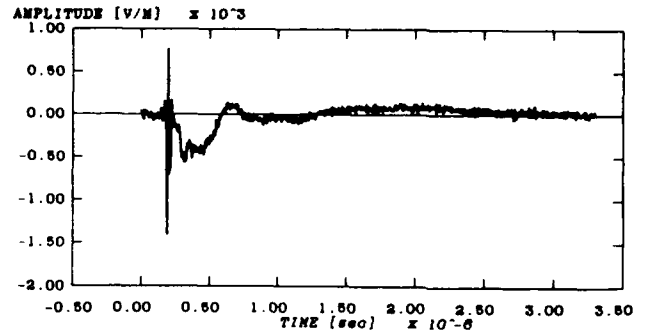
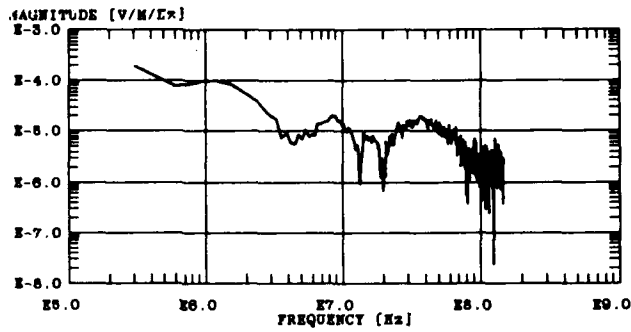
E-field at this location couples to the vertically oriented cable. Except for this difference, these waveforms resemble those of figures B-9 (a) and (b), as they should.

Figures B-11 (a) and (b) are the measured current on the dc power line from the RF-3236R power supply in Test Configuration IB with the transceiver and Test Configuration II, respectively. Both measurements show a damped sinusoid at a frequency of 273 kHz. This frequency component is due to the response of the transformer in the power supply, which acts as a bandpass filter. Figure B-11 (b) has the additional early-time response from the vertical E-field coupling to the vertical section of the power cable. Figures B-12 (a) and (b) are the measured shield current on the dynamic and electret microphone cables, respectively. For these measurements, the microphone cable was extended vertically downward a distance of about 1 m, which in effect produced a vertically oriented monopole antenna. The different current amplitudes in these two measurements are due to the different impedances of these two microphones and how they load the monopole antenna. The 20-MHz resonant frequency is much lower than expected and indicates the top-loaded effect of the microphone impedance and the inductive base-loaded effect of the audio input on the monopole antenna model of this cable.

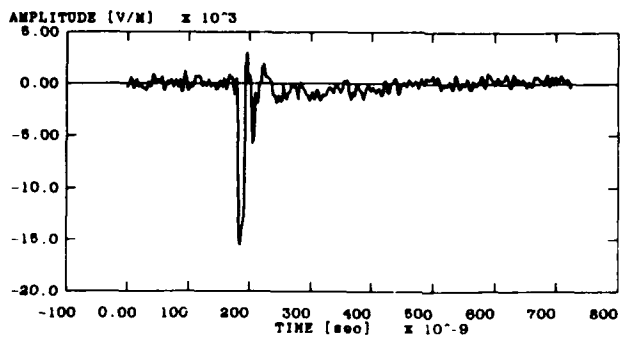
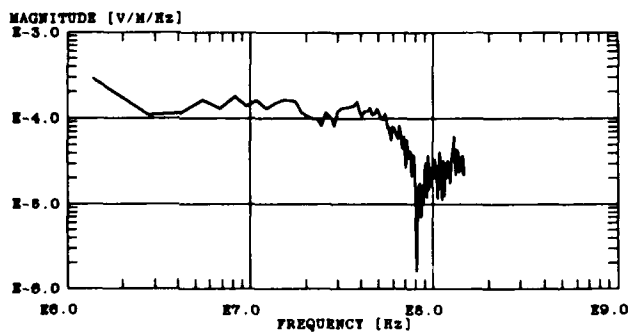
Figures B-13 (a) and (b) are Test Configuration II measurements on the coaxial cable shield at the coupler rf I/O and at the transceiver, respectively. Again, note the early-time response from the vertical cable coupling which precedes the slower pulse from the horizontal cable coupling. This is because the vertical cable coupling follows the vertical E-field while the horizontal cable coupling is proportional to the pulsewidth of the horizontal E-field. Figures B-14 (a) and (b) are Test Configuration II measurements of the ground strap current at the coupler and the transceiver, respectively. Note the similarity of these waveforms to those of figures B-13 (a) and (b). These measurements indicate that the coaxial cable shield current flows to ground at both the coupler and the transceiver. Note that the transceiver ground strap current in figure B-14 (b) includes a contribution from the induced current on the ac power neutral line.

# Appendix B

(a)



(b)



(c)

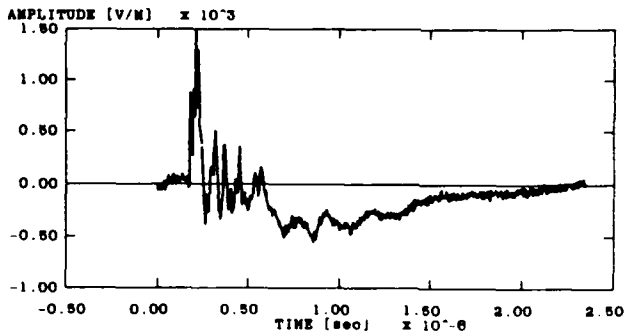
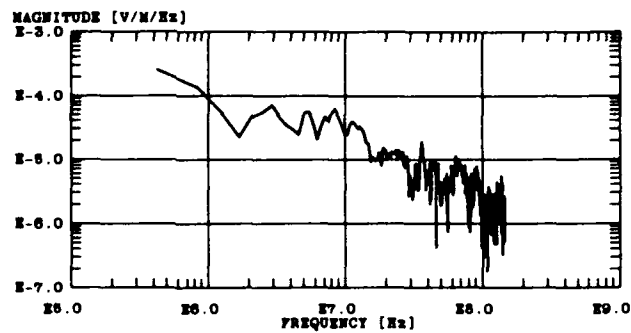
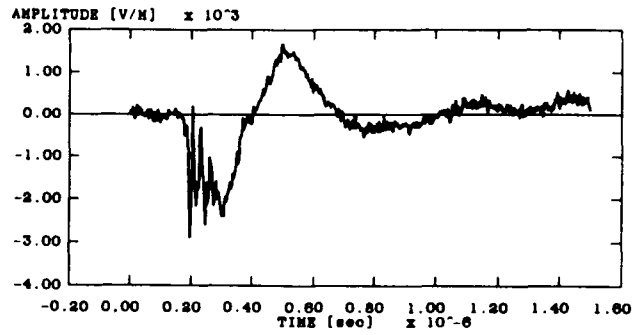
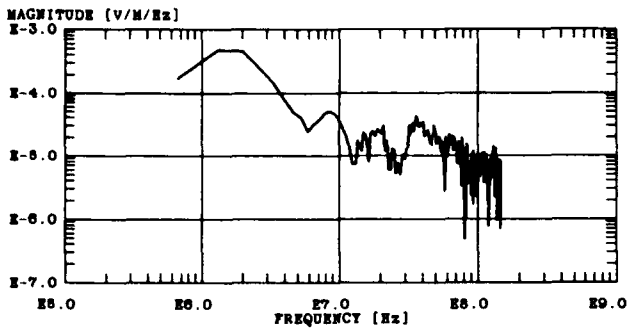
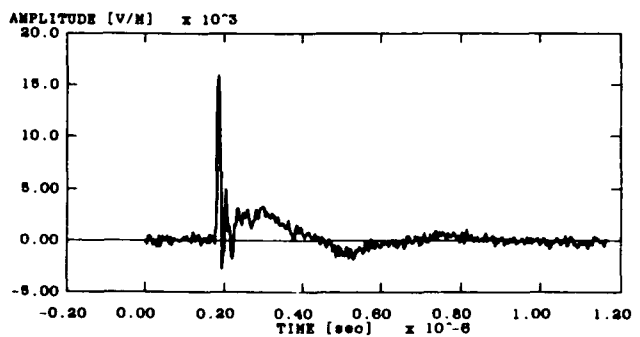
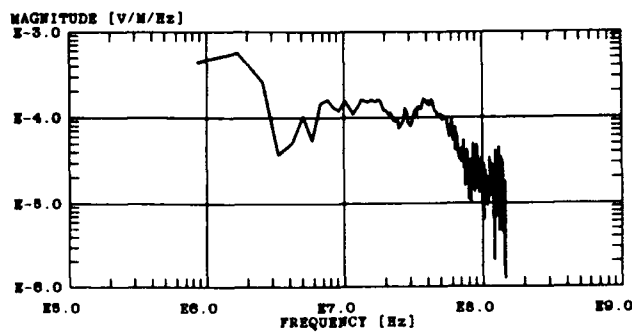


Figure B-1. Measured electric field components, magnitude and amplitude, at location (18, 0, 1):  
 (a) radial (x-component), (b) horizontal (y-components), and (c) vertical (z-components).

(a)



(b)



(c)

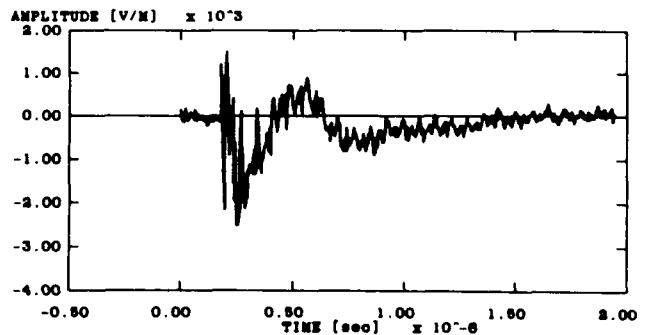
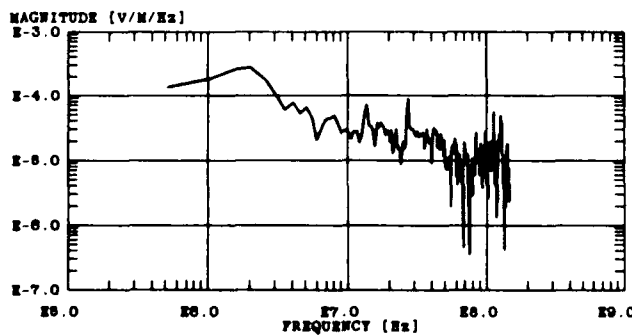
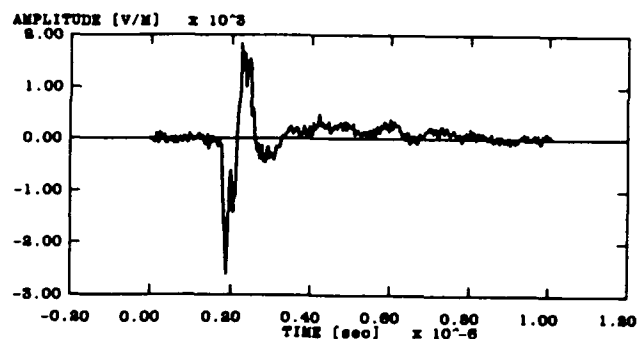
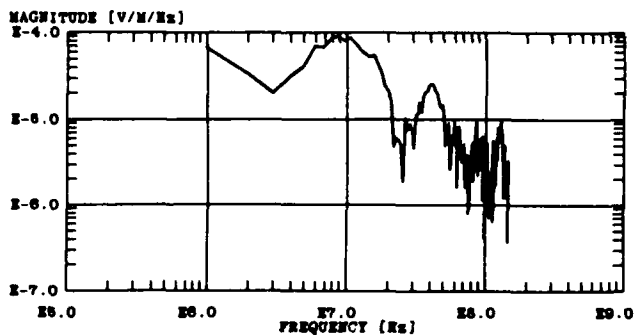


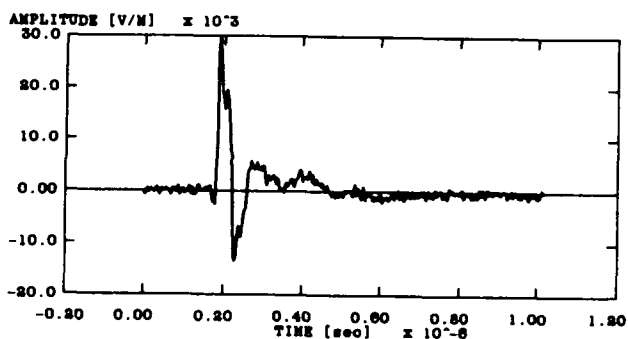
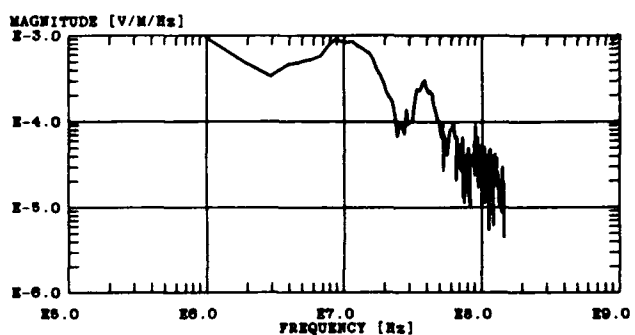
Figure B-2. Measured electric field components, magnitude and amplitude, at location (6, 0, 1): (a) radial (x-components), (b) horizontal (y-components), and (c) vertical (z-components).

# Appendix B

(a)



(b)



(c)

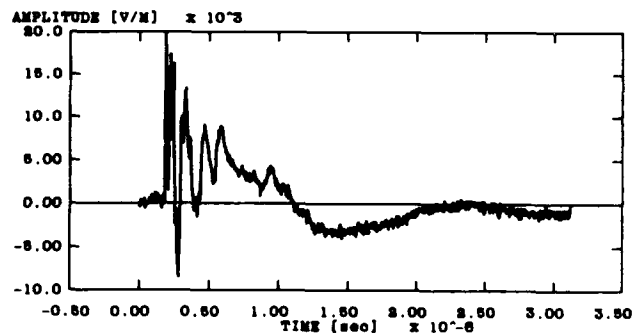
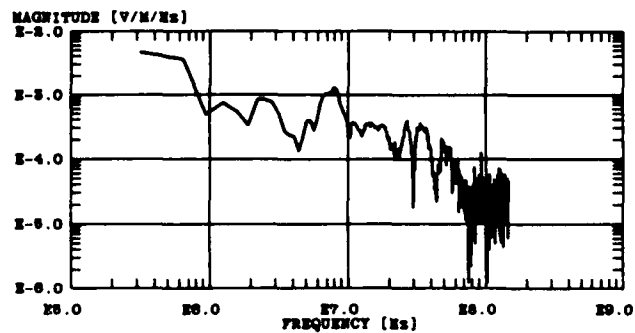


Figure B-3. Measured electric field components, magnitude and amplitude, at location (0, 0, 5):  
 (a) radial (x-components), (b) horizontal (y-components), and (c) vertical (z-components).

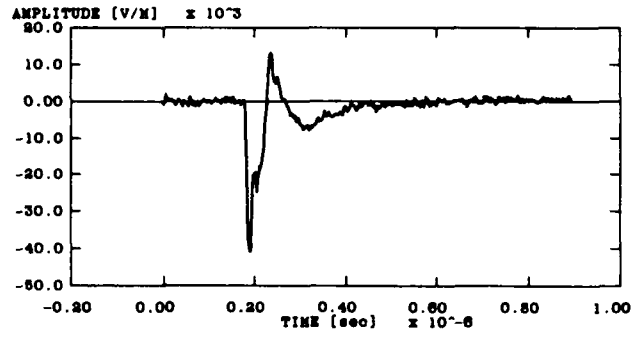
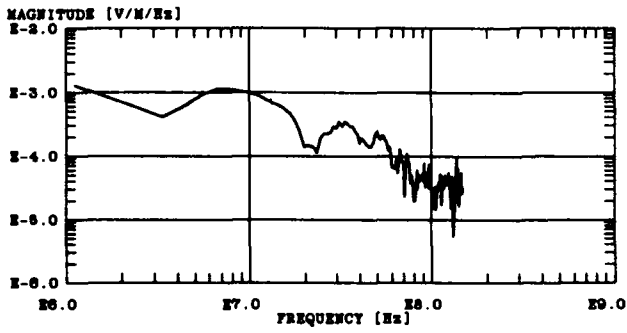
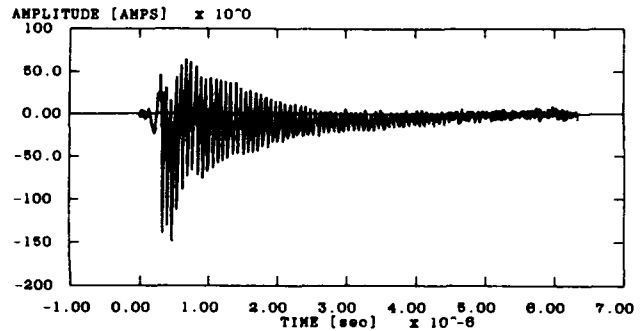
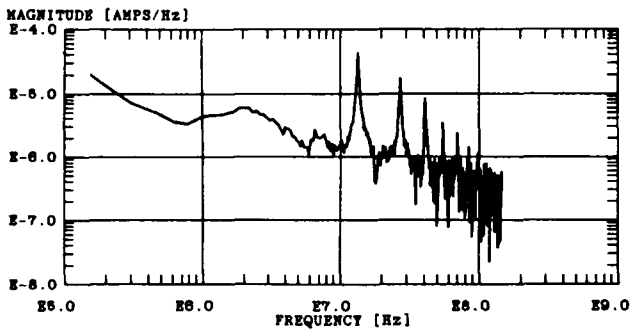


Figure B-4. Measured horizontal electric field (y-component) at location (6, 0, 9).

(a)



(b)

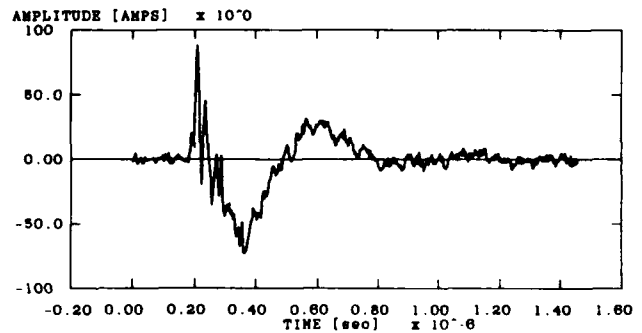
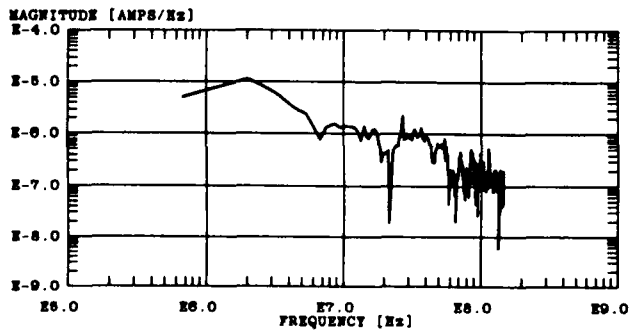
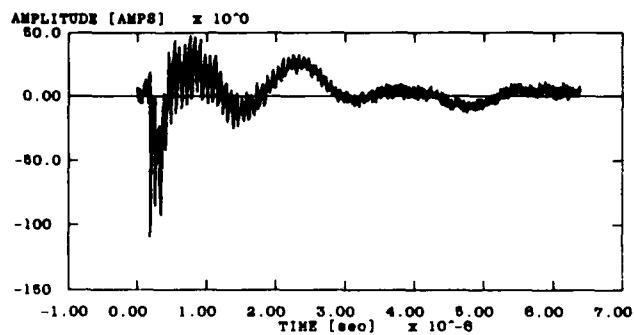
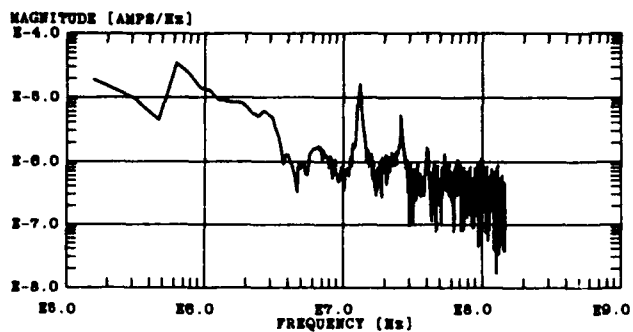


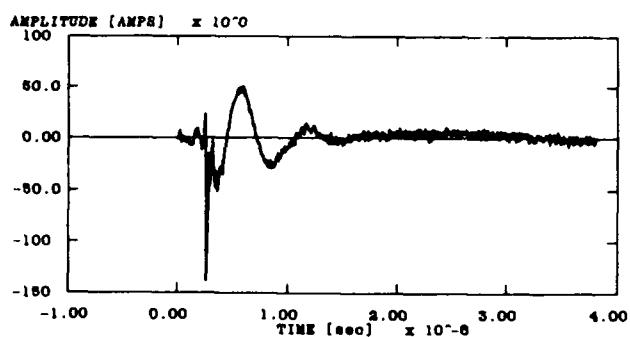
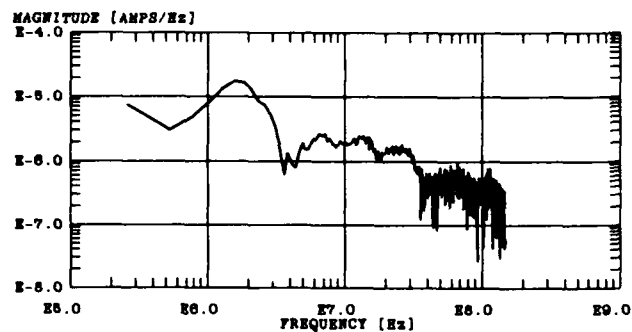
Figure B-5. Measured RF-1912 antenna current: (a) both leads shorted, one lead measured, and (b) both leads shorted, both leads measured.

# Appendix B

(c)



(d)



(e)

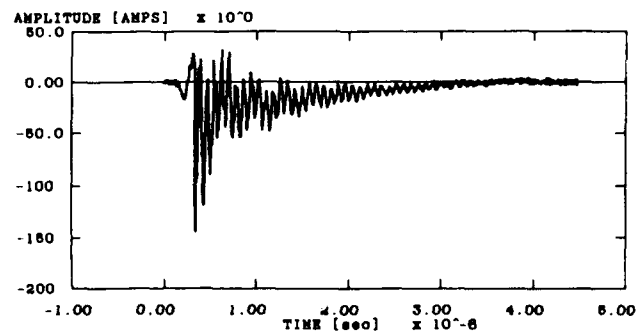
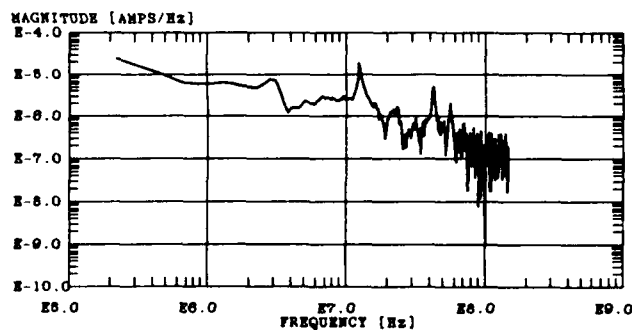
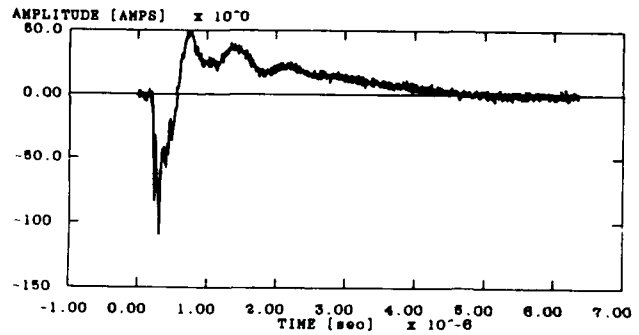
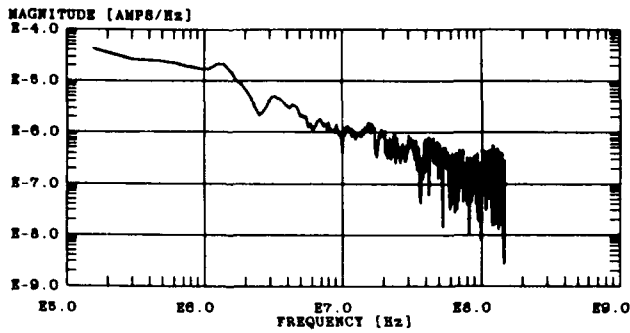


Figure B-5 (cont'd). Measured RF-1912 antenna current: (c) coupler terminated into  $50 \Omega$  (shot #16839), (d) coupler terminated into  $50 \Omega$  (shot #16840), and (e) coupler terminated into transceiver.

(a)



(b)

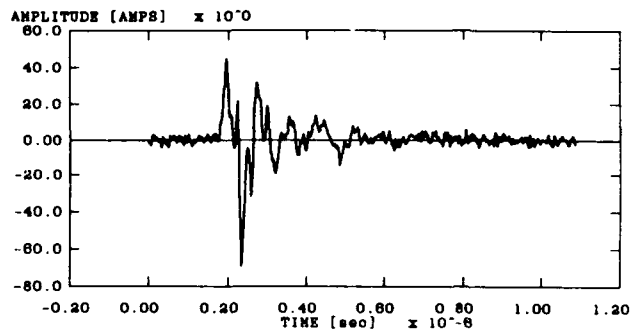
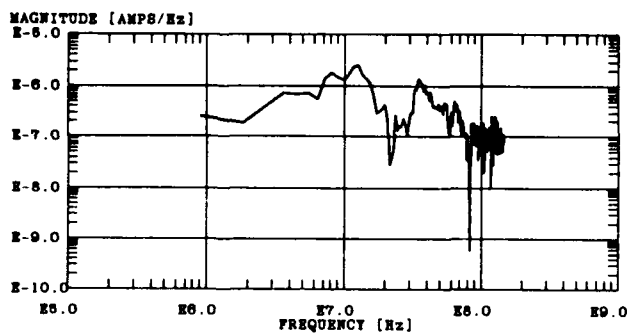


Figure B-6. Measured RF-1940 antenna: (a) horizontal dipole with the coupler terminated into  $50 \Omega$  and (b) vertical monopole with the coupler terminated into the transceiver.

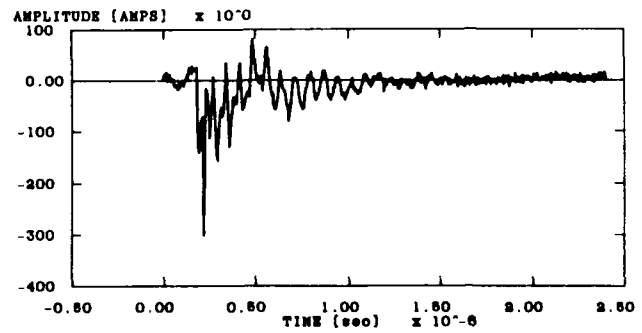
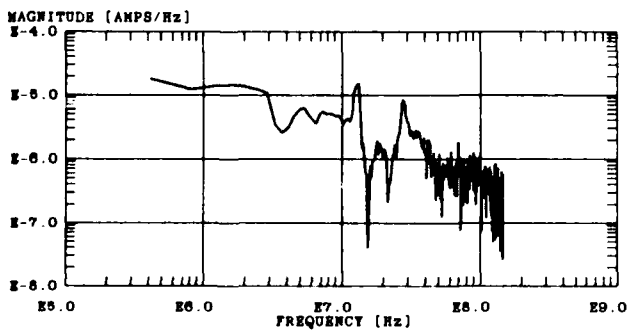
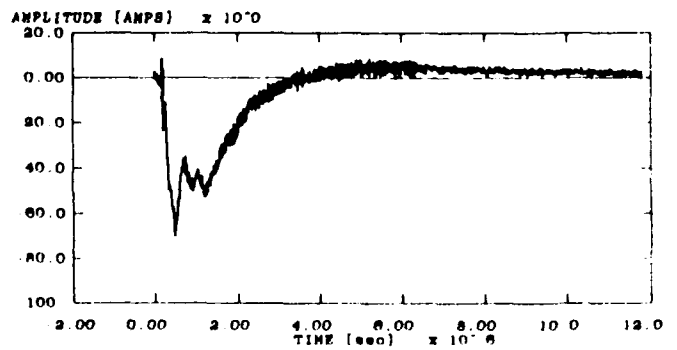
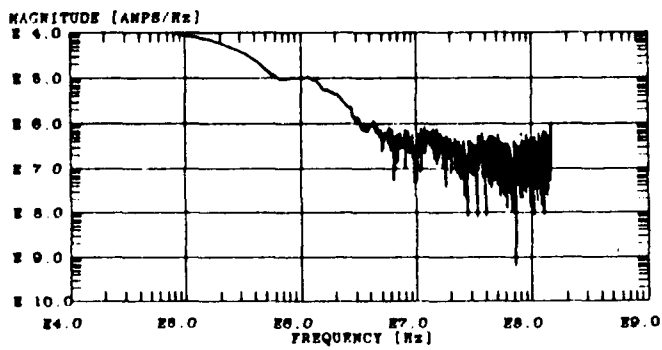


Figure B-7. Measured RF-1940 and RF-1912 combined antenna current: (a) magnitude and (b) amplitude.

# Appendix B

(a)



(b)

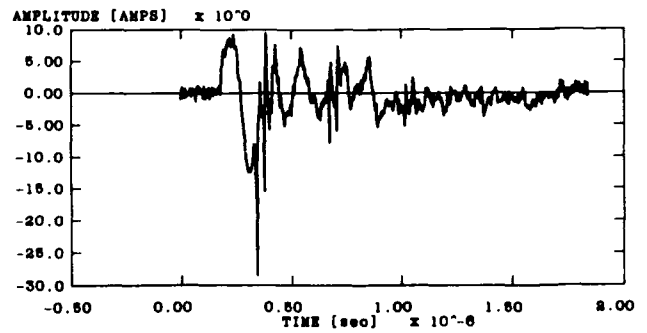
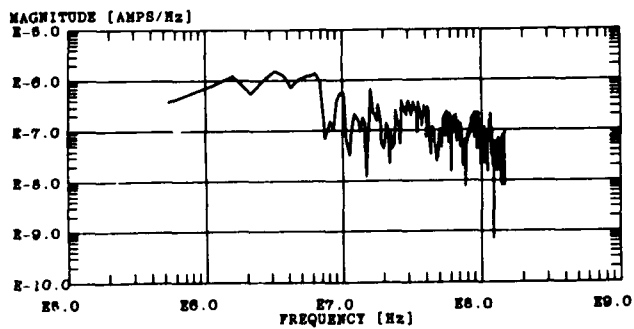
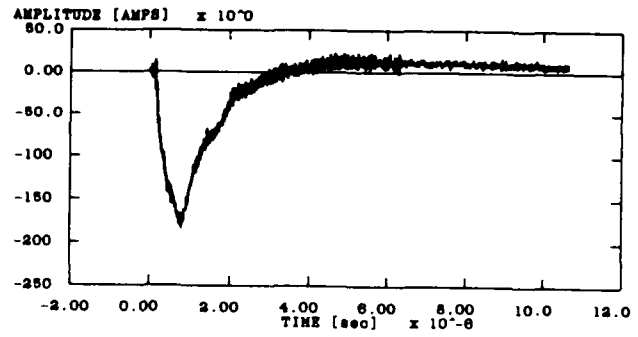
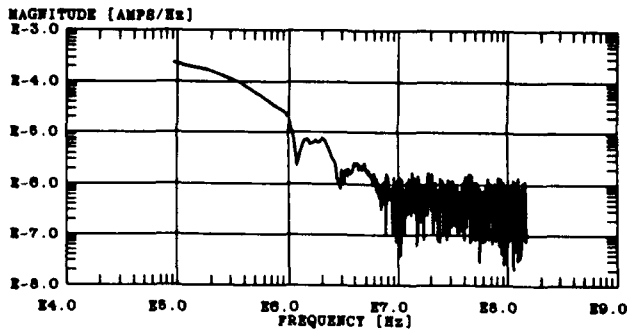


Figure B-8. Measured RG-214/U coaxial cable current in test configuration IB: (a) shield current and (b) center conductor current.

(a)



(b)

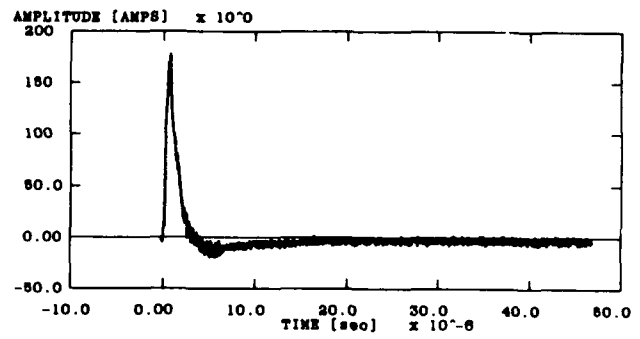
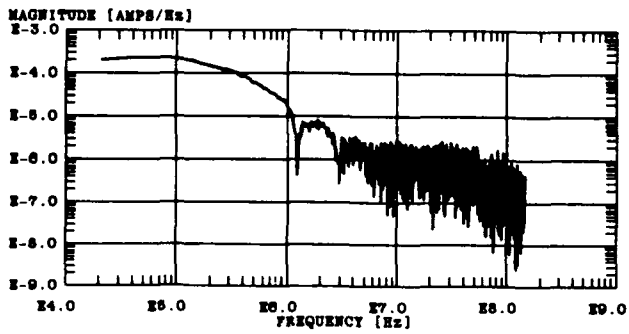
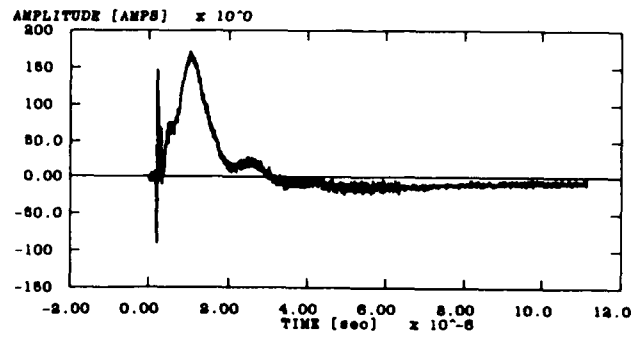
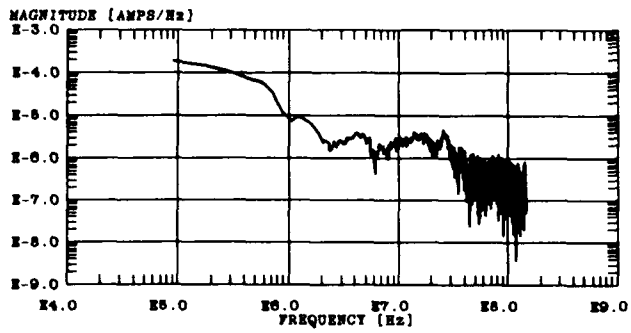


Figure B-9. Measured ac power bulk cable current in test configuration IB: (a) before power line protector and (b) after power line protector.

# Appendix B

(a)



(b)

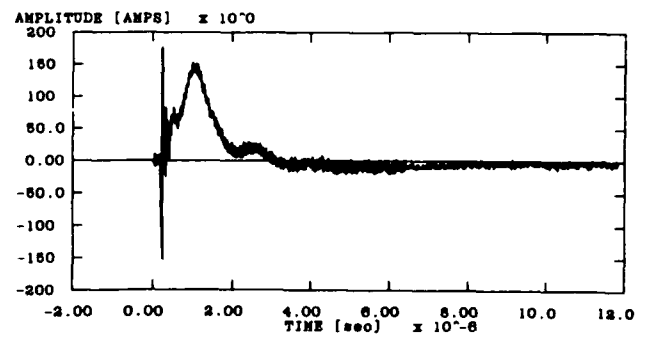
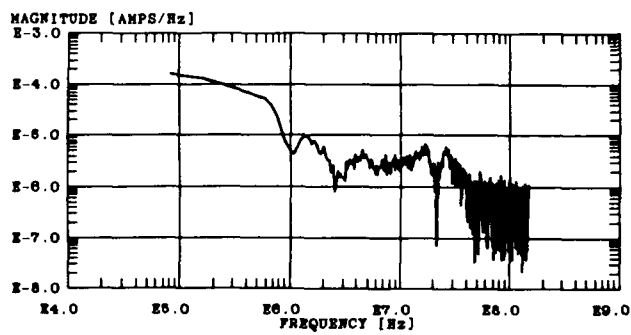
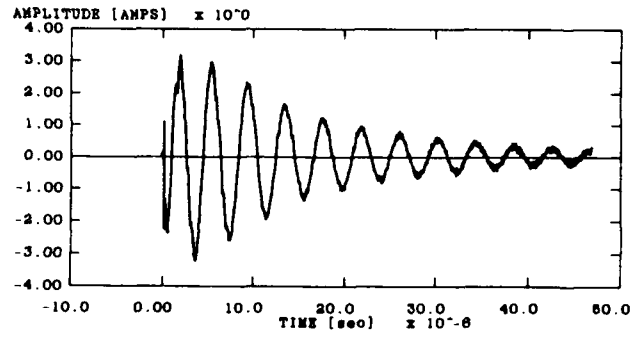
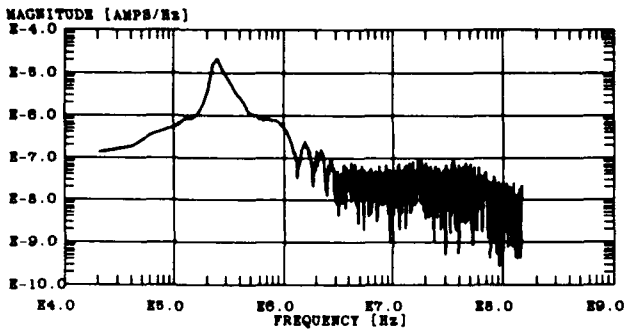


Figure B-10. Measured ac power bulk cable current in test configuration II: (a) before power line protector and (b) after power line protector.

(a)



(b)

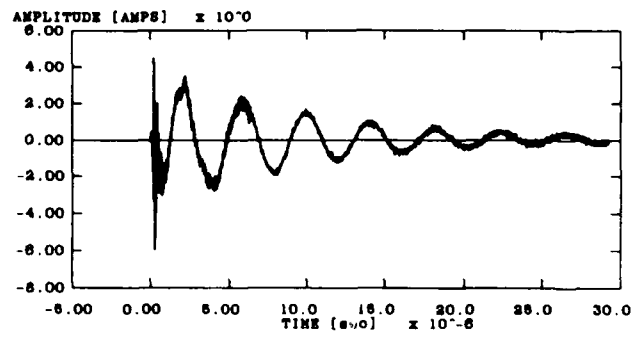
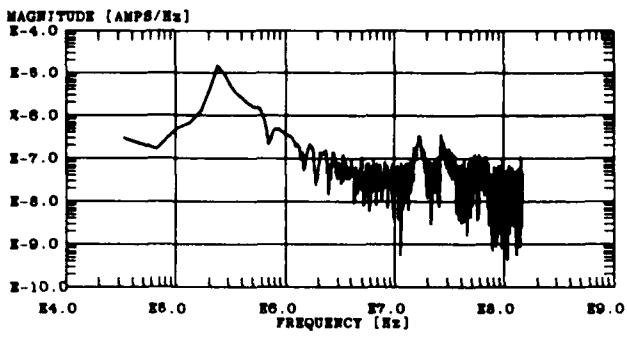
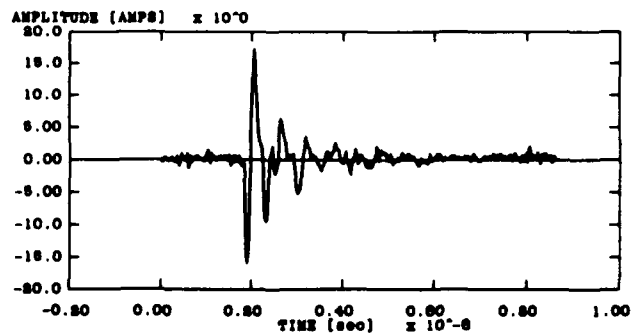
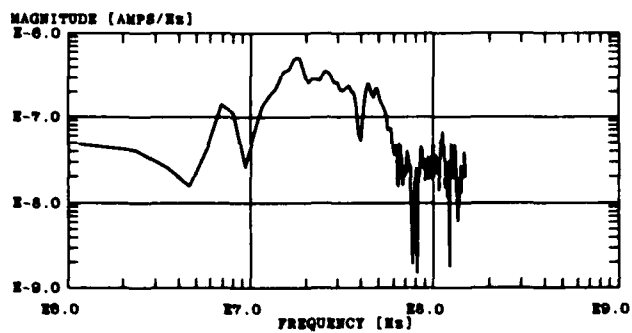


Figure B-11. Measured dc power bulk cable current: (a) test configuration IB and (b) test configuration II.

## Appendix B

(a)



(b)

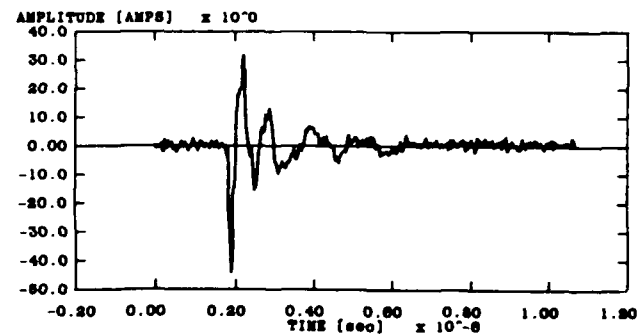
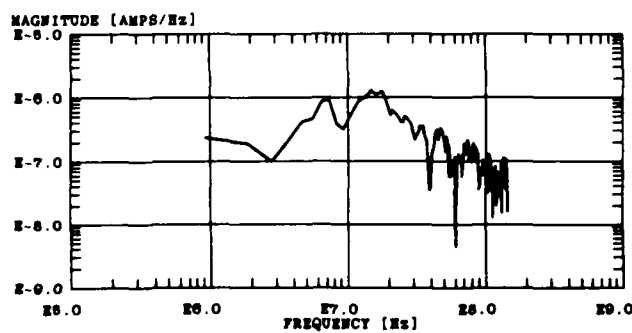
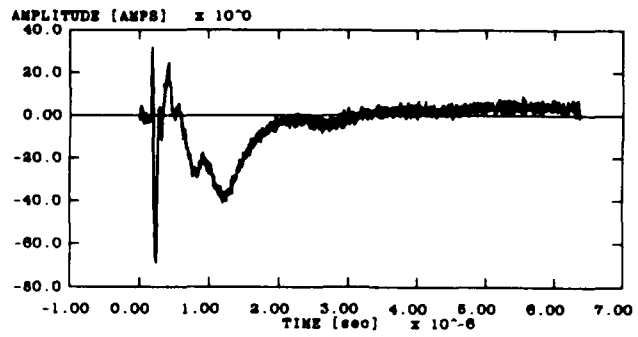
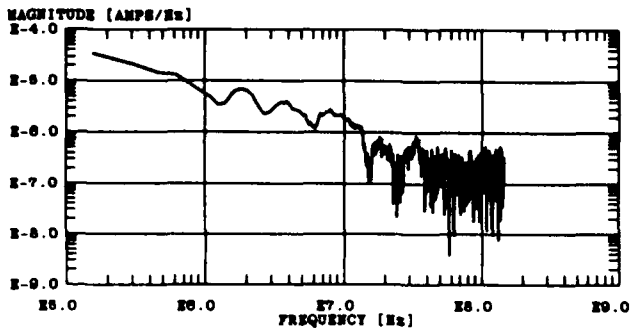


Figure B-12. Measured microphone bulk cable current: (a) dynamic microphone and (b) electret microphone.

(a)



(b)

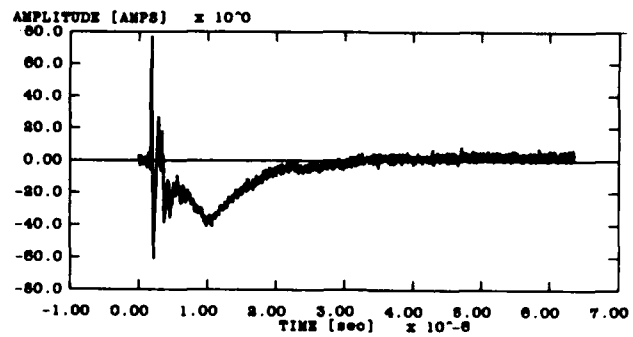
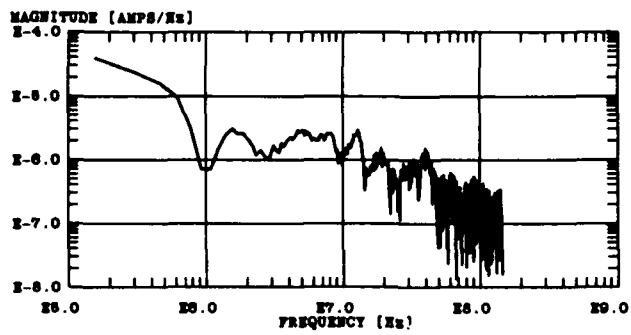
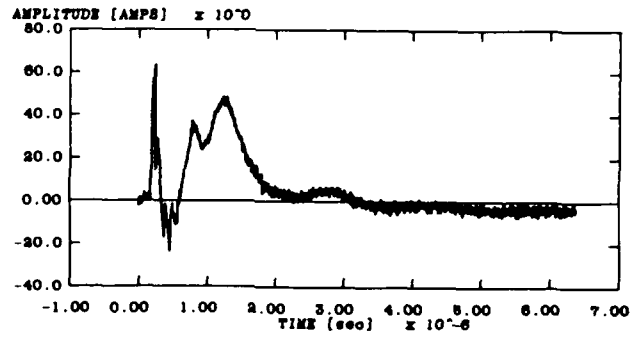
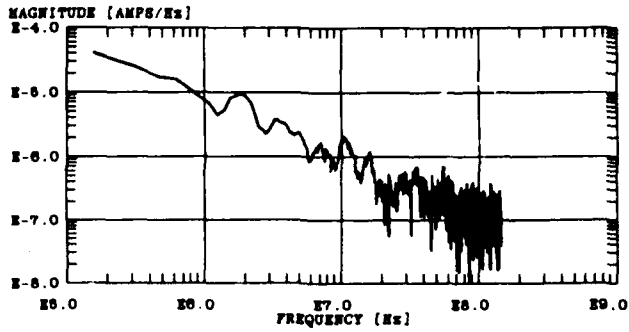


Figure B-13. Measured RG-214/U coaxial cable shield current in test configuration II: (a) at the coupler and (b) at the transceiver.

Appendix B

(a)



(b)

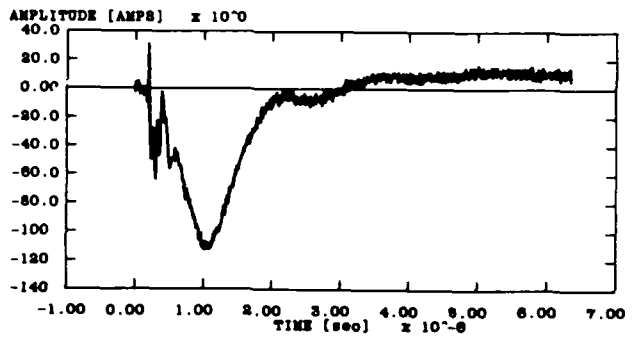
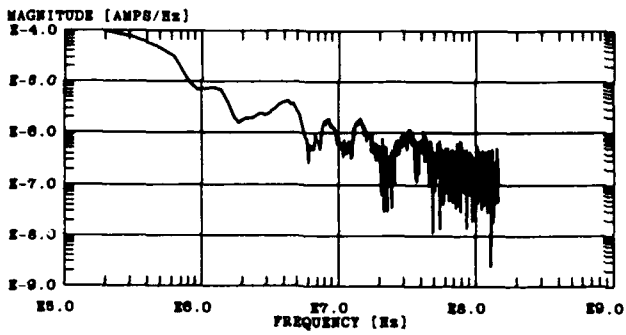


Figure B-14. Measured ground strap current: (a) at the coupler and (b) at the transceiver.

## Distribution

Administrator  
Defense Technical Information Center  
Attn: DTIC-DDA (2 copies)  
Cameron Station, Building 5  
Alexandria, VA 22304-6145

Director  
Defense Intelligence Agency  
Attn: DIO/SPRD, D. Spohn  
Attn: RTS-2A, Technical Library  
Washington, DC 20301

Director  
Defense Nuclear Agency  
Attn: RAEE, EMP Effects Division  
Attn: RAAE, Atmospheric Effects Div,  
B. Prasad  
Attn: RAEV, Electronics Vulnerability Div  
Attn: TISI-Scientific Information Div  
6801 Telegraph Road  
Alexandria, VA 22301-3398

Commander  
Atmospheric Sciences Laboratory  
Attn: STEWS-IM-ST, Technical Library  
White Sands Missile Range, NM 88002-5030

Deputy Director for Research and Engineering  
(Science and Technology)  
Attn: Room 3E118  
Pentagon  
Washington, DC 20301-3080

Director  
US Army Ballistics Research Laboratory  
Attn: SLCBR-DD-T (STINFO)  
Aberdeen Proving Ground, MD 21005

Commander  
US Army Materiel Command  
Attn: AMCAM-CN  
5001 Eisenhower Avenue  
Alexandria, VA 22333-0001

Director  
US Army Missile Command (USAMICOM)  
Attn: AMSMI-RD-CS-R, Documents  
Redstone Arsenal, AL 35898-5400

Commander  
US Army Nuclear & Chemical Agency  
Attn: MONA-NU, R. Pfeffer  
Attn: MONA-NU, A. Renner  
7500 Backlick Road, Bldg 2073  
Springfield, VA 22150

Director  
US Army TMDE Activity  
Attn: AMXTM-S-A, C. Bosco  
Redstone Arsenal, AL 35898-5400

Naval Research Laboratory  
Attn: 4200, Center for Space Sensing  
Attn: 4600, Condensed Matter and Radiation  
Sciences  
Attn: 4700, Plasma Physics Division  
Attn: 5700, Tactical Electronic Warfare  
Division  
Attn: 6800, Electronic Science & Technology  
Division  
Attn: 8000, Center for Space Technology  
Attn: 4820, Technical Info Div  
4555 Overlook Avenue SW  
Washington, DC 20375-5000

Naval Surface Warfare Center, Dahlgren  
Division  
Attn: Code E231, Technical Library  
Dahlgren, VA 22448-5020

Air Force Phillips Laboratory  
Attn: PL/WSR, C. Baum  
Albuquerque, NM 87116

Department of the Air Force  
Attn: HQUSAFA/DFSELD  
USAF Academy, CO 80840-5701

## Distribution

Lawrence Livermore National Laboratory  
Attn: L-156, M. Bland  
Attn: L-86, H. S. Cabayan  
PO Box 808  
Livermore, CA 94550

Sandia National Laboratories  
Attn: Organization 3141, Reports Acquisition  
PO Box 5800  
Albuquerque, NM 87185

National Institute of Standards and  
Technology  
Attn: V. Ulbrecht, Research Information  
Center  
Room E01, Building 101  
Gaithersburg, MD 20899

US Army Laboratory Command  
Attn: AMSLC-DL, Dir Corp Labs

USAISC  
Attn: AMSLC-IM-VA, Admin Ser Br  
Attn: AMSLC-IM-VP, Tech Pub Br (2 copies)

Harry Diamond Laboratories  
Attn: Laboratory Directors  
Attn: SLCHD-SD-TL, Library (3 copies)  
Attn: SLCHD-SD-TL, Library (Woodbridge)  
Attn: SLCHD-CS, Chief Scientist  
Attn: SLCHD-NW, Director  
Attn: SLCHD-NW-E, Deputy Director  
Attn: SLCHD-NW-EP, Chief  
Attn: SLCHD-NW-ES, Chief  
Attn: SLCHD-NW-HPM, Chief  
Attn: SLCHD-NW-P, Chief  
Attn: SLCHD-NW-RF, Chief  
Attn: SLCHD-NW-RP, Chief  
Attn: SLCHD-NW-RS, Chief  
Attn: SLCHD-NW-TN, Chief  
Attn: SLCHD-NW-TS, Chief  
Attn: SLCHD-ST, Director  
Attn: SLCHD-TA, Director  
Attn: SLCHD-NW-EP, W. O. Coburn  
(5 copies)